A study on assessing systemic inflammation due to malignant cells and pesticide exposure

（悪性細胞と農薬曝露による全身性炎症の評価に関する研究）

July, 2021

Doctor of Philosophy (Engineering)

THOMAS TIONG KWONG SOON

トーマス　ティオン　クオン　スン

Toyohashi University of Technology

別紙４－１（課程博士（英文））

Date of Submission（month day，year）： 09th July 2021

Department of Applied Chemistry and Life Science	Student ID Number	D143440
Applicant's name	Thomas Tiong Kwong Soon	

Supervisors	Toshihiko Eki Kazunori Takashima Sachiko Yoshida

Abstract（Doctor）

Title of Thesis	A study on assessing systemic inflammation due to malignant cells and pesticide exposure

Approx. 800 words

Inflammation plays an important role in body defense mechanism as it fights off the invasion of foreign substances such as pathogens are trying to compromise our defense system. Our body usually response with the release of pro-inflammatory cytokines in order to recruit cells such as macrophage and resident microglia to eliminate the pathogens. There are two common types inflammation which are acute inflammation and chronic inflammation. Acute inflammation is a rapid response from initial insult to initiate healing process, while chronic inflammation usually occurs across a longer period of time when the body is under continuous and prolonged perturbation. Both are equally dangerous as the progression of inflammation may lead to systemic inflammation. Systemic inflammation is a result of circulating pro-inflammatory cytokines which can cause multiple reactions before disease manifestation. Therefore, it is hard to pinpoint the exact assault that causes systemic inflammation, making it a prominent target in multiple fields involving medicine, biology, chemistry and physiology. This study proposes an assessment involving cellular biology, signal processing, rat study and genetic engineering in order to evaluate the alterations coming from systemic inflammation.

Chapter 1 consisted of the general introduction of this thesis, explaining the background, motivations and objectives and the structure of this thesis.

Chapter 2 discussed on the evaluation of the cellular dynamics through malignant cells using scanning acoustic microscope. Development of non-invasive observational tool to assess the changes in cellular level is necessary as conventional approaches focus more on tissue and organ. This study focused on the dynamic cellular changes during mitotic phase as cell nucleus facilitates most of the cell activities, making it a prime target in disease study and drug design. Malignant cells were arrested in mitotic phase by cell cycle synchronization using demecolcine, a typical anticancer drug mostly used in chemo-radiotherapy. The dynamic changes of the cell nucleus during mitotic phase were successfully captured using scanning acoustic microscope and confirmed using confocal microscopy.

This result provided valuable insight in understanding the alteration of cell nucleus in real time and allowed us to explore the possibility to improve drug design and elucidate the disease mechanism. This is an important advancement to bring scanning acoustic microscope closer to application in biomedical field.

Furthermore, this study explored the potential causes and effects of systemic inflammation through pesticide exposure in rat study. Glyphosate, an active ingredient of Roundup®, with gathering controversies around its usage was chosen. Daily exposure to such xenobiotics is proven to be unsafe to human as the continuous exposure might cause systemic inflammation which is easy to be overlooked. Emerging evidences suggest that glyphosate is a potential health risk and jeopardize the environment, thus making it a suitable target to trigger systemic inflammation in rat study. Chapter 3 explored whether the transient inflammation observed in previous chapter is systemic or not by looking at the gut-brain axis. Gut-brain axis is a bidirectional relationship that affect each other. One of the feasible factors is through the metabolites produced by the gut bacteria. The changes of the gut microbiota and metabolites are indicative of inflammation-mediated alteration. The result showed that there is a strong association in between the cerebellar developmental anomalies and disrupted gut microbiota and metabolites production. These changes pointed towards systemic inflammation as the major propagator that might further irritate the symptoms.

Chapter 4 focused on the effects of prenatal exposure on the cerebellar development in offspring. Prenatal exposure was chosen because multiple biological and physiological events happened during pregnancy, making pregnant dam more susceptible to alterations. The result showed that alteration occurred in the offspring cerebellum inferring that glyphosate might be developmental neurotoxic. Chapter 5 described the alteration of pro-inflammatory cytokine found in offspring cerebellum. Since the alteration observed in previous chapter might be mediated by systemic inflammation, hence, finding out the production of pro-inflammatory cytokines during early development is essential to understand the mechanism behind the alteration. The result showed that transient inflammation occurred in the cerebellum of juvenile male rat although the production timing differed.

Chapter 6 expanded the research scope into adulthood by examining the social behavioral changes in matured animal. Animal behavior study is essential in understanding the brain alteration and disease phenotype. The result demonstrated that adult male rats born from prenatal glyphosate exposed dam animals were less explorative, not grooming as much and more anxious in social interaction. This implied cognitive impairment, and hence, the result inferred that the effects of prenatal GP exposure carried on into adulthood.

Taken together, scanning acoustic microscope has the potential to bridge current approaches in cellular study to translational research. Tracing the living cellular dynamics change might reveal more on the alteration caused by systemic inflammation. Prenatal glyphosate exposure successfully triggered systemic inflammation in the F1 male rat even when they entered adulthood. The effects were significant and assessable through methodology proposed in this study. This implied that the proposed methodology is translatable in human study in order to elucidate disease mechanism.

Table of contents

List of Figures

List of Tables

Chapter 1 General Introduction

1.1 Background

Inflammation is a complex biological process involving crosstalk within the cellular community, elicit signals such as heat, swelling and redness in order to coordinate the immune defense when the body is under attack. Under normal circumstances, inflammation is beneficial but there are times when it can be harmful. For instances in some cases, the body may start to attacks its own cells or tissues(*1–5*).

The common reason for inflammation is from fatal injuries involving tissue lacerations and necrotic cells from infection. This type of inflammation is known as acute inflammation which takes place in a sudden onset and short duration. Example of such inflammation are allergy, trauma injuries and fatal bacterial or viral infection. The immune defense system usually works swiftly in this case to completely eliminate the foreign insult and initiate the healing process(*6*, *7*). On the other hand, chronic inflammation often occurs in a gradual onset and long duration, while triggering multiple reaction as the symptoms progressed(*8*).

Inflammation is importance for several reasons. First, it served as one of our defense mechanisms against foreign substance invasion. Inflammation is also sometimes expressed as symptoms of various diseases and the hallmark for terminal diseases(*9*). In some case, the inflammatory cytokines released after inflammation occur may help in regulate cell proliferation and differentiation.

In the inflammatory process, if exudation and proliferation prevail, then the inflammation will gradually develop in the direction of healing. Conversely, if injurious changes predominate, inflammation gradually increases and can spread systemically. The spread is usually facilitated by blood flow, sending pro-inflammatory cytokines such as TNF-α and IL-1 around the body making it hard to pinpoint the ground zero for the first assault(*10–13*).

These inflammatory cells can activate granulocytes to cause endothelial cell damage, platelet adhesion, release oxygen radicals and lipid metabolites. Widespread tissue and cell damage caused by

excessive inflammatory responses will eventually instigate systemic inflammation. In addition, as the pro-inflammatory cytokines spread systemically through the whole body, this may lead to multiple organ dysfunction syndrome. This is life-threatening in most cases upon discoveries because all early symptoms are usually insignificant. Therefore, curing systemic inflammation is challenging as many mechanisms behind the phenomenon itself still remained unclear.

1.2 Motivations and objectives

This study proposes an assessment involving cellular biology, signal processing, rat study and genetic engineering in order to evaluate the alterations coming from systemic inflammation. Since systemic inflammation is caused by circulating blood flow, assessing the alterations involved in systemic inflammation is quite challenging. The first part of this thesis focuses on the evaluation of the cellular dynamics through malignant cells using scanning acoustic microscope. Development of non-invasive observational tool to assess the changes in cellular level is vital as conventional methodology focus more on tissue and organ. This study focus on the cell nucleus dynamic changes during mitotic phase as cell nucleus facilitates most of the cell activities, making it a prime target in disease study and drug design. Malignant cells were arrested in mitotic phase by cell cycle synchronization using Demecolcine, a typical anticancer drug mostly used in chemo-radiotherapy.

In the other half of this study, the potential causes and effects of systemic inflammation through pesticide exposure in rat study was explored. Glyphosate (GP), an active ingredient of Roundup®, with gathering controversies around its usage was chosen. Daily exposure to such xenobiotics is proven to be unsafe to human as the continuous exposure might cause systemic inflammation which is easy to be overlooked. Emerging evidences suggest that GP is a potential health risk and jeopardize the environment, thus making it a suitable target to trigger systemic inflammation in rat study. Further evaluation through genetic engineering and animal behavior study will help us better understand how the triggered systemic inflammation affected the development of F1 male rat, from neonatal into adulthood.

1.3 Structure of thesis

This thesis consisted of 7 chapters as described below.

Chapter 1 focused on general introduction of this thesis which cover the background of this study, the motivations and objectives, and the structure of this thesis.

Chapter 2 discussed about the observation of the cellular dynamic using scanning acoustic microscope. Development of non-invasive observational tool to assess the changes in cellular level is vital as conventional methodology focus more on tissue and organ. Previous studies demonstrated that scanning acoustic microscope is able to map the cell as the cytoskeleton correspond with cell elasticity. By cell cycle synchronization, the malignant cells were arrested at mitotic phase to reveal the intracellular contents in order to understand the effects of systemic inflammation. The dynamic changes of the cell, especially the cell nucleus during mitotic phase were successfully captured using scanning acoustic microscope and confirmed using confocal microscopy. Cell nucleus is an important cell organelle as it is the target of most therapeutic drugs. This result provided valuable insight in understanding the alteration of cell nucleus in real time and allowed us to explore the possibility to drug design and unveil disease mechanism. This is an important advancement to bring scanning acoustic microscope closer to application in biomedical field.

Chapter 3 discussed the potential causes and effects of systemic inflammation through pesticide exposure via gut-brain axis. Gut-brain axis suggested that the brain and the gut are in a bidirectional relationship that affect each other via various routes. One of the feasible factors is through the metabolites produced by the gut bacteria. The changes of the gut microbiota and metabolites are indicative of inflammation-mediated alteration. In this chapter, investigation of the active ingredient of commercial herbicides, Roundup®, which is GP, on the pregnant rat model is employed to evaluate the alterations happened in the gut flora. DNA sequencing and bioinformatics were employed in order to elucidate the possible mechanism behind the systemic inflammation caused by prenatal chemical exposure and how it affected the offspring. The result confirmed that disrupted gut microbiota and metabolites production in

male offspring born from dam that was prenatally exposed to GP. These changes pointed towards systemic inflammation as the major propagator that might further irritate the symptoms.

Chapter 4 explored the potential causes and effects of systemic inflammation through pesticide exposure. It is a growing concern that the pesticides we used in the agriculture to enhance the crops production might harm us. This thesis focused on the active chemical ingredient in widely used herbicides, Roundup®, which is GP. GP was once considered safe but emerging evidences suggest that it is a potential health risk and jeopardize the environment. However, less is known about its effect in cerebellar development. Therefore, this thesis attempted to evaluate the effects of prenatal exposure to GP on the development of offspring cerebellum on both acute and chronic exposure. The result showed that alteration occurred in the offspring cerebellum inferring that GP might be developmental neurotoxic.

Chapter 5 described the alteration of pro-inflammatory cytokine found in offspring cerebellum. Significant alteration of cerebellar development observed in previous chapter might be mediated by systemic inflammation as both acute and chronic exposure showed significant changes. Therefore, finding out the production of pro-inflammatory cytokines during early development is essential to understand the mechanism behind the observed alteration. The result showed that transient inflammation occurred in the cerebellum of juvenile male rat although the production timing differed for the tested pro-inflammatory cytokines, which are inducible nitric oxide synthase (iNOS) and interleukin-1β (IL-1β).

Chapter 6 expanded the research scope into adulthood by examining the effects of prenatal GP exposure on the social behavioral changes in matured animal. Animal behavior study is essential in understanding the brain alteration and disease phenotype. In this thesis, basic motor function and social behavior of adult male rat were observed to determine whether the transient inflammation occurred in early cerebellar development would affect their motor and cognitive function. The result demonstrated that adult male rats born from prenatal GP exposed dams were less explorative, not grooming as much and more anxious in social interaction. Less interested in exploration, decreased grooming frequency and anxiousness is indicative of cognitive impairment, and hence, the result inferred that the effects of prenatal GP exposure carried on into adulthood.

Chapter 7 summarized the overall impacts of systemic inflammation observed in cellular study and animal study.

Chapter 2 Observation of the Cellular Dynamic Using Scanning Acoustic Microscope

2.1 Introduction

This chapter discuss the utilization of scanning acoustic microscope in visualizing cellular dynamics, especially the cell nucleus at mitotic phase (M phase) by Demecolcine treatment through cell cycle synchronization. Cell at different stages within G2 and M phase were successfully mapped using scanning acoustic microscope and verified by confocal microscopy.

2.1.1 Scanning acoustic microscope (SAM)

Ultrasonic microscope is divided into a sound speed microscope and an acoustic impedance microscope. The sound speed microscope is a microscope which irradiates a pre-prepared specimen sample with pulsed ultrasonic waves, in which the reflection of the glass and reflection of the glass through the tissue is analyzed by digital signal analysis. The reflection signals are then converting into a propagation time difference to produce sonic speed image. Meanwhile, in acoustic impedance microscope, an image of the sample is acquired from the ratio of the emitted signal of the sound pressure on the tissue surface in contact with the substrate and the reflected signal.

Both microscopes are used in living tissue observation without staining. In Japan, researchers began to explore capabilities of ultrasound for medical diagnostic. In 1991, Saijo et al. has successfully developed transmission and reflection mode of scanning acoustic microscope to develop new biological microscope(*14*). The simplicity of reflection mode is favored by most researchers till this day. Based on this technique, acoustic intensity, speed of sound, attenuation and thickness of target can be measured. By improving this technique, viscous-elastic properties of biological target can be obtained, which gives us a better chance to distinguish healthy and cancerous cells.

2.1.2 Importance of living cells and tissues observation

Pathological diagnosis in cancer diagnosis plays a very important role because this may prolong patients' survival while reduce the morbidity. It is divided into cell diagnosis, tissue diagnosis, biological tissue diagnosis, surgical material pathology diagnosis, intraoperative rapid pathological diagnosis, intraoperative rapid cell diagnosis, special pathology diagnosis and so on. In cell/tissue diagnosis, cancer cells/tissues or normal cells/tissues are identified from cell/tissue morphology using an optical microscope. One of its advantages is that it provides very high spatial resolution. However, it requires staining, which is time-consuming and invasive. For that reason, it can only distinguish between the living cells and the dead or damaged cells.

Therefore, we propose ultrasonic microscope for cell observation that targets cell morphology based on their elasticity, as it is reported that the elasticity between healthy cells and cancer cells are different(*15*). It is a powerful tool for living observation of intracellular condition(*16*). Generally, the relationship between the wavelength and the frequency of the ultrasonic wave is expressed by the following equation.

$$\lambda = \frac{C}{f} \qquad (1)$$

Here, λ is the wavelength of the ultrasonic wave, C is the sound speed of the tissue and f is the frequency of the ultrasonic wave. Generally, the sound velocity of living soft tissue is around 1600 ms^{-1}, so the wavelength is determined by frequency in the above equation. Also, the relationship of the beam diameter of the ultrasonic wave is represented by the following equation.

$$BD = 1.02\,{}^{F_c}/_{fD} \qquad (2)$$

BD is the beam width at which the intensity from the center is decreased by 6 dB, F is the focus length, and D is the aperture of the transducer. From these equations, by increasing the frequency of the ultrasonic wave, the distance resolution and the azimuth resolution of the ultrasonic diagnostic apparatus can be improved.

Frequencies used in clinical ultrasonic diagnostic apparatus generally called echocardiography or abdominal echo are 2.5 to 5 MHz and the sound velocity of the soft tissue of the living body is 1600 ms^{-1}, the wavelength is about 0.5 mm. For intravascular ultrasound and ultrasound endoscopes, frequencies of 20 to 40 MHz are used, and the wavelength and resolution are on the order of tens of microns. Therefore, by further increasing the frequency, the resolution generates is on the order of several microns, and the object is also miniaturized from the period level to the organization level.

Next, the Time-Domain Reflectometry (TDR) method used in this microscope system measures the impedance of a sample by giving a high-speed pulse signal to the sample and capturing its reflected wave with a sampling oscilloscope. Reflection occurs in the mismatched portion of the impedance and its reflection coefficient *R* is shown as below.

$$\boldsymbol{R} = \frac{\boldsymbol{Z_2 - Z_1}}{\boldsymbol{Z_2 + Z_1}} \qquad (3)$$

Here, Z_2 and Z_1 respectively indicate the acoustic impedance in certain two media. Therefore, if Z_1 is known, Z_2 can be obtained by measuring the reflectance.

$$\boldsymbol{Z_2} = \frac{\boldsymbol{1+R}}{\boldsymbol{1-R}}\boldsymbol{Z_1} \qquad (4)$$

The acoustic impedance of the object is obtained based on the value of reflectance R. This is the principle of the TDR method. The characteristic of the TDR method is that the horizontal axis of the observation result is the time axis. Since impedance changes are observed at different positions on the time axis if the reflection points are different, two-dimensional information such as time (position) and impedance is obtainable. This is the reason why the TDR method is an effective measurement method. The acoustic impedance calibration method is shown in Figure 2.1.

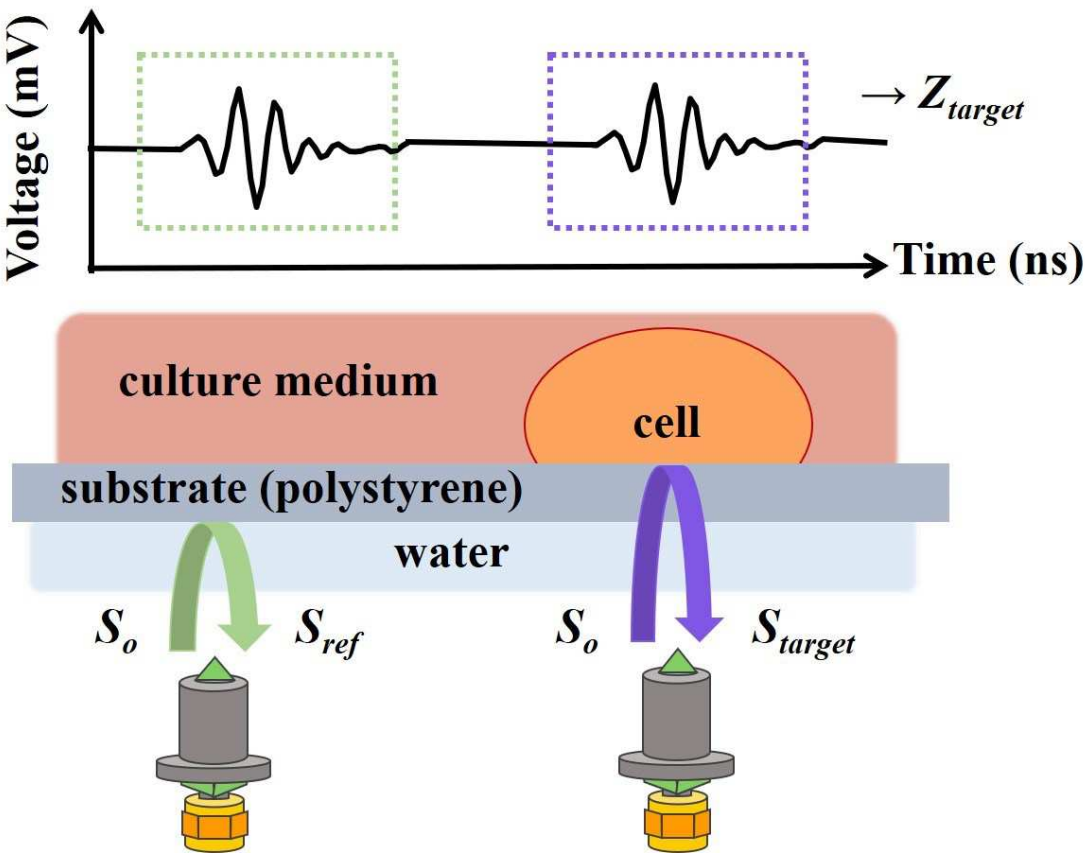

Figure 2.1 Calibration of acoustic impedance

The acoustic impedance of this system is calculated from the equation of sound pressure reflectance (3). The sound pressure reflectance is expressed by the ratio of the reflected signal from the target and the reflected signal from the reference substance. Considering the reflection coefficient, the signal from the target, S_{target} is shown as follows (5).

$$\boldsymbol{S_{target}} = \frac{\boldsymbol{Z_{target} - Z_{sub}}}{\boldsymbol{Z_{target} + Z_{sub}}} \boldsymbol{S_0} \qquad (5)$$

Here, the frequency component of the signal at an arbitrary frequency is denoted by S, and Z_{target} and Z_{sub} are the acoustic impedance of the target tissue and the substrate, respectively. S_0 is the transmission and is always constant during the observation. On the other hand, the reflected signal from the reference material is shown as follows (6).

$$\boldsymbol{S_{ref}} = \frac{\boldsymbol{Z_{ref}-Z_{sub}}}{\boldsymbol{Z_{ref}+Z_{sub}}}\boldsymbol{S_0} \qquad (6)$$

Z_{ref} is the acoustic impedance of the reference material. S_{target} can be measured directly and Z_{ref} is known. Although S_0 cannot be measured in the current system, it can be calculated from equation (6) as follows (7).

$$S_o = \frac{Z_{ref}+Z_{sub}}{Z_{ref}-Z_{sub}} S_{ref}. \qquad (7)$$

Therefore, the acoustic impedance of the target tissue is calculated as a solution of simultaneous equations relating to Z_{target} and S_0. The reflection waveform from the target and the reflection waveform from the reference material are acquired by the TDR method. After the waveform parameter is extracted, acoustic impedance is calculated from (8) and calibrated.

$$\boldsymbol{Z_{target}} = \frac{1+\frac{S_{target}}{S_0}}{1-\frac{S_{target}}{S_0}} Z_{sub} = \frac{\boldsymbol{1-\frac{S_{target}}{S_{ref}}\times\frac{Z_{sub}-Z_{ref}}{Z_{sub}+Z_{ref}}}}{\boldsymbol{1+\frac{S_{target}}{S_{ref}}\times\frac{Z_{sub}-Z_{ref}}{Z_{sub}+Z_{ref}}}}\boldsymbol{Z_{sub}} \qquad (8)$$

2.1.3 Malignant cells

Malignant cells refer to cells that grow rapidly and uncontrollably as their genetic makeup allowed them to circumvent programmed cell death. These are the significant characteristics of cancer cells. Cancer remains a leading cause of morbidity and mortality across the globe as. Since the prognosis of most cancers is still poor, it affects the quality of life (QOL) of cancer patients(*17*). Moreover, cancer possesses several hallmarks that make treatment extremely difficult(*9*). In this study, we focus on tumor promoting inflammation as the release of pro-inflammatory cytokines will circulate within the body through blood circulation. This leads to systemic inflammation which makes metastasis happened easily.

In cases of inoperable cancers, patients often undergo aggressive treatments which may drastically impact the QOL of the patients. This is the reason chemotherapy is preferable as it is less invasive. Chemotherapy utilizes anticancer drugs to either kill the cancer cells or inhibits its proliferation. Although anticancer drugs are given with curative intent, most of them are proven to be toxic to even normal cells,

which is hazardous to cancer patients. Thus, quantitative evaluation of the effects of anticancer drugs on both normal cells and cancer cells is extremely essential.

Breast cancer

Breast cancer is the most common malignant tumor among women around the world (25.2% of the total). It can be either ductal carcinoma, which is the most common type that begins in milk duct and lobular carcinoma, which starts in lobules. Despite of being the most prevalent cancer, breast cancer has a relatively low fatality rate(*17*). This is due to the increase in awareness of the symptoms and advances in screening and treatment. The risk factors for breast cancer are age, genetic, dense breast tissue and so on. Breast cancer is staged based on the size of the tumor and whether it has spread to other parts of the body, from Stage I (often limited to within a duct and have not invades surrounding tissues) to Stage IV (the tumor is up to 5 cm across and has spread to distant organs).

The most common breast cancer screening involves mammogram, ultrasound scan and MRI scan. A mammogram is X-ray imaging commonly used in early breast cancer scan. Although it is the most common screening tool for breast cancer detection, it can sometimes produce ambiguous results. Meanwhile, ultrasound scan is used in breast cancer screening by detecting the changes of mechanical properties causes by abnormal growth. The sensitivity and specificity in detecting malignancy of breast cancer is 50% and 91.8%, respectively(*18*).

2.1.4 Cell nucleus

The nucleus is a highly specialized organelle that serves as the information processing and administrative center of the cell. This organelle has two major functions: it stores the cell's hereditary material, or DNA, and it coordinates the cell's activities, which include growth, intermediary metabolism, protein synthesis, and reproduction(*19*).

The spherical nucleus typically occupies about 10 percent of a eukaryotic cell's volume, making it one of the cell's most prominent features. A double-layered membrane, the nuclear envelope, separates the contents of the nucleus from the cellular cytoplasm. The envelope is riddled with holes called nuclear pores

that allow specific types and sizes of molecules to pass back and forth between the nucleus and the cytoplasm. It is also attached to a network of tubules and sacs, called the endoplasmic reticulum, where protein synthesis occurs, and is usually studded with ribosomes. In acoustic impedance measurement, mapping the morphological changes in cell nucleus is infeasible as it is surrounded by all these organelles. Hence, we coined the phrase nuclear complex (Figure 2.2) that describes all the organelles mentioned above as a unit of target to study the mechanical properties of the cell nucleus.

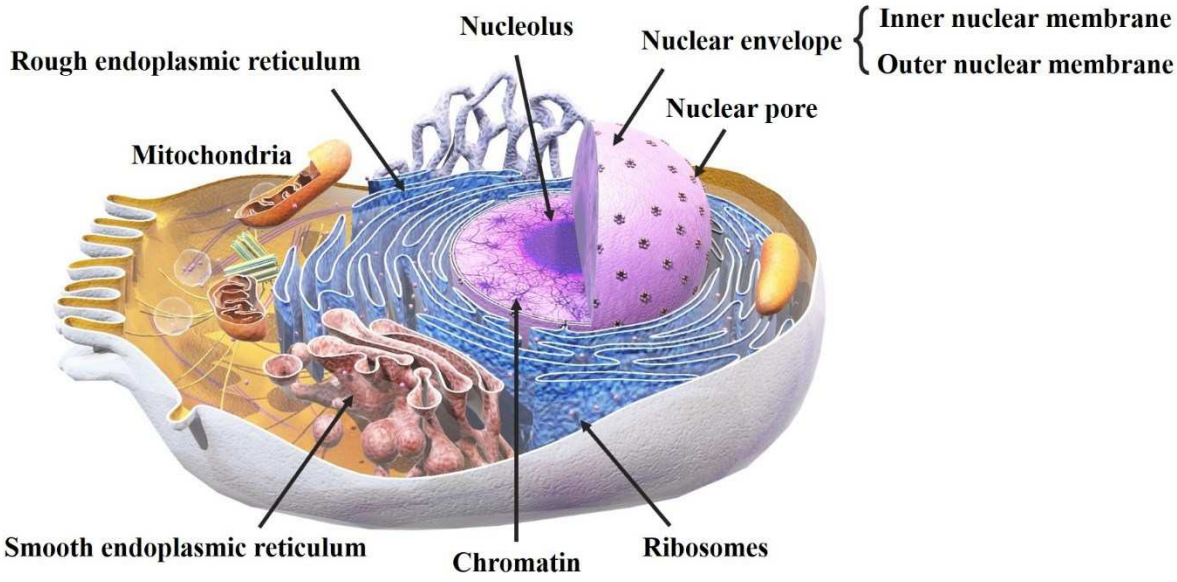

Figure 2.2 The nuclear complex(*19*)

Thus, the interaction between cell nucleus and other organelles, for example, mitochondria and microtubules play an important role in anticancer drug study. This is because stresses induced by anticancer drugs initiate cell death by perturbing cellular homeostasis. Moreover, cell nucleus contains chromatin which is deeply involved in gene expression, cell division, survival, and differentiation. In cancer cell, the chromatin often undergone post-translational modification such as DNA methylation and histone acetylation which can lead to epigenetic modifications. Inhibitors of the enzymes can reverse these modifications which often happen in cancer cell. This is known as epigenetic therapy which has been gaining more attention across the year.

DNA

DNA or deoxyribonucleic acid is the basic unit of heredity in all known forms of life. It consists of polynucleotide chains comprise of sugar phosphate backbone with four different nitrogenous bases which are adenine (A), guanine (G), thymine (T), and cytosine (C) through phosphodiester bond. Two complementary polynucleotides chains form double helix structure (Figure 2.3) by hydrogen bonds in between complementary pairs which are G-C, and A-T. The two strands of the helix are arranged in an anti-parallel manner. The upper end of one strand is labeled five prime (5'), and the lower end of the same strand is labeled three prime (3'). The upper end of the opposite strand is labeled 3', and the lower end of the same strand is labeled 5'. As a result, the 5' end of one strand matches up with the 3' end of the other strand on each end of the double helix. The distance between two base pairs is 0.34 nanometers. The length of one turn of the double-helix is 3.4 nanometers. The width of the DNA molecule is 2 nm(*20*).

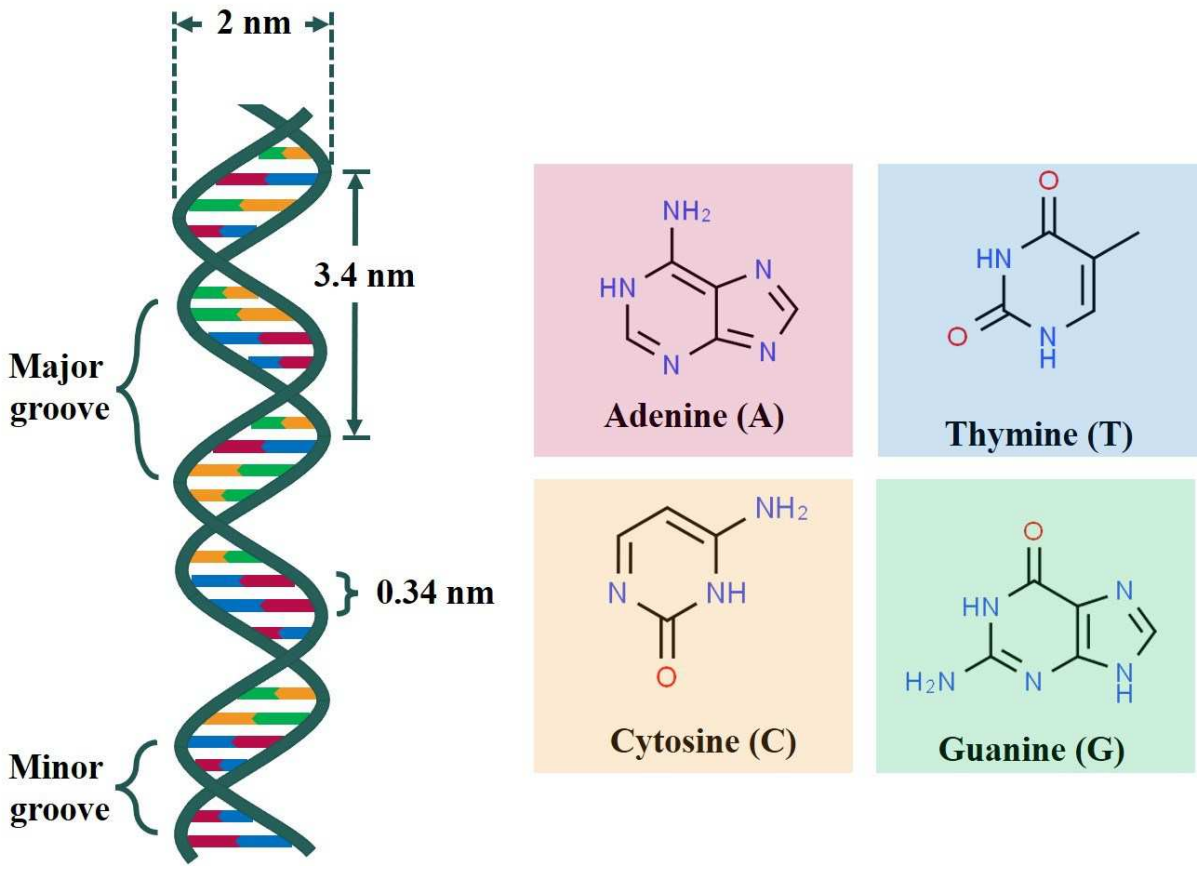

Figure 2.3 The DNA structure(*21*)

Histone and nucleosome

Histones are DNA-binding proteins found in the chromatin of all eukaryotic cells. They associate with DNA in the nucleus and help condense it into chromatin. Histones are basic proteins, and their positive charges allow them to associate with DNA, which is negatively charged. Some histones function as spools for the thread-like DNA to wrap around. Nuclear DNA does not appear in free linear strands; it is highly condensed and wrapped around histones in order to fit inside of the nucleus and take part in the formation of chromosomes. They are highly conserved and can be grouped into five major classes: H1, H2A, H2B, H3, and H4. Two each of the histones H2A, H2B, H3, and H4 come together to form a histone octamer (Figure 2.4), which binds and wraps approximately 1.7 turns of DNA, or about 146 base pairs. This structure is known as nucleosome core particle. The chain of nucleosomes is then wrapped into a 30 nm spiral called

a solenoid, where additional H1 histone proteins are associated with each nucleosome to maintain the chromosome structure(*22*, *23*).

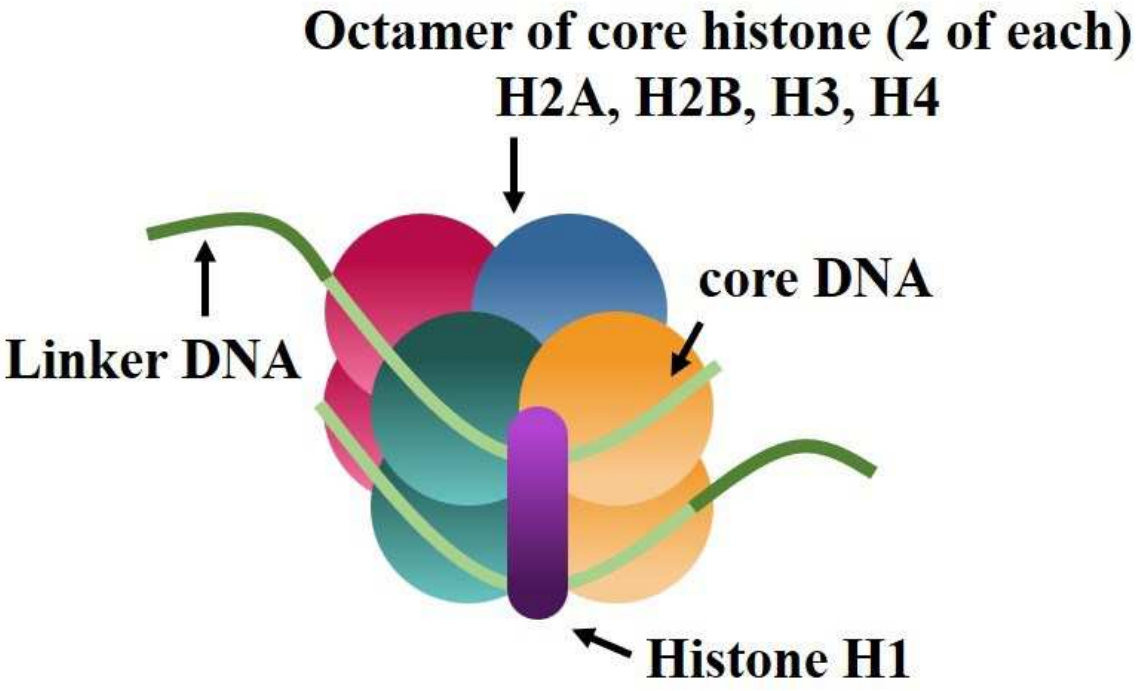

Figure 2.4 The structure of histone and nucleosome(*24*, *25*)

The histone proteins play an important role in gene regulation through post-translational modifications, such as methylation and acetylation (Figure 2.5). Acetylation of the lysine residues at the N terminus of histone proteins removes positive charges, thereby reducing the affinity between histones and DNA. This makes RNA polymerase and transcription factors easier to access the promoter region. Therefore, in most cases, histone acetylation enhances transcription while histone deacetylation represses transcription. Histone acetylation is catalyzed by histone acetyltransferases (HATs) and histone deacetylation is catalyzed by histone deacetylases (denoted by HDs or HDACs)(*26*, *27*). The process of histone acetylation is tightly involved in the regulation of many cellular processes including chromatin dynamics and transcription, gene silencing, cell cycle progression, apoptosis, differentiation, DNA replication, DNA repair, nuclear import, and neuronal repression. Meanwhile, an imbalance in the equilibrium of histone acetylation has been

associated with tumorigenesis and cancer progression. For example, HDAC inhibition displays significant effects on apoptosis, cell cycle arrest, and differentiation in cancer cells. HDAC inhibitors are currently being developed as anticancer agents(*28*, *29*).

On the other hand, histone methylation is defined as the modification of certain amino acids in a histone protein by the addition of one, two, or three methyl groups.by histone methyltransferases (HMTs). HMTs control or regulate DNA methylation through chromatin-dependent transcriptional repression or activation. In the cell nucleus, when histone methylation occurs, specific genes within the DNA complexed with the histone may be activated or silenced. either by loosening their tails, thereby allowing transcription factors and other proteins to access the DNA, or by encompassing their tails around the DNA, thereby restricting access to the DNA. This modification alters the properties of the nucleosome and affects its interactions with other proteins.

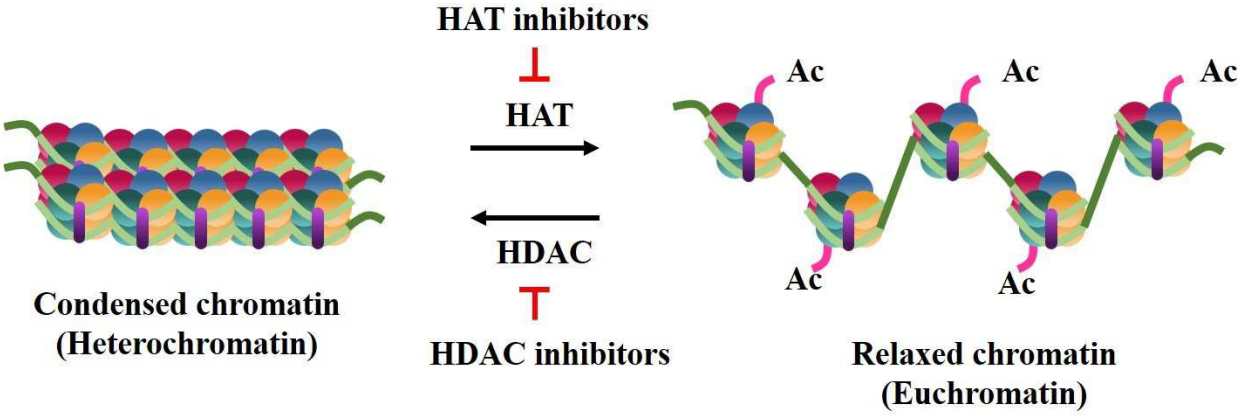

Figure 2.5 Schematic diagram depicting histone acetylation and deacetylation(*29–31*)

Chromatin

Chromatin is a complex of DNA and proteins that compress into compact unit so that it will be less voluminous and can fit within the nucleus. Chromatin exists in two forms. One form, called euchromatin, is less condensed and can be transcribed. Most chromatin remains in this relaxed form and the DNA is

exposed in euchromatin, allowing replication and DNA transcription to take place. During transcription, the DNA double helix unwinds and opens to allow the genes coding for proteins to be copied. DNA replication and transcription are needed for the cell to synthesize DNA, proteins, and organelles in preparation for cell division (mitosis or meiosis). The second form, called heterochromatin, is highly condensed and is typically not transcribed. A small percentage of chromatin exists as heterochromatin during interphase. This chromatin is tightly packed, not allowing gene transcription to take place. This structure is further categorized into facultative heterochromatin, consisting of genes that are organized as heterochromatin only in certain cell types or at certain stages of development, and constitutive heterochromatin that consists of chromosome structural components such as telomeres and centromeres. Under the microscope in its extended form, chromatin looks like beads on a string, in which the beads are called nucleosomes. During cell division, the structure of the chromatin and chromosomes are visible under a light microscope, and they change in shape as the DNA is duplicated and separated into two cells.

In eukaryotes, epigenetic modifications exert effects on the chromatin environment and gene expression, so that an ostensibly identical gene exhibits different patterns in a temporal and spatially dependent manner. Moreover, the chromatin variants with different structure, be it relaxed or compacted, are playing important roles in gene regulation. Since the acoustic properties are influenced by the hydrophobicity of the substance, it is feasible to distinguish the various structure of chromatin as mentioned previously using ultrasonic microscope. Although the cytoskeleton has the most influence on cellular acoustic impedance change through actin polymerization and depolymerization, obtaining the dynamic information on cell nucleus is equally crucial. Thus, the study of the dynamic change of these structures in cellular or genetic events might contribute new insights on how the nucleus reacts upon anticancer drugs application through ultrasonic microscope. Consequently, this may take us closer to the development of personalized medicine in treating various diseases.

2.1.5 Cell cycle synchronization by demecolcine

Different anticancer drugs work differently as they target different cell cycle phase which is vital to cell proliferation and DNA replication. Cell cycle is an event where the existing cells reproduce by duplication and division. It consists of 5 phases: the G0, G1, S, G2, and M phases (Figure 2.6). G0 is the phase where the cells have left the cycle, stopped dividing and entering differentiation. Meanwhile, G1, is when the cells increase the supply of proteins, number of organelles and grow in size. The cells then enter S phase, in which DNA synthesis commence, and the chromosome duplication occurs. After that, the cells enter G2 phase.

During this phase, the cells undergo rapid growth and protein synthesis to prepare for mitosis. This is when the microtubules reorganize to form spindle fiber. As the preparation for mitosis is completed in S phase, the cells move into M phase, in which the cells divide into two identical daughter cells. Two major events occur in this phase which are nuclear division, or mitosis, in which the duplicated chromosomes are distributed into a pair of daughter nuclei; and cytoplasmic division, or cytokinesis, when the cell splits into two identical daughter cells.

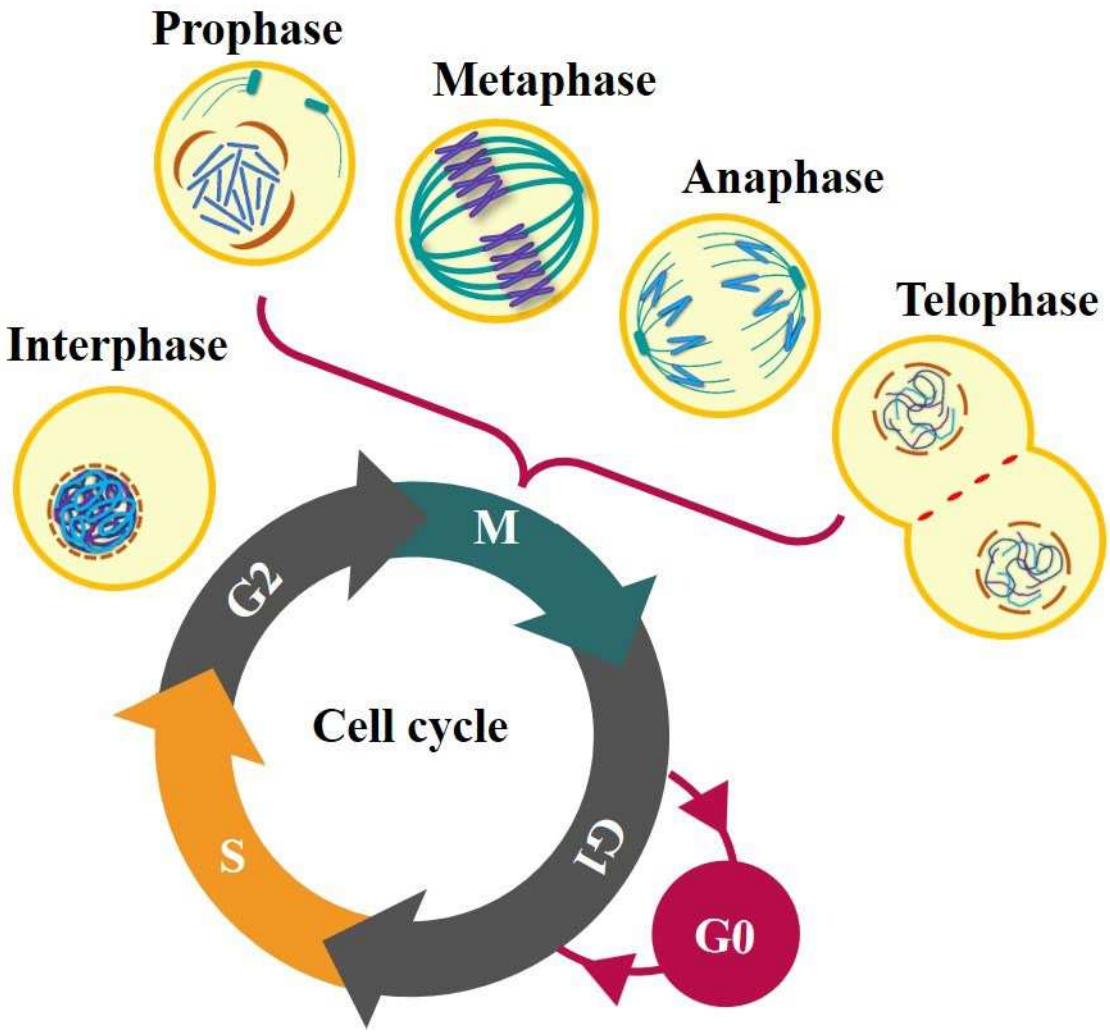

Figure 2.6 Cell transition from G2 phase to M phase(*32*, *33*)

Anticancer drugs that act during specific portion of the cell cycle are known as cell cycle specific drugs, whereas those that act on any phase, including G0 are known as cell cycle non-specific drugs. Cell cycle specific drugs mostly targets S, G2 and M phases, when DNA duplication and cell division occur as they are high in growth factors. Therefore, the cells in these phases are more susceptible to the effects of cell cycle specific drugs. On the other hand, cell cycle non-specific drugs targets both proliferating and non-proliferating cells. Hence, in chemotherapy, cell cycle specific drugs were used to arrest cancer cells in

certain phase in order to debulk the tumor and then kill the remaining cancer cells using cell cycle non-specific drugs.

However, there are still some side effects concerning the usage of anticancer drugs. First, even if the cancer cells were shrunk or reduce to harmless size, there is no guarantee recurrence and metastasis will not occur. Moreover, as most anticancer drugs targets cells that proliferate rapidly, normal cells or tissues that proliferate quickly inside our body is subjected to the effects of anticancer drugs too. For example, hair follicles and cells in digestive tract. This is the reason cancer patients undergo chemotherapy suffer from nausea, hair lose, vomiting and so on. Therefore, development of novel anticancer drugs that targets only cancer cells is essential to limit their cytotoxicity towards normal cells.

Demecolcine, also known as colcemid is an anticancer drug which is closely related into the natural alkaloid colchicine. It is commonly used in chemotherapy and research. It targets microtubules and hindered microtubules formation(*34*). It acts by two distinct mechanisms. At very low concentration it binds to microtubule plus end to suppress microtubule dynamics. Recent study has found at higher concentration colcemid can promote microtubule detachment from microtubule organizing center. Detached microtubules with unprotected minus end depolymerize with time. Cytotoxicity of the cells seems to correlate better with microtubule detachment. Lower concentration affects microtubule dynamics and cell migration. This causes inactivation of spindle fiber formation, and hence arresting cancer cells in metaphase. Therefore, it is utilized in chemo-radiotherapy by synchronizing tumor cells at metaphase which is radiosensitive stage of the cell cycle. In cancer research, it is often employed to arrest cancer cells to study the process of apoptosis and changes in nucleus.

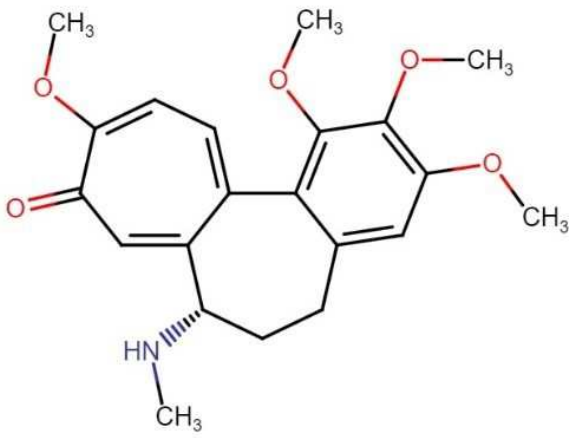

Figure 2.7 Structural formula of Demecolcine

2.2 Experimental section

2.2.1 Cell culture

Culturing cells *in vitro* enable us to administer substances that do not exist in the body into the cell to study the changes. Also, it is easier to control the cell culture than living cells or tissues *in vivo*. In recent years, there has been a great advance in cell culture technology, in which media, antibiotic and serum suitable for cell growth *in vitro* is created. Therefore, it is easier for researcher around the world to conduct physiological and pharmacological study using cell culture. In this study, C127I murine breast cancer cells were proliferated in suitable condition.

2.2.2 Sterilization

1. Autoclave

Bottle containing the prepared medium or calcium/magnesium free phosphate buffered saline solution (CMF-PBS), pipette tip, and lid of a reagent bottle were sterilized at 121℃, 2 atmospheric pressure for 20 minutes.

2. Dry heat sterilization

It is used for sterilizing glassware (dish, reagent bottle, pipette, etc.) at 110℃. for 70 minutes.

3. UV sterilization

   Clean bench and culture vessel are sterilized by direct UV irradiation.

4. Flame sterilization

   It is used for auxiliary sterilization of glassware (pipette, cap and mouth of reagent bottle, etc.) by flaming using a gas burner inside the clean bench.

5. Ethanol sterilization (70%)

   70% ethanol is Used to disinfect hands, fingers, experimental animals, surgical tweezers, scissors and knives, and clean bench before experiment.

2.2.3 C127I murine breast cancer cells culture

Immortalized C127I cell line (EC90060504-F0) is an epithelial tumor cell line derived from mouse murine mammary tumor that was purchased commercially (DS Pharma Biomedical Co. Ltd, Japan). C127I breast cancer cells were proliferated in Dulbecco's Modified Eagle Medium: Nutrient Mixture F-12 (DMEM/F12) supplemented with 10% immobilized fetal bovine serum, and 1% kanamycin (Wako Pure Chemical Industries). Thawing, subculture, cryopreservation, medium exchange and cell cycle synchronization of C127I murine breast cancer cells is as described as below:

Thawing

1. Place the vial that contains the frozen C127I murine breast cancer cells into a water bath at 30-37℃.
2. Wash the cells with 1 mL of culture medium, then centrifuge at 10,000 rpm for 30 seconds.
3. Remove the supernatant and then repeat step 2.
4. Remove the supernatant and then resuspend the cells with 1 mL of culture medium.
5. Cultivate cells accordingly.

Subculture

1. Thaw 1.5 mL of 0.25% Trypsin- Ethylenediaminetetraacetic acid (EDTA).

2. Remove all medium from canted neck flask, then add thawed 0.25% Trypsin-EDTA into the flask and wait for 1~2 minutes.
3. Add 1 mL of culture medium then harvest cell using cell scraper.
4. Transfer harvested cells into the 1.5 mL microtube, then centrifuge at 10,000 rpm for 30 seconds.
5. Remove the supernatant and then repeat step 2.
6. Remove the supernatant and then resuspend the cells with 1 mL of culture medium.
7. Cultivate cells accordingly.

Cryopreservation

1. Repeat step 1 to 4 of as described in subculture section.
2. Remove the supernatant and then resuspend the cells with 1 mL of Cell Reservoir One (Nacalai Tesque Inc) for storing.
3. Redistribute the content of step 2 into serum tube and then store the tube in medical freezer at − 80℃.

Medium exchange

In order to ensure optimal survival conditions of cell culture, medium exchange is performed accordingly. This is to reduce irritation; stress induced to the cell culture and replenish the nutrients necessary for cell proliferation. As the temperature of the incubator is different compared to the temperature of medium stock solution store in refrigerator, it is important to exchange medium in room temperature.

Cell cycle synchronization

Cell culture was subjected to cell cycle synchronization once it reached about 70% confluence. 0.05 μg/mL of Demecolcine (Fujifilm Wako, 045-18761, CAS. No 477-30-5) was used to arrest cell culture at mitotic phase (M phase) for 12 hours(*35*).

2.2.4 Culture vessels

Canted neck flask

Corning® 25 cm^2 rectangular canted neck flask (Sigma-Aldrich, 430639) is used in this research for cancer cell sub-culture. This is because the big surface area is suitable for cancer cell growth. In addition, it is user friendly in terms of pipette operation and cell harvest. Furthermore, the lid is a double seal cap (made of high-density polyethylene) and it is structured to seal at both end (the inner circumference and the end of the mouth). Therefore, there is little risk of microbial infection and contamination during experiment and observation.

In this study, subculture of cancer cells was carried out using this culture vessel to obtain large quantity of cells for cryopreservation and experiment.

PS film dish

A new dish type culture vessel is currently developed by Honda electric Co. Ltd. for better acoustic impedance measurement of cultured cell, which is named PS film dish (HPS-3505L, Figure 2.8). PS is the abbreviation for polystyrene, which is the main component of the film used in this culture vessel. It is designed with film thickness of 50 μm and film surface area of 3.2 cm^2. The dish shape design is desirable as it is easier to handle both cell culture from above and acoustic impedance measurement from below the film. It is suitable for confocal microscopy too as the film is even in design. As for ultrasonic microscopy, it can handle both low and high frequency ultrasonic waves although there are some technicalities that need improvement. Overall, it satisfied our needs in this research, both in confocal microscopy and ultrasonic microscopy as most commercially available culture vessel is unsuitable for ultrasonic microscopy.

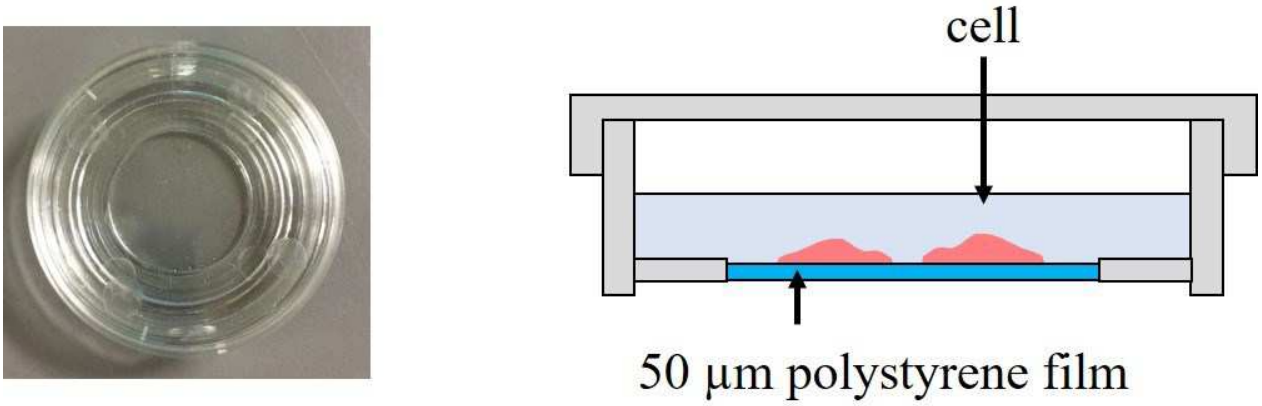

Figure 2.8 PS film dish used for acoustic impedance measurement, left: film dish; right: schematic diagram depicting cell culture using PS film dish

2.2.5 Cell observation

Acoustic impedance measurement

SAM used in this study employed the measurement system described previously(*16*, *36–42*). The images generated for one observation consists of 200 × 200 points (x- and y- resolution), waveform size (t-resolution) 200 samples, sampling with an interval of 125 ps. The specimen was subjected to 8 times of waveform acquisition for noise reduction by averaging(*43*).

The transducer consists of a flat zinc oxide, ZnO as piezoelectric material attached with a sapphire lens of (assumed uniform) half curvature of 60°. Its aperture diameter and focal length (from the bottom of the lens) were 0.43 mm and 0.29 mm, respectively. The central frequency of the transducer was designed as 320 MHz Acoustic pulse wave spreading 200 - 400 MHz was focused on the interface between the cell and the substrate and sent through the substrate. The acoustic wave transmitted and received by the same transducer, was focused on the interface between the substrate and specimen. PS film containing cultured cells in the was placed above the transducer, which mechanically scanned the specimen by attaching it with a stage driver while maintaining the focal point on the rear surface of the film. The reflection from the surface was subsequently interpreted into a two-dimensional profile of reflection intensity(*44–48*). All the

measurements were performed at room temperature. In this research, cell culture was subjected to acoustic impedance measurement by ultrasonic microscope upon anticancer drug application. This is to visualize and evaluate the intercellular dynamics, and hence draw comparison with optical microscopy and confocal microscopy to better understand anticancer drugs in action to eliminate cancer cells.

2.2.6 Immunocytochemistry

Cell fixation

The reason cells must be fixed prior to immunostaining is to permeabilize cells to allow antibodies to access intracellular structures. Without fixation, the structures in cells would fall apart and diffuse away before antibody incubations and wash steps. The mechanism of fixation is dependent on the reagent used. Alcohol based fixations dehydrate cells/tissues, causing proteins to denature and precipitate in situ. Paraformaldehyde causes covalent cross-links between molecules, effectively gluing them together into an insoluble meshwork. In this study, we used 4% paraformaldehyde (Nacalai Tesque, Inc.) to fix our cells before immunostaining and the procedure are described as below:

1. Remove all the medium inside the culture vessel.
2. Add 2 mL of 4% paraformaldehyde into the culture vessel containing cells and wait for 20 minutes.
3. Remove all paraformaldehyde, then add 2 mL of PBS into the culture vessel.
4. After 5 minutes, repeat step 3 twice
5. Remove all PBS, then preserve the cell by adding 2 mL of 0.02% sodium azide solution into the culture vessel.
6. Seal the culture vessel accordingly before storing them inside refrigerator.

Immunostaining

Immunostaining is a method of morphologically detecting a specific molecule (antigen) existed in a tissue or a cell to observe its localization by utilizing a specific binding reaction called an antigen-antibody reaction (Figure 2.9). A good antibody should possess high potency and specificity, while a good antigen should be able to retain its binding to the tissue or cells during and after sample preparation.

In this experiment, we stained mitochondria by incubating living cells with MitoTracker™ Orange CMTMRos (0.5 μM, Invitrogen M7510). The fixed cells were then permeabilized with 0.1% Triton X 100/PBS and incubated for 60 minutes in blocking solution containing 5% goat serum. Permeabilized cells were then incubated overnight in primary antibody solutions. After PBS wash, the samples were incubated overnight again with fluorescence-conjugated secondary antibody solutions. The composition of all antibody solutions was shown in Table 2.1 and Table 2.2. Lastly, all sample were incubated with PBS diluted 4,6-diamidino-2-phenylindole dihydrochloride, DAPI (1:1000, Wako Pure Chemical Industries 340-07971).

Table 2.1 Composition of primary antibody solutions

Target	Primary Antibody	Ratio to blocking solution
Nuclear envelope	rabbit anti Lamin A/C (Abcam EPR4068)	1:100
Actin filament	mouse anti Actin (Invitrogen PA5-27863)	1:1000
Phosphorylated histone	rabbit anti PhH3S10 (Cell Signaling Technology #9701)	1:2000

Table 2.2 Composition of secondary antibodies

Fluorescent- labeled antibody	Ratio to blocking solution
Alexa-Fluor-488-conjugated goat anti-mouse IgG (Invitrogen A-11005)	1:1000
FITC-conjugated goat anti-rabbit IgG (Proteintech SA00003-2)	1:1000
Texas Red-conjugated goat anti-rabbit IgG (Thermo Fisher T2767)	1:1000

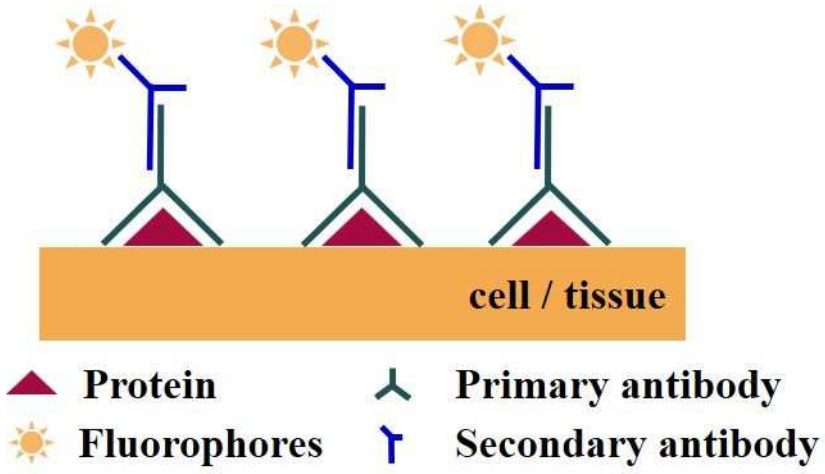

Figure 2.9 Schematic diagram depicting antigen-antibody reaction in immunostaining

Confocal microscopy

Nikon confocal laser microscope A1 is used for fluorescence imaging of sample undergone immunostaining. An optical disc (slit disc) with a lattice-shaped slit was placed at a position conjugate to the focal point of the objective lens, and excitation light was irradiated to the sample through the slit. Fluorescence from the sample passes through the slit again and is imaged by the CCD camera. The light from the focal plane of the specimen passes through the slit, and hence, confocal image without blurred image is obtained. Fluorescent images were captured with an objective lens with 20× magnification, scan size = 2048, scan speed = 0.125, with 8 times image acquisition for clearer image by averaging. For DAPI imaging, fluorescence wavelength = 410 nm, excitation wavelength = 403.2 nm; for lamin A/C and actin imaging, fluorescence wavelength = 488 nm excitation wavelength = 486.8 nm; for PhH3S10 and mitotracker imaging, fluorescence wavelength = 561 nm excitation wavelength = 561.5 nm. The images obtained from confocal microscopy were processed with an open-source image processing software, Fiji (*49*).

2.2.7 Statistical analysis

The data were reported as mean ± standard error of mean (SEM). Dunnett's test was performed to estimate the significance of the result. Data were reported as statistically significance when $p < 0.05$.

2.3 Results and Discussion

C127I cells were mapped using SAM once the cell culture was confluent, and the result of the observation was shown in Figure 2.10. Cells arrested in different mitotic phases such as prometaphase, anaphase, and telophase were successfully captured. Further, as described previously, the changes observed from SAM acquisition reflect the changes in cell elasticity. The strength of the cytoskeleton is strongly associated with the cell elasticity, and hence, higher acoustic impedance region surrounding the cell (high Z ring). A lower acoustic region within the cells (low Z ring) recorded implied that it was cell nucleus, as the description of cell nucleus during mitosis was consistent with our result.

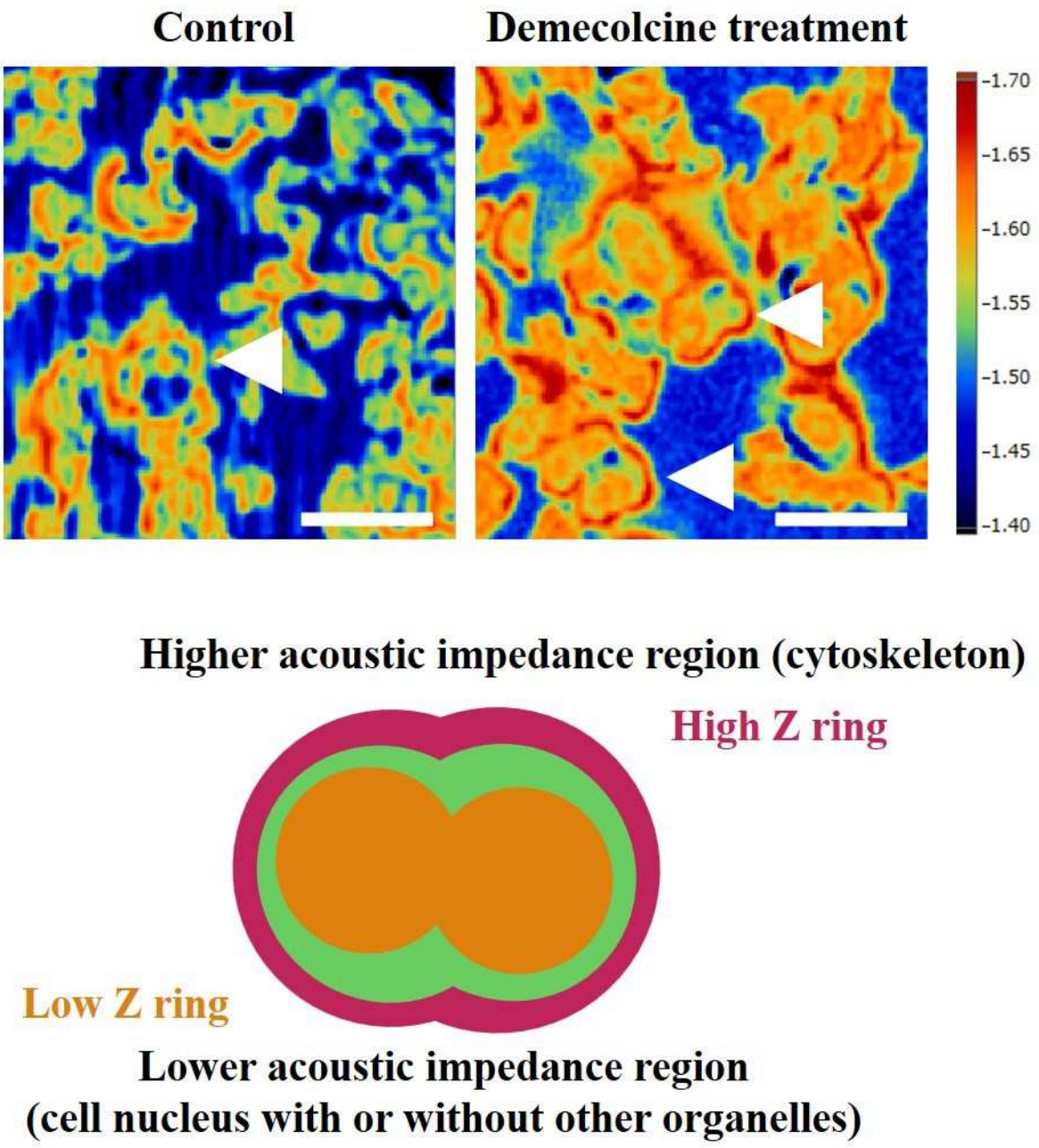

Figure 2.10 Cell morphology of C127I cell culture treated with demecolcine., top: acoustic impedance profile of C127I cells; bottom: schematic diagram depicting C127I cell arrested in mitotic phase that had different acoustic impedance region which resembled multiple cell organelles disintegration/distribution when cell cycle progress from G2 phase to M phase

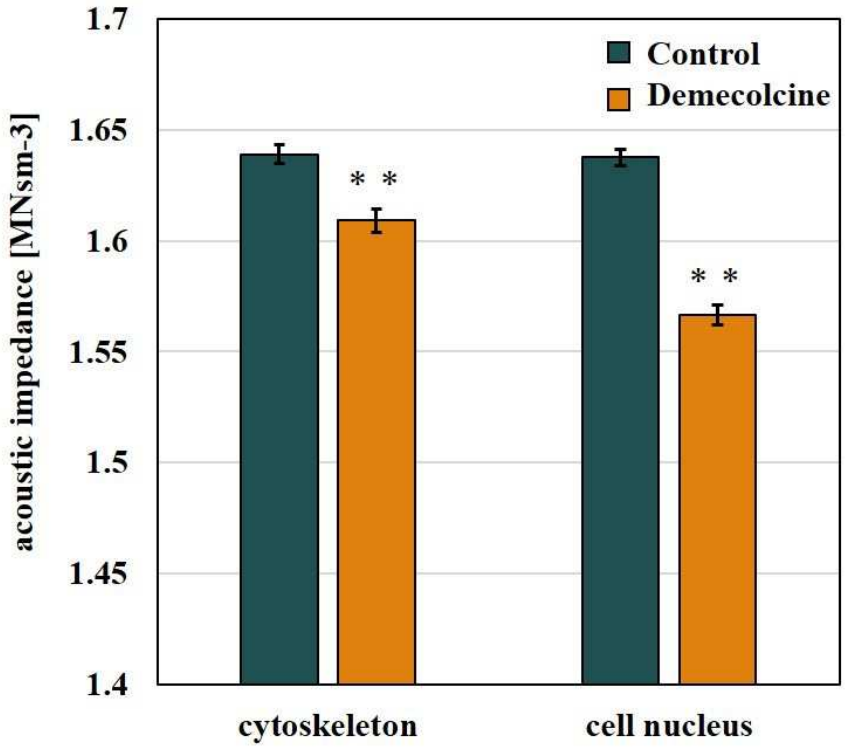

Figure 2.11 The difference of the acoustic impedance of cytoskeleton and cell nucleus with or without demecolcine treatment. Scale bar = 100 μm. Each bar represents mean ± SEM and the significant value was estimated by Student's *t*-test (n = 10 for each sample, ∗∗ $p < 0.01$ compared to control group)

A cell that entered mitosis will enlarge in size as the genetic material doubles to prepare the cell in splitting into two daughter cells. The cell nucleus and the nuclear envelope break down to allow the chromosomes to gather around the midline during metaphase. The spindle fibers then pulled the chromatid pairs that queued along the midline into the opposite end of the cells. These dynamic changes were successfully recorded, as shown in Figure 2.12. This result is confirmed by immunocytochemical analysis, by immunostained the cell nucleus with DAPI and the actin filament with actin. Although the morphology of the cells observed under confocal laser microscopy resembles the one obtained from acoustic impedance measurement, the result is not conclusive. Therefore, immunostaining the cells with different protein marker is carried out.

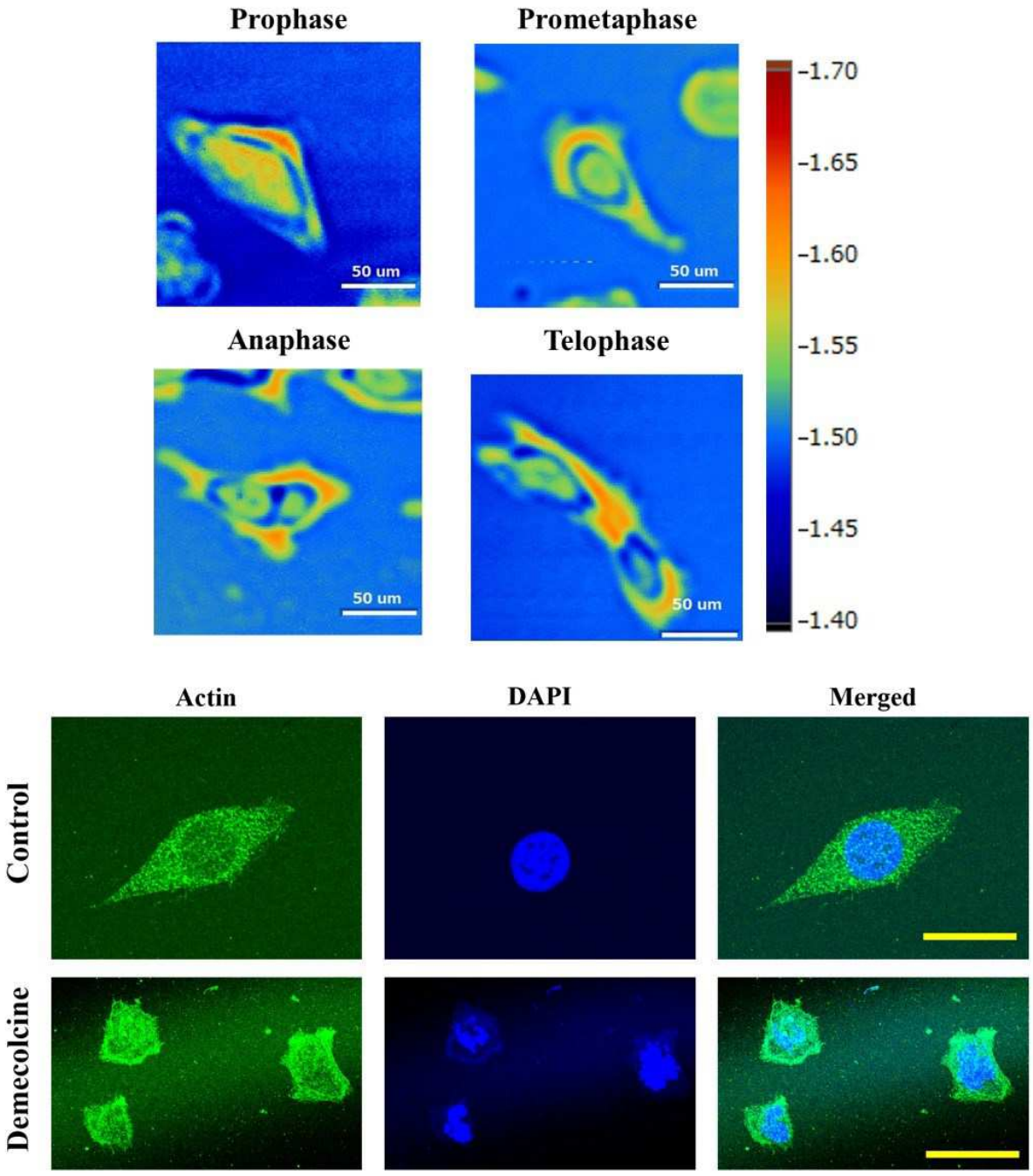

Figure 2.12 Cell arrested in mitotic phase by demecolcine treatment, top: acoustic impedance profile; bottom: confocal microscopy image (green: actin filament; blue: cell nucleus)

As mitosis progress, the chromosomes decondensed, the spindle fibers dissociated, and then the nuclear membrane and cell nucleus started to reform. Also, it is clearly illustrated this alteration as two lower acoustic regions were formed within the cytoskeleton. This phase is known as telophase, and the cell will undergo cytokinesis as it splits into two identical daughter cells. Immunocytochemical analyses were carried out to confirm the result obtained from SAM acquisition. In this study, phosphor-histone H3 (Ser10) or PhH3S10 was used to trace the mitotic phase. Phosphorylation of histone is known to occur during mitosis as the chromatin is condensed. Therefore, the expression of PhH3S10 helps us pinpoint at which stage the cell is during mitosis. The expression of PhH3S10 is obvious in anaphase as the chromatin condensed to allow the splitting (Figure 2.13). This result is consistent with previous reports(*50*, *51*). Moreover, PhH3S10 expression is evident in anaphase and telophase as the cell is coming close to the end of mitosis. This suggested that PhH3S10 plays an important role in initiating the condensation and decondensation of chromatin during mitosis, making it a suitable marker.

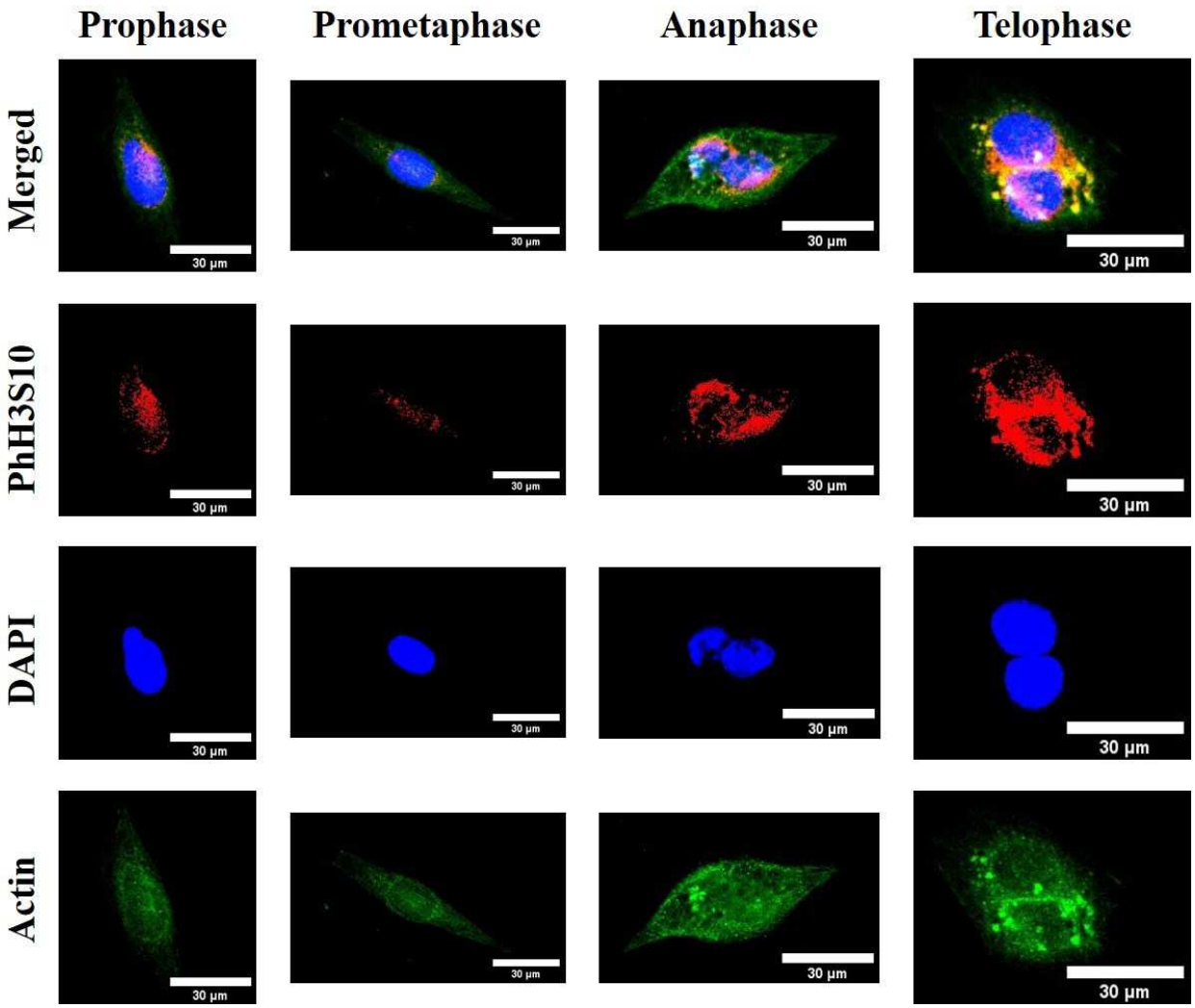

Figure 2.13 Immunocytochemical staining of cell in different mitotic phase (red: phosphorylated histone; blue: cell nucleus; green: actin filament)

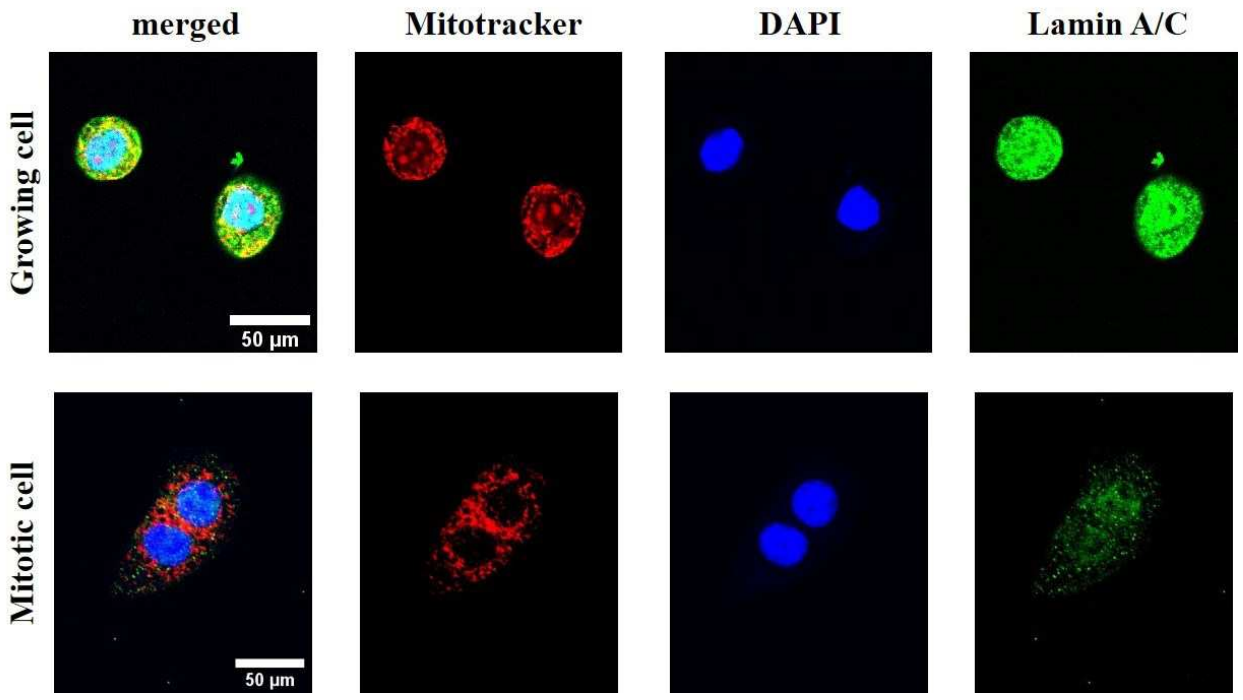

Figure 2.14 Immunocytochemical staining of cell arrested in mitotic phase by demecolcine treatment (red: mitochondria; blue: DAPI; green: nuclear envelope)

Immunocytochemical analyses on other organelles were carried out to further investigate the low Z ring observed before. Considering the size of nucleus, it is safe to assume that low Z ring is the cell nucleus. However, one of the hallmarks of cancer cells is housing enlarged cell nucleus, and sometimes multiple nuclei as they proliferate uncontrollably. Therefore, it is important to determine the exact acoustic impedance value of the cell nucleus. Mitchondria (mitotracker) and nuclear envelope (lamin A/C) were the targets here as the dynamical changes of these organelles are guaranteed as mitosis take place. As shown in Figure 2.14, mitochondria dispersed around the nucleus once the cell was arrested in mitotic phase. On the other hand, nuclear envelope disintegrated to allow the condensation of chromatin once the cell entered metaphase. These changes might disturb the living measurement of the low Z ring, so the area occupied by this low Z ring, roundness and circularity from both acoustic impedance profile and confocal laser microscopy images were analyzed using Fiji. The result is shown in Table 2.3, and this suggest that there is

a slight difference, in which low Z ring acquired by SAM are larger and rounder. Hence, the low Z ring might consist organelles other than cell nucleus.

Table 2.3 Comparison of the area circularity and roundness of the nucleus observed in SAM and confocal laser microscopy. Data were reported as mean ± standard deviation (n = 10 samples each)

SAM	Observation method	Confocal laser microscopy
296.52 ± 55.71	Area (μm^2)	117.77 ± 40.09
0.83 ± 0.09	Circularity	0.67 ± 0.23
0.72 ± 0.15	Roundness	0.76 ± 0.13

2.4 Summary

First, quantitative analysis is feasible to evaluate the cellular dynamic change arrested in different mitotic phase using SAM. This will provide us with more information going forward in developing a powerful observational tool. However, mitosis occur in normal healthy cells too, and hence, labelling the cells for observation is essential to distinguish the differences that might arise during acoustic impedance measurement. The result also showed that other organelles exist in the perinuclear region, making it challenging to determine the exact acoustic impedance of cell nucleus. Further development in analysis and methodology is necessary to counter this problem in order to provide a clearer and cleaner image after data acquisition. Moreover, labelling the cell within the culture vessel is also important, so that comparison of same, exact targeted cells is feasible for confirmation. Taken together, SAM has the potential to bridge current approaches in cellular study to translational research.

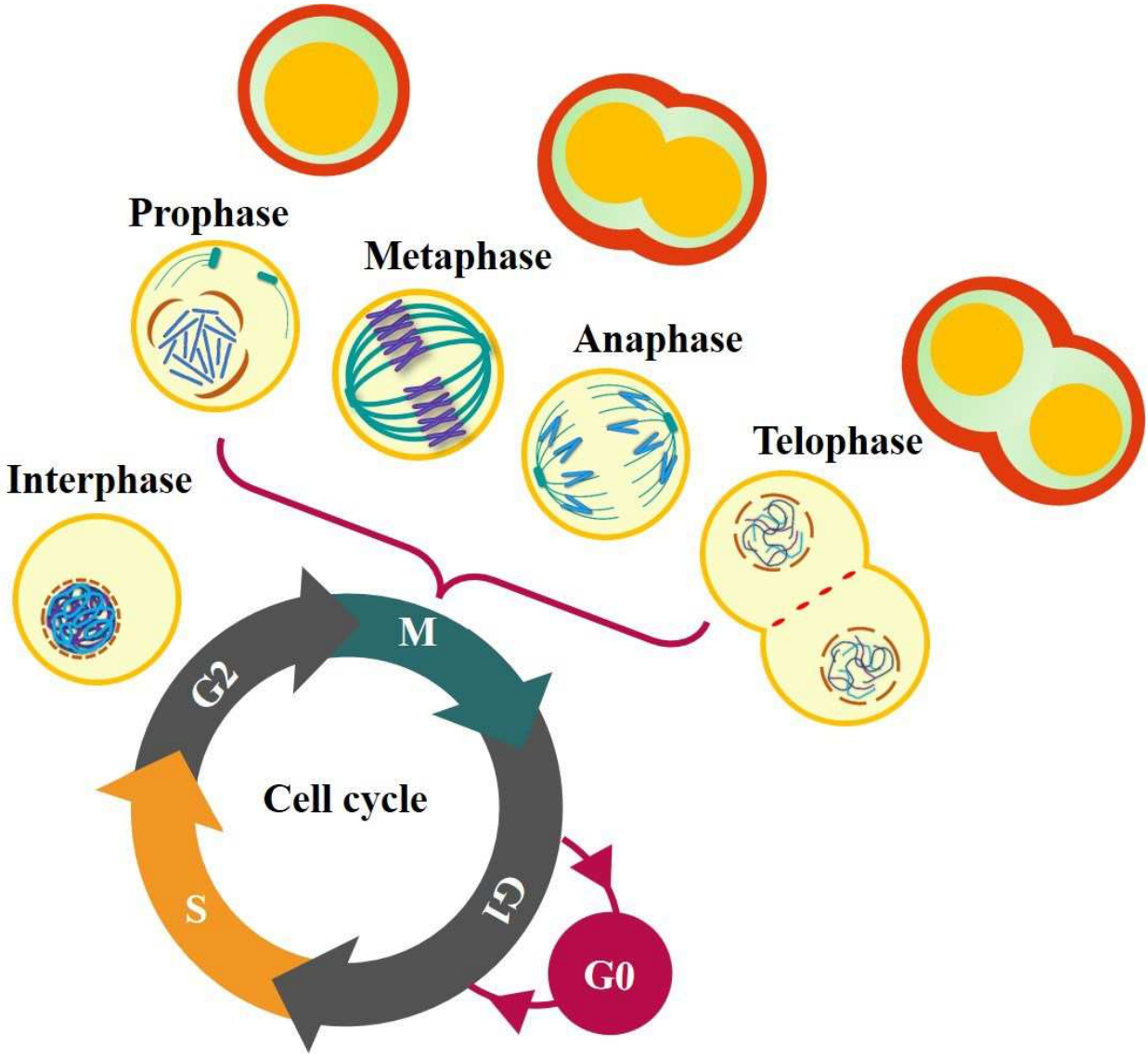

Figure 2.15 Cell morphological changes of C127I cells in different mitotic phases. Similarities in cellular observation were confirmed between the general depiction of mitosis and the acoustic impedance profiles using SAM(*39*)

Chapter 3 Gut-Brain Axis: Alteration of Gut Microbiota of Throughout the Pregnancy and Its Effect on the Offspring

3.1 Introduction

This chapter will discuss the potential causes and effects of systemic inflammation through pesticide exposure via gut-brain axis. Gut-brain axis suggested that the brain and the gut are in a bidirectional relationship that affect each other via various routes. One of the feasible factors is through the metabolites produced by the gut bacteria. The changes of the gut microbiota and metabolites are indicative of inflammation-mediated alteration. In this chapter, investigation of the active ingredient of commercial herbicides, Roundup®, which is GP, on the pregnant rat model is employed to evaluate the alterations happened in the gut flora. DNA sequencing and bioinformatics were employed in order to elucidate the possible mechanism behind the systemic inflammation caused by prenatal chemical exposure and how it affected the offspring. The result confirmed that disrupted gut microbiota and metabolites production in male offspring born from dam that was prenatally exposed to GP. These changes pointed towards systemic inflammation as the major propagator that might further irritate the symptoms.

3.1.1 About glyphosate

The Organization for Economic Co-operation and Development (OECD) has been attempting to standardize tests on the effects of chemical substances in the environment and food on the body. In recent years, it has been suggested that some of the substances conventionally classified as N substances may have developmental toxicity and induce higher brain dysfunction such as depression and autism. In recent years, however, it has been suggested that some of the substances conventionally regarded as N-substances have developmental toxicity and may induce higher brain dysfunction such as depression and autism.

GP (N-phosphonomethylglycine) is the main ingredient of the herbicide Roundup® developed by Monsanto in 1970, registered by the U.S. Environmental Protection Agency (EPA) in 1974, and is an N substance in the OECD test guidelines (Figure 3.1)(*52*). As an herbicide, it inhibits 5-enolpyruvylshikimate-3-phosphate synthase (EPSPS) in the shikimic acid pathway, which synthesizes aromatic amino acids in plants (Figure 3.2). It is also metabolized to AMPA in the soil(*53*). The shikimic acid pathway is found in microorganisms and plants, but is thought to have no effect on the human body because it is a metabolic pathway not found in animals. The NOAEL for the developing nervous system is 1000 mg/kg for rats and 100 mg/kg for humans(*54*). On the other hand, the apparent half-life of GP is estimated to be 3.1 hours in humans (NOAEL)(*55*) and 14.38 hours in rats (NOAEL)(*56*), and it is thought to be almost completely eliminated via the renal pathway.

However, since the shikimic acid pathway is not present in animals, it has been reported that prenatal exposure to GP induces neurobehavioral abnormalities and autism(*57*, *58*). In this laboratory, we have reported that prenatal GP exposure induces developmental neurotoxicity, behavioral abnormalities, and intestinal bacterial abnormalities. In this study, we observed changes in the cerebellum caused by exposure to low concentrations of GP or its metabolite, aminomethyl-phosphonic acid (AMPA), during fetal life, and investigated the effects of GP exposure on developmental neurotoxicity due to chemical effects(*57*, *58*). Developmental neurotoxicity is a widely known concept, but in developmental disorders, there may be disorders caused by neural changes that do not fit into the conventional toxicity concept. However, in developmental disorders, there are disorders caused by neural changes that do not fit into the conventional concept of toxicity, and we have clarified the effects and mechanisms of developmental neurotoxicity.

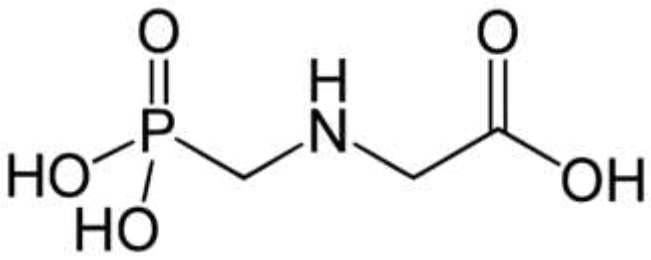

Figure 3.1 Structural formula of GP

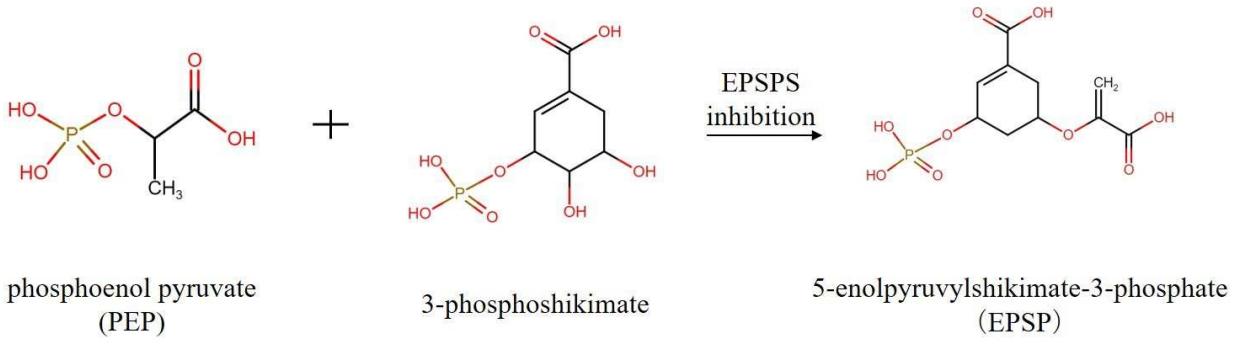

Figure 3.2 Mechanism of action of GP

There are two pathways of GP degradation by plants and microorganisms: the pathway that forms sarcosine and glycine intermediates, and the pathway that forms AMPA (Figure 3.3)(*59*). In the pathway to form sarcosine and glycine intermediates, the C-P bond is cleaved by C-P lyase to produce phosphate and sarcosine. Next, sarcosine is degraded by sarcosine oxidase to glycine and formaldehyde. Formaldehyde enters the pathway induced by tetrahydrofolate, and glycine is metabolized by the standard pathway. Finally, it is degraded to CO_2 and NH_3.

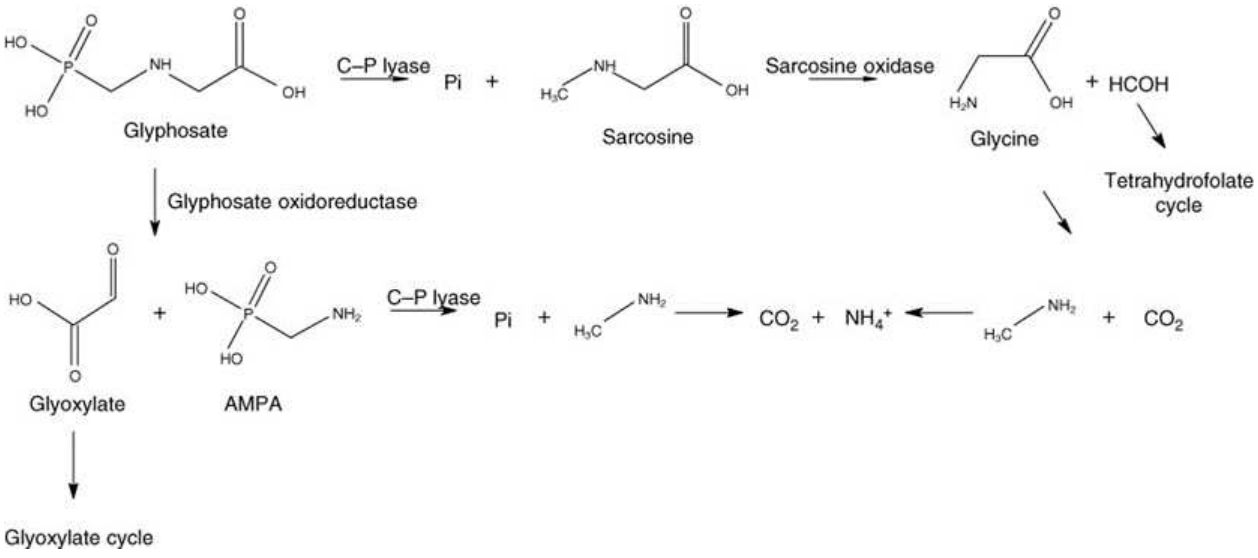

Figure 3.3 Degradation of GP by microorganisms

On the other hand, in the AMPA formation pathway, AMPA and glyoxylic acid are generated by the cleavage of C-P bonds by glyphosate oxidoreductase. Next, glyoxylate is further metabolized by breaking the glyoxylate circuit, and AMPA is cleaved by the enzyme C-P lyase to produce inorganic phosphate and methylamine. Finally, it is decomposed into CO_2 and NH_3.

3.1.2 Gut-brain axis

Gut flora is the complex community of microorganisms that live in our digestive tracts. It not only plays important roles in digestion, immune responses and diseases and also contributes to modulate the cross communication in between the gut and the brain, known as gut-brain axis. It has been reported that the brain and gastrointestinal system are closely related via the autonomic nervous system, vagus nerve and humoral factors such as hormones and cytokines(*60–66*).

Gut microbiota, as the name implies, are bacteria that are resident in the intestines of living organisms, and there are more than 1000 types and 100 trillion bacteria in the human intestine. Gut microbiota is roughly divided into three types: (a) good bacteria, which are responsible in maintaining the homeostasis in the gut, helping in the digestions and synthesizing vitamins such as niacin and folic acid; (b) bad bacteria, which are mainly pathogens that disrupt the gut environment, producing endotoxin, causing inflammation that might increase permeability of the intestines; (c) opportunistic bacteria, which are resident gut microbes that occupied most of the gastrointestinal system remained neutral unless there is a perturbations in the gut that shift them into helping bad bacteria. The composition of the gut microbiota varies in individual depends on the races, diet and country of residence. It has also been reported that although the number of bacteria varies with age, the type of bacteria hardly changes throughout life. Over 99% of the intestinal bacteria consists of the following phyla: Firmicutes, Bacteroidetes, Proteobacteria, and Actinobacteria(*61–63*, *65*).

Gut-brain axis is gaining a lot of attention in recent years, as its relevance to disease is greatly investigated. There are several factors that can affect the gut-brain axis, for example tobacco,

chemical exposure, diet, substance abuse and so on. These factors are well studied over the years but how they come in play with the gut microbiota remained unclear. This is because the huge number of different types of bacteria resided in our gut make it hard to pinpoint the causes that are observed in the studies. However, advancement in the genome sequencing technique improved the precision and accuracy in profiling the gut microbiota. This is known as taxonomic profiling, which allow us study the change in the trend of the microbiota composition under different circumstances. The relationship between diseases such as type II diabetes, Parkinson's disease, autism spectrum disorder and gut microbiota are well studied and the results are fascinating. This is because alterations of gut microbiota over time is indicative of disease manifestation. These alterations are usually mediated through inflammation that occurred in the gastrointestinal tracts.

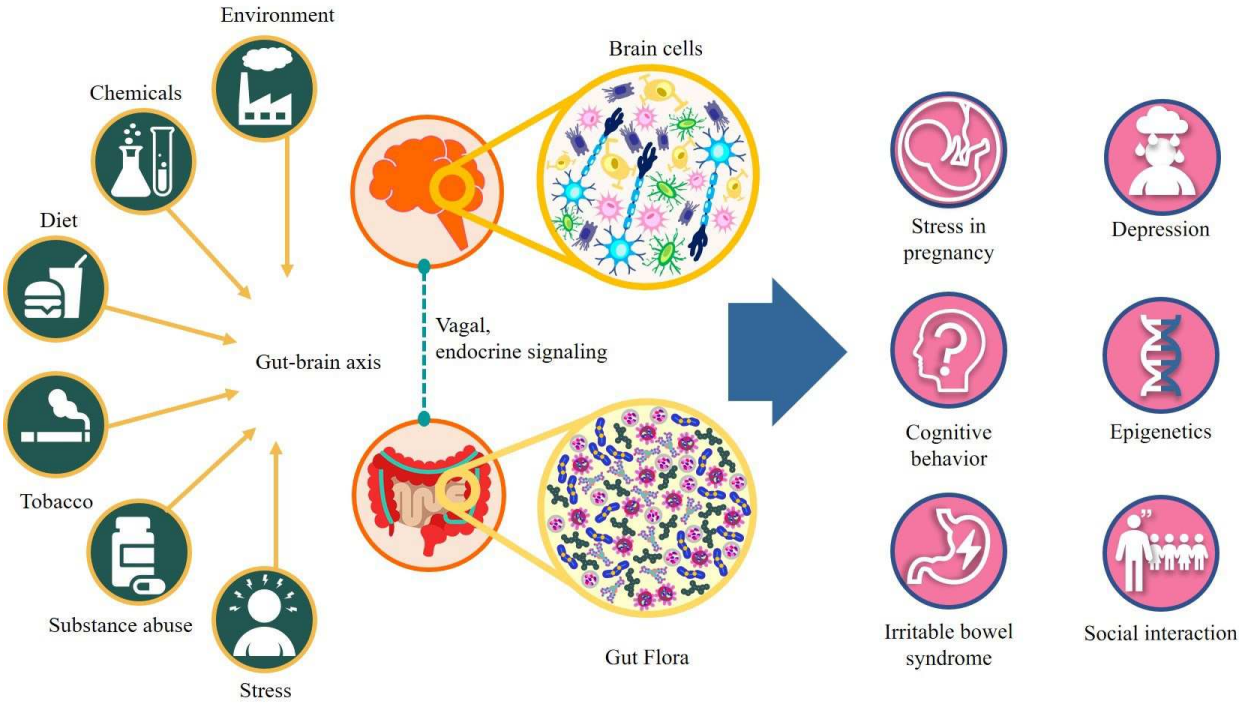

Figure 3.4 Gut-brain axis: what could affect this bidirectional relationship and the possible outcomes that come with it(*61*, *62*, *66*)

3.1.3 Metabolites

Short-chain fatty acids (SCFA) are indigestible components of fermented products in the large intestine. Common SCFAs are acetic acid, propionic acid and butyric acid. Butyric acid, acetic acid and propionic acid are metabolized and utilized in the liver and muscle, and butyric acid is used as an energy source for colonic epithelial cells.

Some of the SCFA are consumed by the epithelial cells of the anterior stomach and large intestine, while the rest reach the liver via the portal vein and are used as substrates for fat synthesis. The rest is used as an energy source for cells throughout the body and as a substrate for fat synthesis. SCFA are important energy nutrients that cover 80% of basal metabolism in ruminants and, in some cases, 20% or more in humans. It is characterized by its ability to be taken up by cells without depending on insulin action and to cross the blood-brain barrier. Lactic acid and succinic acid are hardly absorbed and do not serve as an energy source for epithelial cells.

3.2 Experimental section

3.2.1 Animal preparation

Animal experiments were carried out in accordance of the protocol approved by the committee for the use of animals in Toyohashi University of Technology. The Wistar rats used in this study were obtained from Japan SLC, Inc. In-house breeding was carried out once the rats were sexually matured (12 weeks old). The pregnant dam was isolated from then buck after mating and confirming plaque. They were kept in the same cage with their pups until weaning. The temperature of the animal facility was kept at 23 ± 3°C and at 40-60% relative humidity with 12 hours light/dark cycle.

Pregnant dam was subjected to acute exposure with 250 mg/kg body weight (GPa) on E16. For chronic exposure (GPc), 15.625 mg/kg/day was administrated by oral gavage to the pregnant dam for 16 days, starting from E5 until E20. The control animals were prepared by oral gavage of phosphate-buffered

saline, 1× PBS diluted from 10× PBS. The concentration of GP used in this study was based on the reported toxic effect on the neurobehavioral function of F1 offspring upon acute prenatal exposure to 250 or 500 mg/kg/day (*67*). Moreover, the dose of GP used in this study is lower than the No Observed Adverse Effective Levels (NOAEL) established by the Food Safety Commission of Japan in 2016 based on the developmental toxicity study (1000 mg/kg body weight/day).

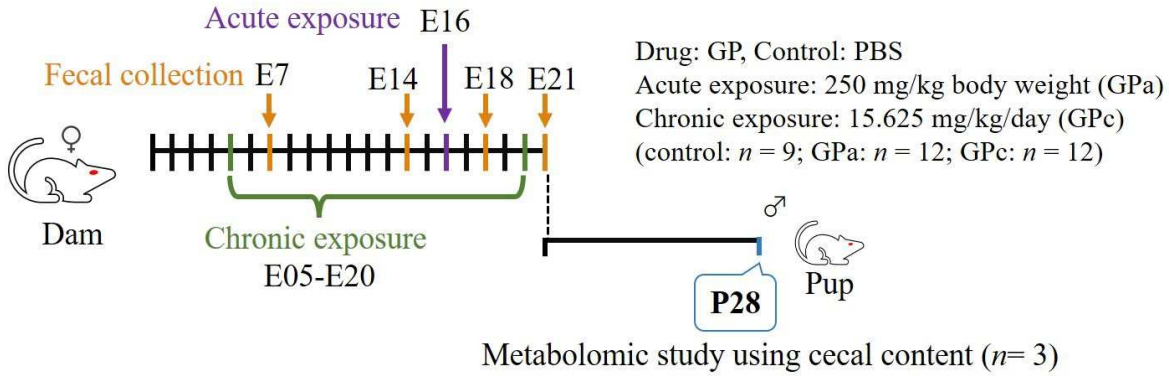

Figure 3.5 The study design to assess the alteration of gut microbiome of both dam and F1 male offspring and metabolomic changes in F1 male offspring

3.2.2 Fecal sampling

Rat feces were collected as depicted in the timeline as shown in Figure 3.3. The animals were isolated from their cage in order to avoid contamination during collection. All samples were collected using autoclaved toothpicks, put in microtube and stored at −20 °C before DNA extraction.

3.2.3 Fecal DNA extraction

Rat fecal DNA was extracted using the QIAmp DNA stool Mini Kit following the protocol from the manufacturer (Qiagen). The brief description was listed below.

1. Weigh 180-220 mg stool in a 2 mL microcentrifuge tube and place tube on ice.
2. Add 1 mL InhibitEX Buffer to each stool sample. Vortex continuously for 1 min or until the stool sample is thoroughly homogenized.
3. Heat the suspension for 5 min at 90°C. Vortex for 15 sec.

4. Centrifuge sample for 1 min to pellet stool particles.
5. Pipet 15 µL Proteinase K into a new 1.5 mL microcentrifuge tube.
6. Pipet 200 µL supernatant from step 4 into the 1.5 mL microcentrifuge tube containing Proteinase K.
7. Add 200 µL Buffer AL and vortex for 15 sec.
8. Incubate at 70°C for 10 min.
9. Add 200 µL of ethanol (96–100%) to the lysate, and mix by vortexing.
10. Carefully apply 600 µL lysate from step 9 to the QIAamp spin column. Close the cap and centrifuge for 1 min. Place the QIAamp spin column in a new 2 mL collection tube, and discard the tube containing the filtrate.
11. Carefully open the QIAamp spin column and add 500 µL Buffer AW1. Centrifuge for 1 min. Place the QIAamp spin column in a new 2 mL collection tube, and discard the collection tube containing the filtrate.
12. Carefully open the QIAamp spin column and add 500 µL Buffer AW2. Centrifuge for 3 min. Discard the collection tube containing the filtrate.
13. Place the QIAamp spin column in a new 2 mL collection tube and discard the old collection tube with the filtrate. Centrifuge for 3 min.
14. Transfer the QIAamp spin column into a new, labeled 1.5 mL microcentrifuge tube and pipet 200 µL Buffer ATE directly onto the QIAamp membrane. Incubate for 1 min at room temperature, then centrifuge for 1 min to elute DNA.

3.2.4 PCR

Amplicon PCR

Amplicon PCR was carried out following the parameter listed in the tables below.

Table 3.1 Composition of reagents used in amplicon PCR

Microbial genomic DNA (5 ng/μL in 10 mM Tris pH 8.5)	2.5 μL
Amplicon PCR Forward Primer 515F with MiSeq tail (1μM) 5`-TCGTCGGCAGCGTCAGATGTGTATAAGAGACAGGTGCCAGCMGCCGCGGTAA	5 μL
Amplicon PCR Reverse Primer 806R with MiSeq tail (1μM) 5`-GTCTCGTGGGCTCGGAGATGTGTATAAGAGACAGGGACTACHVGGGTWTCTAAT	5 μL
DNA polymerase, 2x KAPA HiFi HS ReadyMix (Nippons Genetics KK2602)	12.5 μL
Total	25 μL

Table 3.2 Thermal cycling parameter for amplicon PCR

95℃	3 min	1 cycle
95℃	30 sec	35 cycles
55℃	30 sec	
72℃	30 sec	
72℃	5 min	1 cycle
4℃	forever	

DNA purification by AMpure Beads XP

The DNA samples were further purified using AMpure Beads XP (Beckman A63880) as described in Figure 3.3. Brief description of the procedure was listed below. The total concentration of purified DNA was determined using NanoDrop spectrophotometer (Thermo Fisher).

1. Vortex AMpure Beads XP (Beckman A63880) before use. Add 20 μL of it to the PCR product. Mix by pipetting and incubate for 5 minutes at room temperature.

2. Collect the beads on a magnetic stand and discard the supernatant.
3. Add 180 µL of 80% ethanol to 2, and discard the supernatant after a while. Repeat this procedure twice.
4. Dry the sample at room temperature for 5 minutes.
5. Remove the sample from the magnetic stand, and add 52.5 µL of 10 mM Tris-HCl (pH 8.5) to 4. Mix by pipetting and incubate for 2 minutes at room temperature.
6. Collect the beads on a magnetic stand and transfer 50 µL of the supernatant to a new PCR tube.

The purified PCR products were confirmed via 1% agarose gel electrophoresis. 1 kbp plusladder (Life Technologies, 10787-018) was used as molecular weight marker.

Index PCR

Index PCR was carried out following the parameter listed in the table below.

Table 3.3 Composition of reagents used in Index PCR

1. Purified DNA	2.5 µL
2. Nextera Index Primer 1 (N7xx)	2.5 µL
3. Nextera Index Primer 2 (S5xx)	2.5 µL
4. 2x KAPA HiFi HotStart ReadyMix	12.5 µL
5. PCR grade water	5 µL
Total	25 µL

Table 3.4 Thermal cycling parameter for Index PCR

95℃	3 min	1 cycle
95℃	30 sec	8 cycles
55℃	30 sec	
72℃	30 sec	
72℃	5 min	1 cycle
4℃	forever	

The product of Index PCR was purified as described in DNA purification by AMpure Beads XP section with slight modification on step 1, 5 and 6. 28 μL of beads solution and 10 mM Tris-HCl (pH 8.5) used was and in this purification process and 25 μL of purified DNA was collected for further use. The concentration of the PCR product was verified by NanoDrop spectrophotometer (Thermo Fisher).

3.2.5 16S rRNA sequencing

Sequentially hyper-variable V4 region of bacterial 16S rRNA gene was PCR amplified using universal primer 515F/806R with MiSeq tails. The resulting ~300-bp sized amplicons were pooled and Qubit dsDNA HS assay kit (Life technologies, Q32850) was used to determine the concentration of the DNA library. Pooled DNA library was diluted to a concentration of 4 nM and then sequenced with the Illumina MiSeq 2x250 paired-end sequencing platform. Brief description of the procedure was listed below.

1. Add 5 μL of 0.2 M NaOH to 5 μL of the DNA library diluted to 4 nM, and incubate at room temperature for 5 minutes.
2. Add 990 μL of buffer HT1 to the reaction at step 1 on ice (20 pM denaturing DNA library).
3. Mix 150 μL of denaturing DNA library with 50 μL of denaturing PhiX library and then add 400 μL of buffer HT1 (5 pM final concentration of the library).
4. Incubate the DNA library in a heat block at 96°C for 2 minutes for further heat denaturation.

5. Incubate on ice for 5 minutes.
6. Place 600 μL of the reaction solution into port 17 of the reagent cartridge of the MiSeq Reagent kit v2 500 cycle.
7. Set up the flow cell, reagent cartridge, and buffer bottle, and start the run.

3.2.6 Data analysis

Qiime2 (2020.08 ver.)

QIIME 2 is a powerful, extensible, and decentralized microbiome analysis package with a focus on data and analysis transparency. In this study, we utilized the 16S rRNA sequencing data to build taxonomic profile to understand the gut microbiota alteration(*68*, *69*).

R studio (4.0.4 ver.)

R studio is a free software that comes with many useful packages for statistical computing and graphics. Raw data processed and integrated by Qiime2 are processed by using the following packages(*70*).

- **Vegan**: contain tools for diversity analysis, ordination methods and tools for the analysis of dissimilarities(*71*).
- **mixOmics**: offers a wide range of multivariate methods for the exploration and integration of biological datasets with a particular focus on variable selection(*72*).
- **ggplot2**: provide elegant graphics for data analysis(*73*).
- **Ellipse**: functions for drawing ellipses and ellipse-like confidence regions(*74*).
- **PLS-DA (Partial Least Squares Discriminant Analysis)**

  This is a discrimination method based on PLS regression, and is one of the multivariate analyses employed to identify the changes in the gut microbiota and the major variables that cause such discrimination depending on the administration method. The confidence level of a pairwise confidence region is by default 0.95 for a 95% region.

- **VIP (Variable Importance in Projection) score**

  This score estimates the importance of each variable in the projection used in a PLS model and is often used for variable selection. A variable with a VIP Score closes to or greater than 1 (one) can be considered important in given model.

3.2.7 Determination of SCFA from cecal content

Adult F1 male rat was defined as pup that reached the age of P28, in which weaning occurred. The adult F1 male rat was anesthetized using 2-Bromo-2-chloro-1,1,1-trifluoroethane (Sigma-Aldrich) before sacrifice. The animal was placed on its back on the dissection table and with their limbs fixed after they reach a deep anesthesia state. The skin of the abdomen was first removed before making a cut to reveal the inside of the lower abdomen. After that, the gastrointestinal organs were evacuated from the cavity to isolate cecal from the intestines. Cecal was obtained by removing it from the colon and the ileum. Cecal obtained from the adult F1 male rat was kept in 5 mL microtube and stored in deep freezer (－80℃) for further use.

The SCFA contents from the cecal were analyzed through derivatization using high performance liquid chromatography, HPLC (YMC Co. Ltd.) as described previously (*75*, *76*). Brief description of the procedure was listed below.

1. Weigh 200 mg of cecal contents from thawed sample.
2. Fill one third of the vessel with zirconia beads and crush the contents with a vortex mixer.
3. Add 800 µL of distilled water to the crushed suspension prepared in step 2.
4. After centrifugation (3500 rpm, 4°C), transfer 200 µL of the supernatant into a test tube with a stopper, and add 100 µL of 10 mmol/L 2-ethylbutyrate solution as an internal standard.
5. Add 200 µL of Reagent A and 200 µL of Reagent B respectively, cap the tube tightly, and then mix by shaking. Heat the specimen at 60°C for 20 minutes.
6. Add 200 µL of Reagent C, cap tightly and shake to mix. Then heat the specimen at 60 °C for 15 min, and cool to room temperature afterwards.

7. Add 4 mL of Reagent D and 5 mL of n-hexane to step 6, cap tightly, shake thoroughly, and centrifuge (3,500 rpm, 4°C).
8. Discard the supernatant and add 5 mL of n-hexane to, cap tightly, shake thoroughly, and centrifuge (3,500 rpm, 4°C). Remove the upper layer so that approximately 3 mL of the lower layer remained.
9. Add 5 mL of diethyl ether to 8, shake thoroughly, and centrifuge (3,500 rpm, 4°C). Then, transfer most of the upper layer into another test tube with a stopper.
10. Add 3 mL of distilled water to the mixture, shake thoroughly, centrifuge (3,500 rpm, 4°C), and divide the upper 2 mL into 9-mL screw-tube bottles.
11. Dissolve the residue with 200 µL of methanol, after the diethyl ether in the screw tube bottle was removed by centrifugal evaporator.
12. Analyze 11 using HPLC.

3.2.8 Statistical analysis

Data are reported as mean ± standard error of the means (SEM). For statistical significance, Wilcoxon test and Kruskal-Wallis test were performed accordingly. Data were statistically significant when $p < 0.05$.

3.3 Results and Discussion

A total of 1,152,290 sequenced were obtained from the 16S rRNA sequencing, with an average of 34,918 reads per sample, ranging from 10,061 to 131,885. At phylum level, the dominant taxa were composed of Bacteroidetes, Firmicutes Proteobacteria, Cyanobacteria and Tenericutes in rat fecal samples (Figure 3.6). The changes in early pregnancy are not significant, and hence, the comparison of E21 dam and P28 male offspring which involved *Bacteroidetes* and *Firmicutes* (Table 3.5). Overall, the changes in the phylum Bacteroidetes and Firmicutes in both E21 dam and P28 male offspring is indicative of balance shift when disturbance occurred to disrupt the homeostasis.

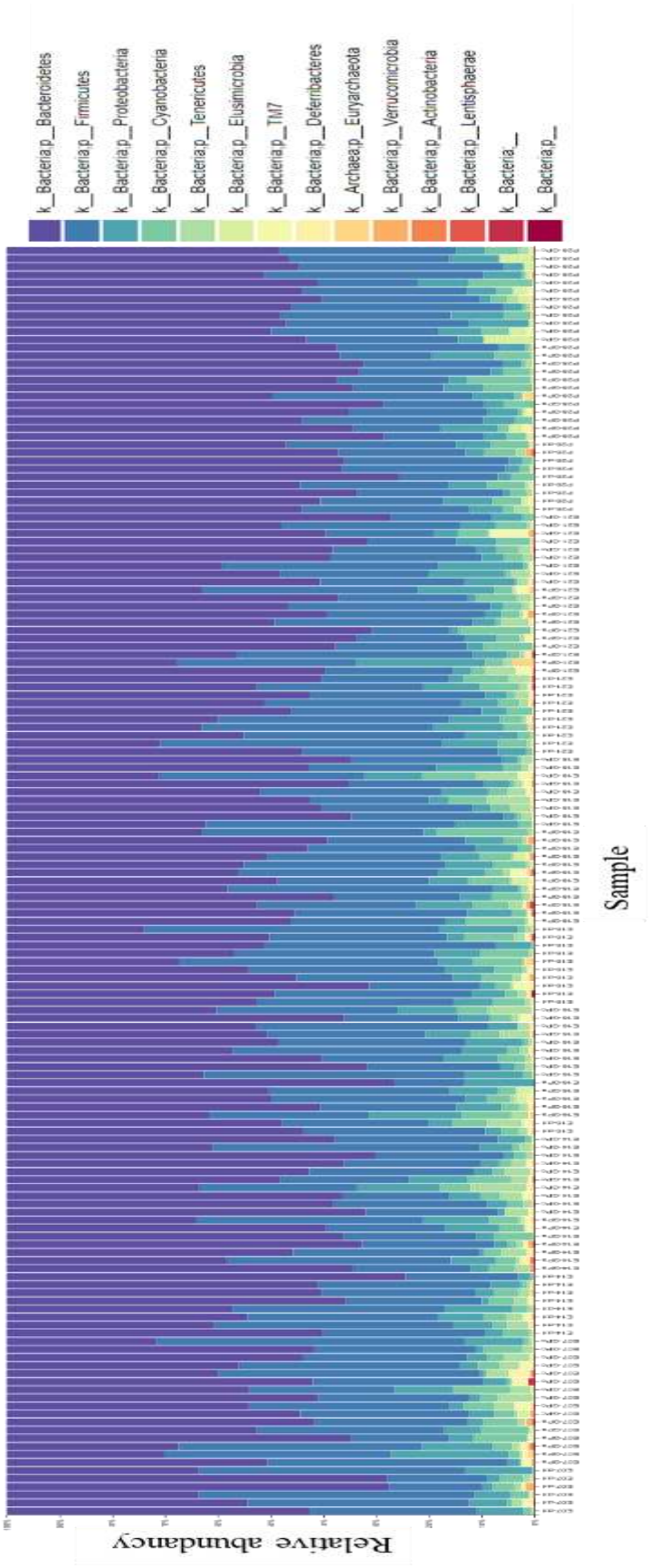
k__Bacteria;p__Bacteroidetes
k__Bacteria;p__Firmicutes
k__Bacteria;p__Proteobacteria
k__Bacteria;p__Cyanobacteria
k__Bacteria;p__Tenericutes
k__Bacteria;p__Elusimicrobia
k__Bacteria;p__TM7
k__Bacteria;p__Deferribacteres
k__Archaea;p__Euryarchaeota
k__Bacteria;p__Verrucomicrobia
k__Bacteria;p__Actinobacteria
k__Bacteria;p__Lentisphaerae
k__Bacteria;__
k__Bacteria;p__
Relative abundancy
Sample

Figure 3.6 Overall gut microbiota changes in phylum level

Table 3.5 Alteration of gut microbiota in phylum level in E21 dam and P28 male offspring

age	phylum	Relative abundance [-]	*p* value (Wilcoxon test)
P28	Bacteroidetes	Decrease	0.0093 (GPc vs ctrl)
		Decrease	0.0001 (GPc vs GPa)
P28	Firmicutes	Increase	0.0399 (GPc vs ctrl)
		Increase	0.0049 (GPc vs Gpa)
E21	Bacteroidetes	Increase	0.0209 (GPc vs ctrl)
E21	Firmicutes	Decrease	0.0061 (GPc vs ctrl)

Biodiversity within the sample was determined by running alpha diversity test, using two indexes that are Peilou's evenness and Faith's phylogenetic diversity (Figure 3.7). Peilou's evenness measures the relative evenness of species richness while Faith's phylogenetic diversity measures the biodiversity that incorporate phylogenetic difference between species. The result showed that the gut microbiota is less diverse and homogenous in the both GPa and GPc. The result is more significant in the P28 male offspring when compared to the E21 dam. This suggested the treatment group had more effects on the P28 male offspring than E21 dam. Although weaning happened on P28, the male offspring stayed with the dam until then in the same cage. If maternal colonization is successful, the biodiversity and gut microbiota composition of the P28 male offspring are not supposed to divert this much from E21 dam. This suggests that prenatal GP exposure will have a continuous effect on the composition of gut microbiota after birth and weaning.

At genus level, the supervised clustering PLS-DA analysis suggested that the overall microbial communities were clustered differently, in which the control group and GPa group are highly similar while dispersion observed I GPc group. This result is consistent across treatment group (Figure 3.8), E21 dam

(Figure 3.9) and P28 male offspring (Figure 3.10). The top contributors that to differentiate the changes observed were determined by VIP score (higher than 1) and the result is as shown in Table 3.6, Table 3.7, and Table 3.8.

In between treatment group, *Ruminococcaceae* differentiate the changes. *Ruminococcaceae* is a butyric acid producing bacteria(*77*, *78*)that is susceptible to the adverse effects coming from GP exposure. This result implied that GP treatment affected the abundance of the butyric acid producing bacteria. On the other hand, alteration observed from the gut flora of E21 dam were greatly affected by bacteria that play important roles in energy metabolism such as *Oscillospira* and *Lachnospiraceae*(*79–81*). This suggests prenatal GP exposure might inhibit the energy metabolism in the dam in late pregnancy which might be a risk that endanger both the dam and unborn pups. Meanwhile, the bacteria that differentiate the microbial communities in P28 male offspring, such as *Prevotella* and *Phascolarctobacterium*(*82*) is similar to the gut microbiota changes as observed in neurodevelopmental and neurodegenerative disorder.

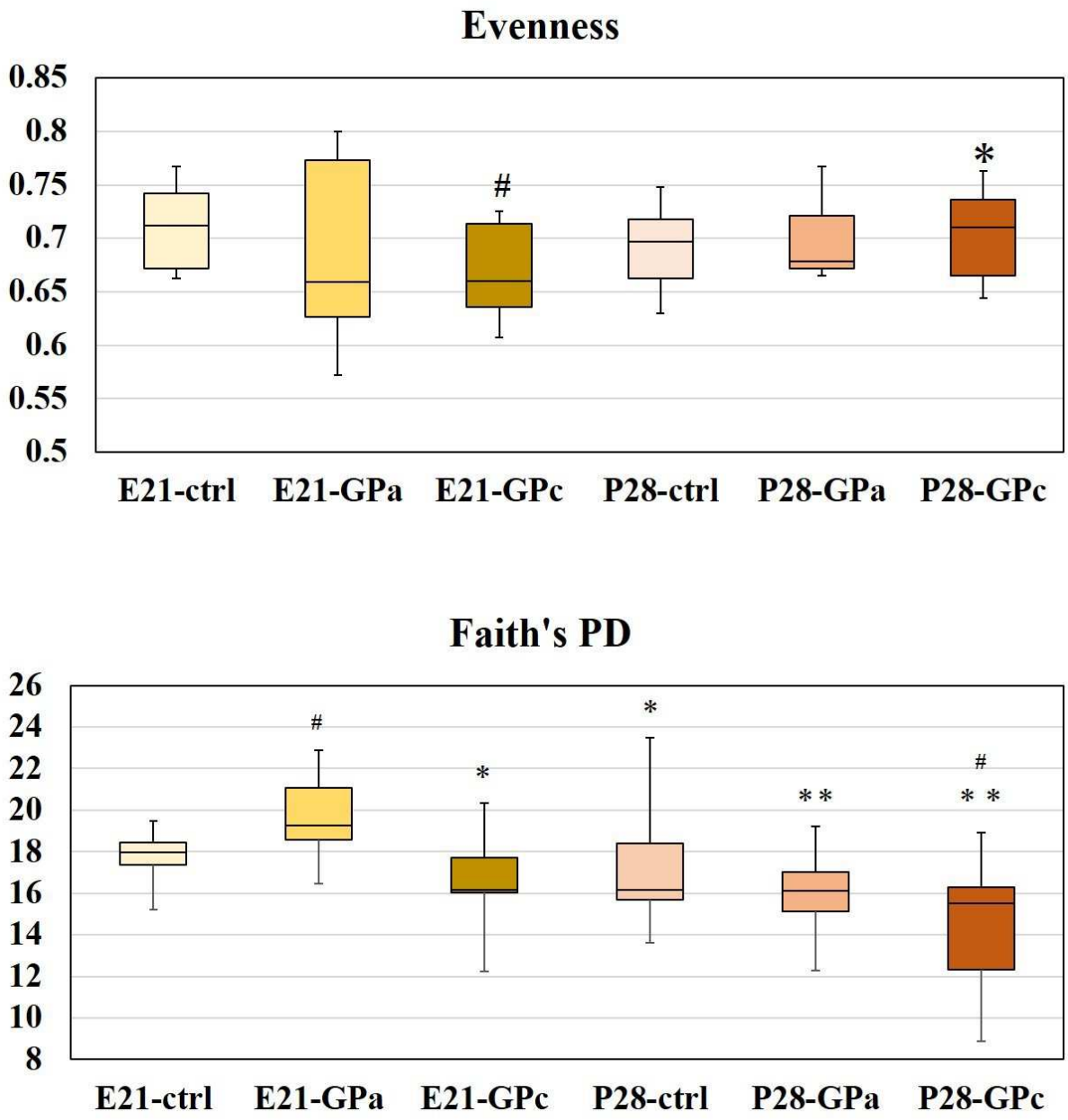

Figure 3.7 Alpha diversity across sample with significant changes in E21 dam and P28 male offspring, Peilou's evenness (top), Faith's phylogenetic diversity (bottom). The significant value was estimated by Kruskal-Wallis test ($** p < 0.01$ $* p < 0.05$ compared to E21-GPa, $\# p < 0.05$ compared to control group)

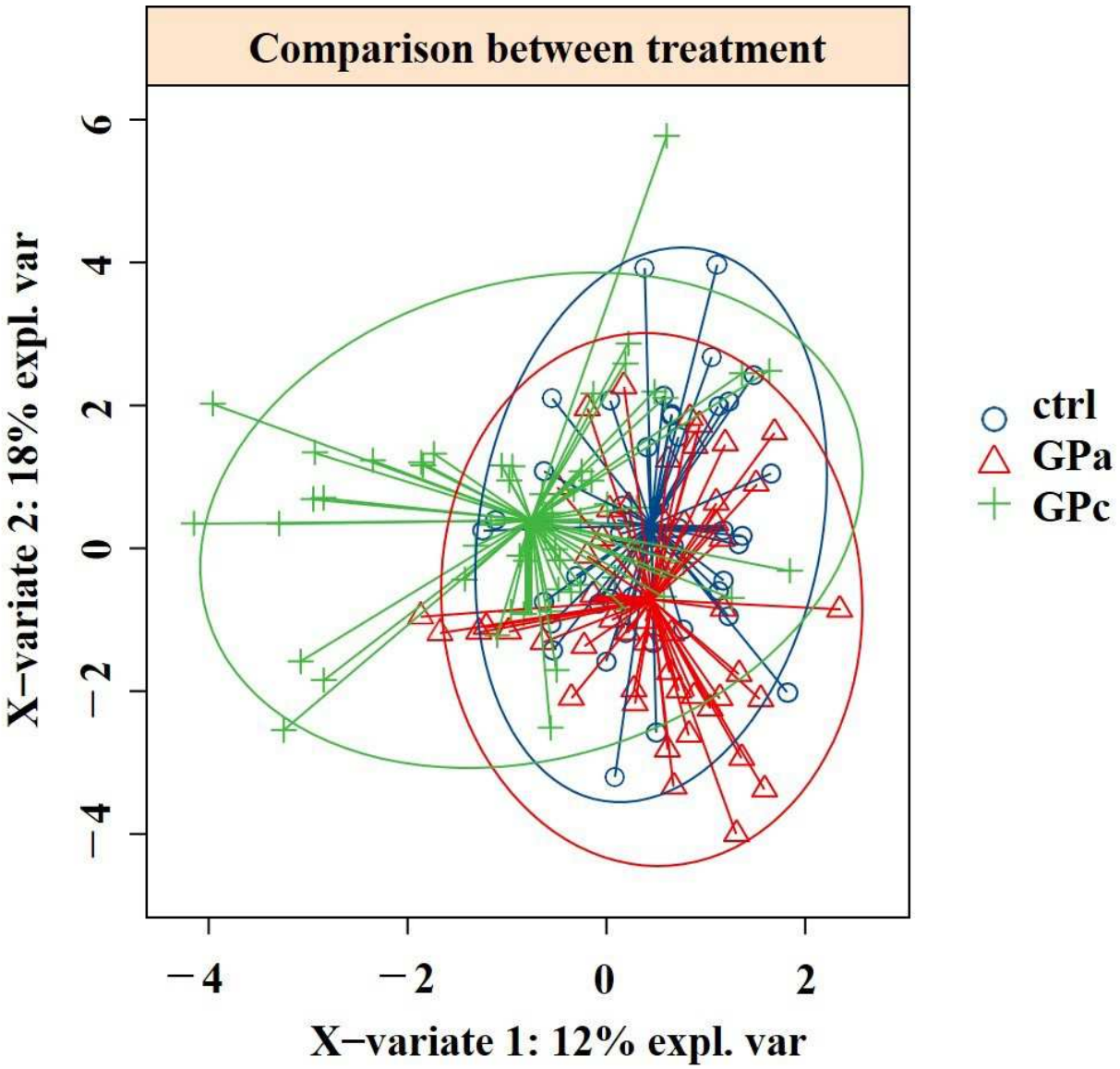

Figure 3.8 Comparison of gut microbiota in between treatment

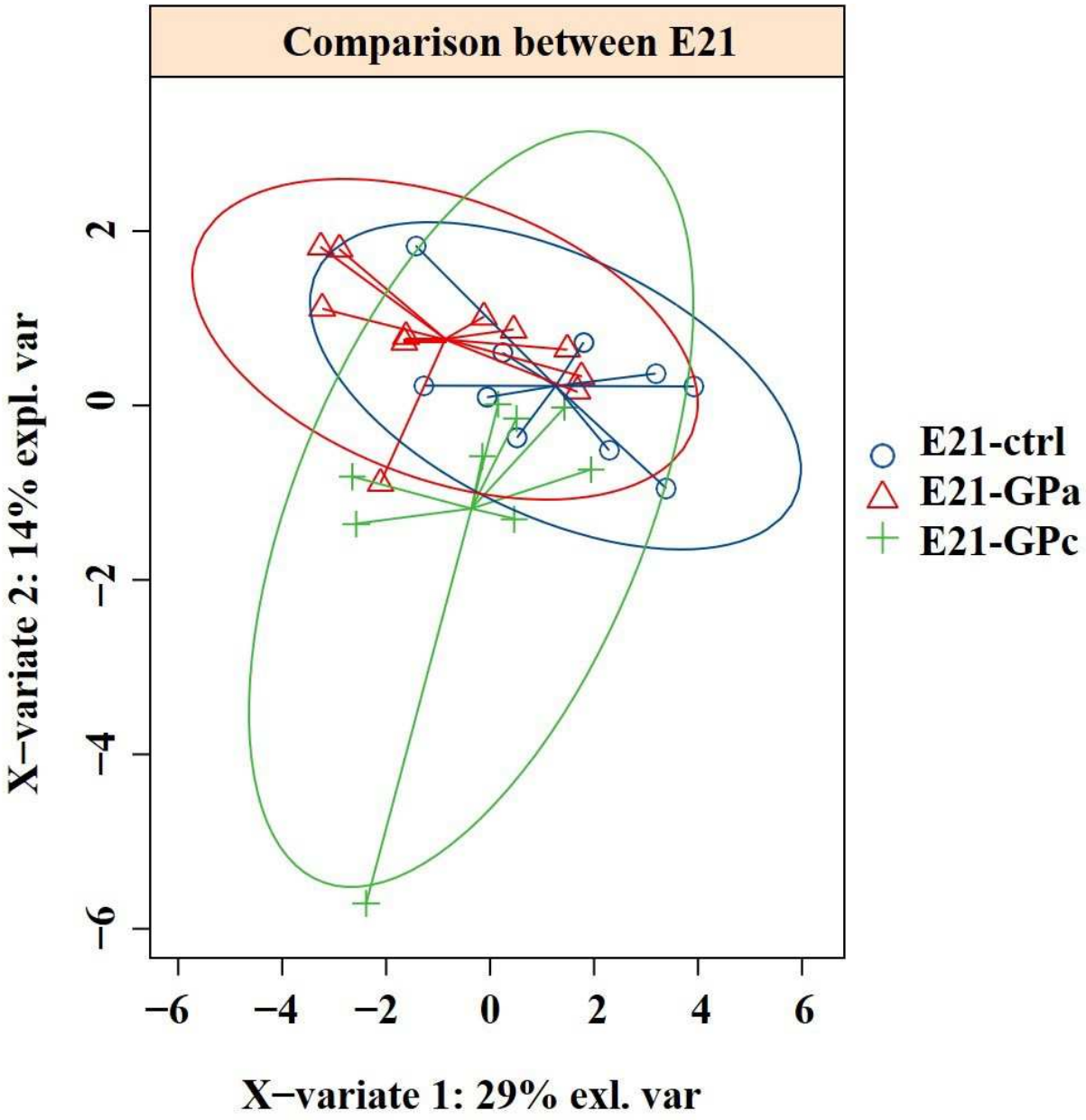

Figure 3.9 Comparison of gut microbiota in between the dam at E21

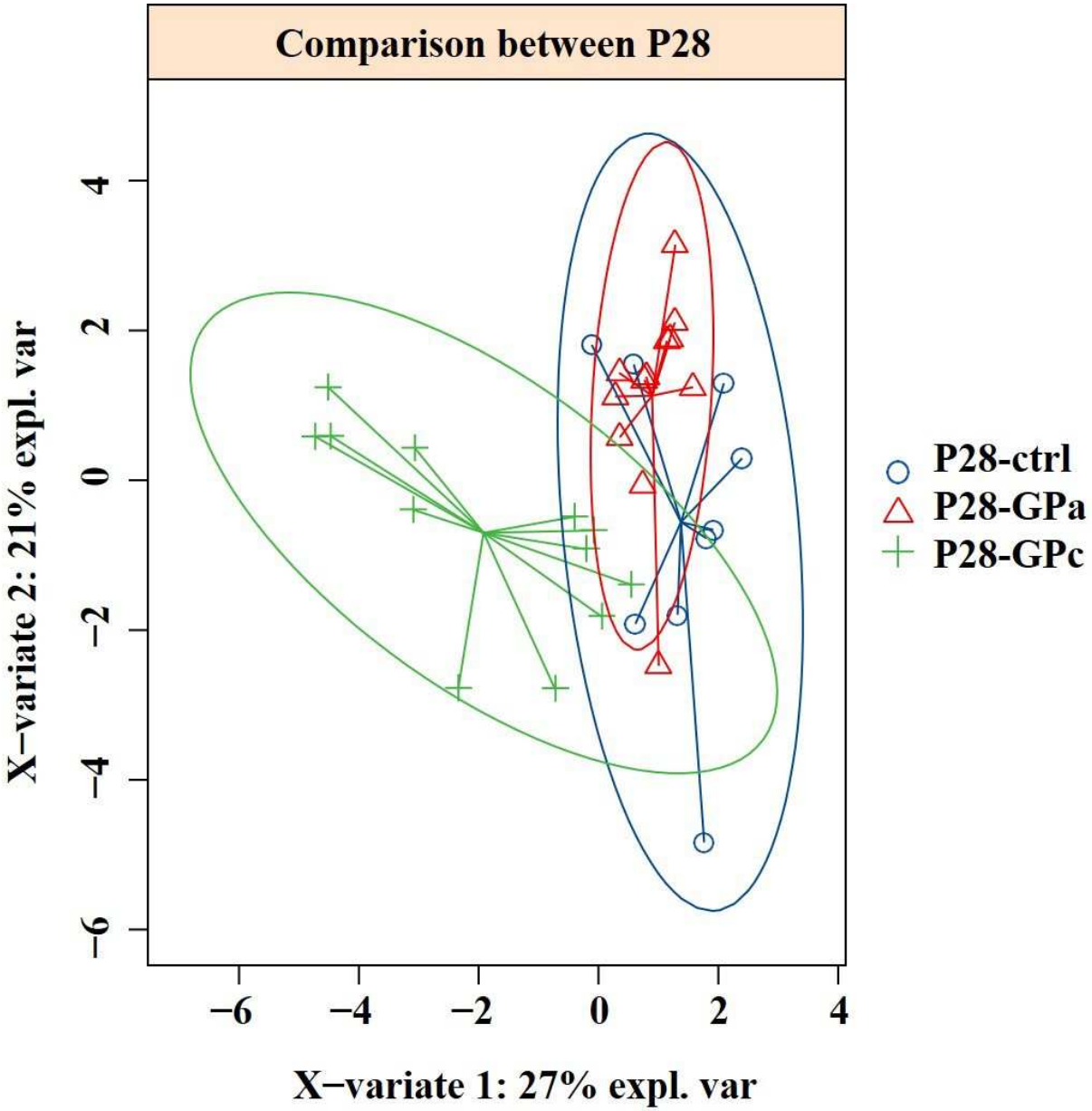

Figure 3.10 Comparison of gut microbiota in between F1 male rat at P28

Table 3.6 Gut microbes in genus level that differentiate the microbial communities in between treatment group

Genus	*p* value (Wilcoxon test)
Rumicoccaceae	0.0048 (GPc vs GPa)
unclassified Tenericutes	0.029 (GPc vs ctrl) 0.0027 (GPc vs GPa)
unclassified Cyanobacteria	0.013 (GPc vs GPa)
unclassified S24.7	0.042 (GPc vs GPa)

Table 3.7 Gut microbes in genus level that differentiate the microbial communities in between E21 dam

Genus	*p* value (Wilcoxon test)
Oscillospira	0.01 (GPc vs GPa)
Lachnospiraceae	0.022 (GPa vs ctrl)
Clostridiales	0.028 (GPa vs)

Table 3.8 Gut microbes in genus level that differentiate the microbial communities in between P28 male offspring

Genus	*p* value (Wilcoxon test)
Bacteroides	0.02 (GPc vs GPa) 0.0024 (GPc vs ctrl)
Lachnospiraceae	0.0068 (GPc vs ctrl) 0.0073 (GPc vs GPa)
Helicobacter	0.023 (GPc vs ctrl)
Prevotella	0.014 (GPc vs GPa) 0.0073 (GPc vs ctrl)
Clostridiales	0.034 (GPc vs ctrl)
Phascolarctobacterium	0.012 (GPc vs ctrl)

The production of SCFAs is determined by running HPLC on the cecal content of P28 male offspring. The result showed that the production of three SCFAs, butyrate, propionate and acetate were affected by GPa exposure (Figure 3.11). This implied that alteration in SCFAs producing bacteria might perturbed intestinal homeostasis, permeability and immune system. This might contribute to the occurrence of systemic inflammation.

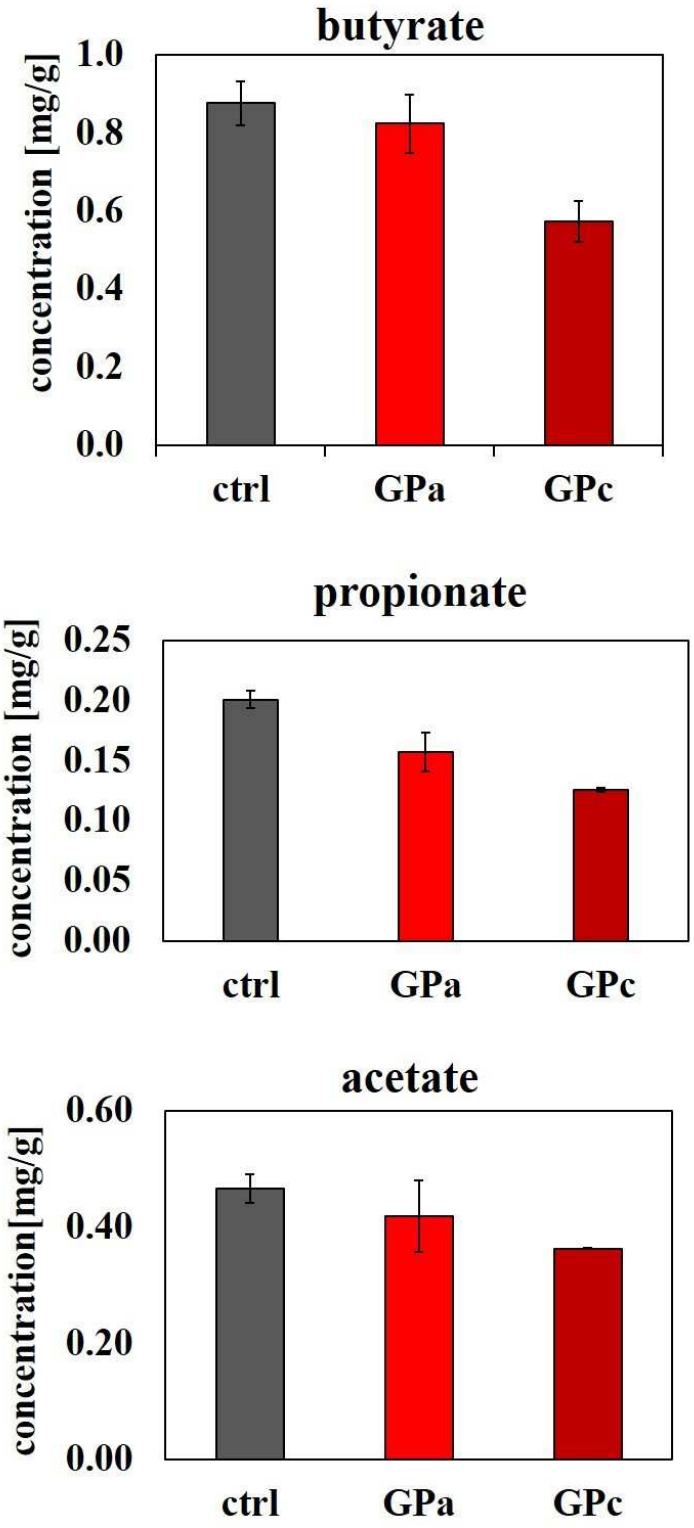

Figure 3.11 Alteration of SCFA produced in the cecal of P28 F1 male rat, butyrate (top), propionate (middle), and acetate (bottom). Each bar represents mean ± SEM (n = 3 for each sample)

3.4 Summary

Investigating the gut brain axis allowed us to dig deeper to unveil the changes occur within our body. The result is evident on gut flora disruption caused by prenatal GP exposure, not only on the pregnant dam but also in the male offspring after weaning. This strongly implicated that prenatal GP exposure agitated the gastrointestinal homeostasis in both the dam and the male offspring. For many years, the fetal intestine is considered to be sterile, and it is thought that intestinal flora formation begins when exposed to mother-derived or environmental-derived bacteria at birth, On the other hand, recent studies have revealed the presence of bacteria in amniotic fluid, endometrium, and placenta, and there are several reports that bacterial exposure has already begun in utero(*83*). As a result, the gut microbiota compositions changed and this perturbation that happened inside the gut affects the metabolism too. Furthermore, the microbial communities were less diverse and homogenous in the treatment group (GPa and GPc) which may elicit immune response. This may exacerbate the altered gut flora by the release of inflammatory cytokines into the bloodstream and thinning the intestinal barriers. This can all contribute to the initiation of systemic inflammation, suggesting that assessment of systemic inflammation is feasible.

Chapter 4 Effects of Prenatal Exposure to Glyphosate on the Development of Offspring Cerebellum

4.1 Introduction

This chapter will discuss about the potential causes and effects of systemic inflammation through prenatal glyphosate exposure. It is a growing concern that the pesticides we used in the agriculture to enhance the crops production might harm us. This thesis focused on the active chemical ingredient in widely used herbicides, Roundup®, which is GP. GP was once considered safe but emerging evidences suggest that it is a potential health risk and jeopardize the environment. However, less is known about its effect in cerebellar development. Therefore, this thesis attempted to evaluate the effects of prenatal exposure to GP on the development of offspring cerebellum on both acute and chronic exposure. The result showed that alteration occurred in the offspring cerebellum inferring that GP might be developmental neurotoxic.

4.1.1 The brain

The brain is composed of six parts: the medulla oblongata, the pons, the cerebellum, the midbrain, the diencephalon, and the cerebral hemisphere. Among them, the pons, midbrain and medulla oblongata are collectively called the brain stem. The cerebellum is located dorsally, with the cerebrum covering the diencephalon and midbrain. Each region cooperates with each other via neural circuits in the brain while processing information with erasure, and produces higher-order functions such as memory, judgment, and emotional thinking.

4.1.2 The cerebellum

The cerebellum intervenes in the pathway that runs between the cerebrum and the spinal cord, and is an important center of the extrapyramidal system. The cerebellum is one of the most important centers of the extrapyramidal system. Although it has been thought that the cerebellum mainly regulates movement and equilibrium, it has recently been revealed that the cerebellum is the center of cognitive and emotional

functions, and it has attracted attention that the cerebellum and higher brain functions are greatly related(*84–86*).

The cerebellum plays an essential role in motor control, learning, and sense of balance. It is composed of cortex, white matter, and cerebellar nucleus, but the cerebellum can be roughly divided into vermis and hemisphere. Both the vermis and the cerebellar hemisphere are divided into several cerebellar lobes by the cerebellar fissure. The sagittal section of the vermis has a basic structure consisting of 10 lobules: lobules I to V correspond to the anterior lobe; lobules VI to IX correspond to the posterior lobe, and the lobules X corresponds to the inferior lobe (Figure 4.1). Further, it can be categorized into three parts: vestibular cerebellum, spinocerebellar cerebellum, and pontine cerebellum, which are responsible for the body balance function, eye movements, smooth movements, and exercise planning. Lobules V to VIII are important areas that control higher-order functions that are said to control cognition and emotions(*87*).

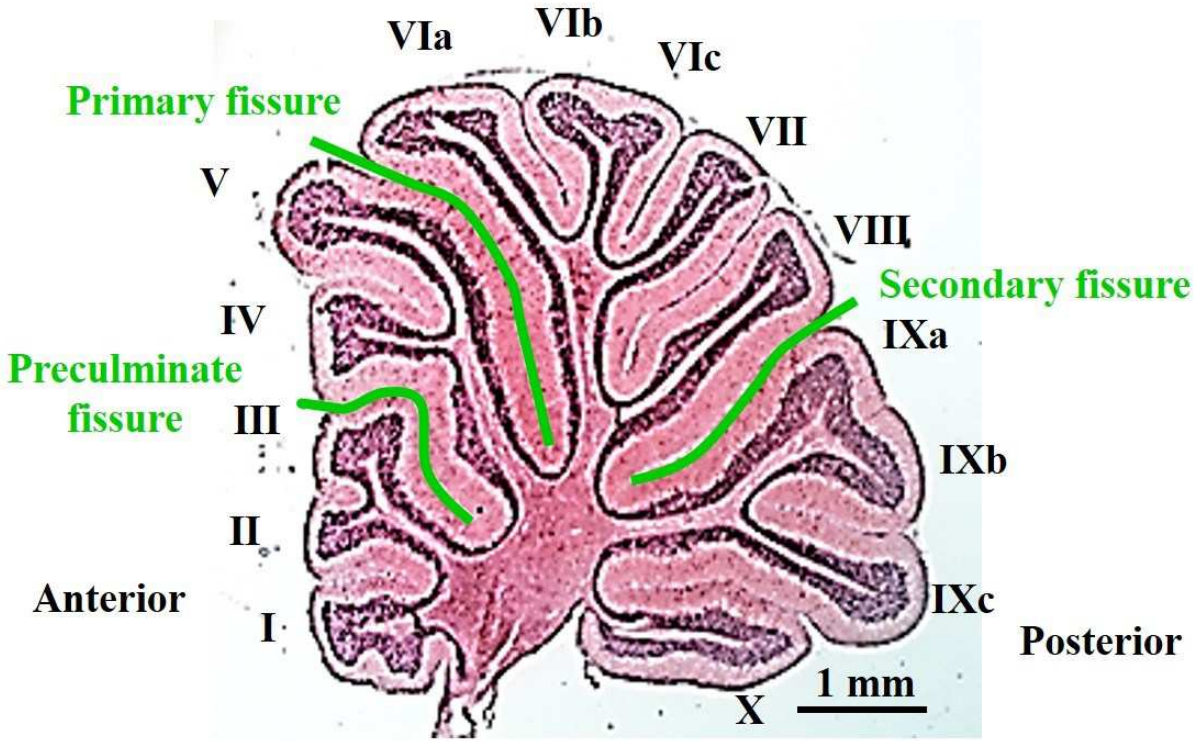

Figure 4.1 Midline cerebellar vermis in sagittal section of rat(*88*)

The cerebellum is composed of the cortex, white matter, and cerebellar nuclei. In the mature cerebellar cortex, there are three layers: the molecular layer, the Purkinje cell layer, and the granule cell layer. The inner part of the granule cell layer is made up of the white matter in which nerve fibers intertwined. There are five main types of neurons in the cortical structure: stellate cells, basket cells, Purkinje cells, granule cells, and Golgi cells. Relatively small stellate cells and basket cells scattered around in the molecular layer. Large Purkinje cells aligned in a single row in the Purkinje cell layer, whereas the granule cells and medium-sized Golgi cells are distributed in the granule layer. Out of these cells, only Purkinje cells extend their axons outside the cortex, while the axons of all other neurons end up inside the cortex. Granule cells are glutamatergic excitatory cells, while all other cells are inhibitory neurons that use gamma-aminobutyric acid (GABA) as their transmitter. There are two types of excitatory input fibers spreading into the cortex: mossy fibers and climbing fibers. The cerebellar cortex enables smooth movement by facilitating the functioning of circuits in the cerebellar white matter and nuclei. The cerebellum contains about 100 billion neurons, which is about seven times more than the cerebrum(*87*).

Neuron

Neuron consists of dendrites, cell body (soma), and a single axon. The soma contains cell nucleus that is essential for the production of RNAs and proteins necessary for the cell survival. Axons are thinner and smoother than dendrites, and do not contain protein synthesizing machinery such as ribosomes. Signals received from the dendrites and soma are send down the axon to the synapses. Here, neurotransmissions occur which allow cross communication in between the neurons. Neurons that send their axons to distant sites are called projecting neurons, while those that stay in the vicinity of the axon are called interneurons. Projecting neurons are comparatively larger than interneurons and they have higher level of metabolism, transcription and translation. Typically, there are three types of neurons, categorized by their function: sensory neurons, motor neurons and interneuron. Sensory neurons respond to stimuli such as sound, light and smell by sending signal to the brain or spinal cord the affect our sensory organ. Meanwhile, motor neurons are neurons that received the signals input by the sensory neurons in order to act in response.

Interneurons are neurons that connect one neuron to the other within then spinal cord and brain, eventually form the large-scale brain network in order to carry out myriad of tasks.

Granule Cells

Granule cells are the only glutamatergic cells among the neurons that make up the cerebellar cortex. They are also the only intrinsic excitatory neurons. The cells are small, approximately 10-15 μm in size. Granule cells receive excitatory inputs from mossy fibers and inhibitory inputs from Golgi cells. They project up through the Purkinje layer and go further into the molecular layer. There, they branched out into the parallel fibers to form an intricated neural circuit using glutamate as a neurotransmitter. However, excessive release of glutamate can cause Purkinje cell death (glutamate excitotoxicity). Low glutamate release causes by the granule cells when they are underdeveloped. But as granule cells develop, glutamate release increases, making glutamate uptake by astrocytes a key factor in maintaining the homeostasis within the neural circuit. Therefore, if the astrocytes are underdeveloped, the glutamate released by the developing granule cells may cause programmed cell death in Purkinje cells(*89*, *90*).

Purkinje cell

Purkinje cells are the only output neurons in the cerebellar cortex, and their activity is regulated by excitatory synaptic inputs from parallel and climbing fibers and inhibitory synaptic inputs from basket cells and stellate cells. The size of the cells is about 25 μm. They also show plasticity other than long-term depression. In addition to long-term depression, there is also long-term potentiation at synapses between parallel fibers and Purkinje cells. Furthermore, at synapses between basket cells and stellate cells and Purkinje cells, long-term potentiation occurs when Purkinje cells are depolarized by excitatory synaptic inputs such as climbing fiber input. This inhibitory synaptic plasticity is suppressed if the presynaptic inhibitory interneuron (basket cell or stellate cell) is activated during Purkinje cell depolarization. It has been suggested that this synaptic plasticity also cooperates with long-term depression and is involved in information processing in cerebellar circuits.

Golgi cells

Golgi cells receive excitatory input from parallel fibers and form a negative feedback circuit of granule cells, Golgi cells, and granule cells. When Golgi cells are killed, the inhibition of the granule cell layer becomes ineffective and motor deficits are exhibited, but the motor deficits are subsequently alleviated.

Stellate cells and basket cells

Both astrocytes and basket cells are inhibitory interneurons to Purkinje cells, and astrocytes are also called outer astrocytes and basket cells (basket cells) are called inner astrocytes. Both are suggested to function similarly, but the outer star cells are smaller and contact fewer (about 12) inhibitory Purkinje cells on the dendrites, whereas the inner star cells are believed to be more influential because they are said to make up many synapses on the Purkinje cell body.

Glial cells

Glial cells or simply glia, are generic terms for non-neuronal cells constituting the central and peripheral nervous system. In the human brain, the number of glial cells is estimated to be 50 times more than neurons. The term derives from a Greek word meaning glue. Glial cells were named in the sense that it plays a role of adhering nerve cells. Previously, it was thought that glial cells were not in involved in neurotransmission but merely provide support and trophic factors.

However, there has been a lot of reports on their important roles in maintaining homeostasis and neuron maturation in recent years. For example, the expression of receptors of a wide variety of neurotransmitters. Moreover, they maintain the ionic milieu of nerve cells, modulating the rate of nerve signal propagation and controlling the uptake of neurotransmitters to regulate synaptic action. Furthermore, in our previous research in our laboratory, we discovered that glial cells play an alternative role of nerve cells in brain function during developmental process, and that they synthesize and release GABA to promote differentiation of nerve cells.

Table 4.1 Different types of glial cells and their functions

Type of glial cells	Function
Astrocyte	• Anchors neurons to capillaries • Forms blood brain barrier
Oligodendrocyte	• Forms myelin sheath • Insulate axon of central nervous system
Ependymal cell	Formation and circulation of cerebrospinal fluid
Microglial	Phagocytosis (dead nerve tissue and microorganisms)

Microglial cells

Microglia account for about 10% of all glial cells. Microglia are resident macrophages of the central nervous system that arise early in embryonic development and provide immune protection and developmental support to the brain. In the adult brain, microglia are involved in the homeostatic functions of the brain and in the interaction between the central nervous system and the gut microbiota.

Microglia are also highly dynamic and are closely related to neurons and astrocytes. Microglia can rapidly respond to changes in the environment and release molecules to regulate neural function and synaptic transmission. Recent reports indicate that microglial activity induces a rapid increase in spontaneous excitatory postsynaptic currents. This regulation is conveyed by the binding of ATP to P2Y1R in astrocytes. In other words, microglia release a small amount of ATP, and then astrocytes amplify this release. P2Y1 stimulation of astrocytes then increases the excitatory postsynaptic current through a glutamate receptor 5-dependent mechanism.

In mice, microglia form the cortex at 11.5 days of age (E11.5). Initially, the cells assemble in the lateral ventricles on the surface and inside the soft membrane, and then they are distributed throughout the cortical wall. The formation of the cortical parenchyma is a multistep process, with a slow increase in

microglia from E10.5 to E14.5, a rapid increase from E14.5 to E15.5, and a slow increase again from E15.5 to E17.5.

When human microglia invade the central nervous system, they become highly proliferative, forming a localized accumulation around the white matter region. Therefore, immature microglia exist in an amoeboid shape to promote sustained cell migration. Later, the microglia form the brain. Initially, microglia migrate tangentially along the surface of the central nervous system, covering the entire CNS layer. Later, they migrate perpendicular to the surface and undergo morphological maturation from an amoeboid to a branched shape.

4.1.3 Differentiation of the cerebellar cortex

In the rat, the cerebellar primordium is formed during the embryonic period (E13-16 days). Purkinje cells and Golgi cells migrate from the neural tube and are distributed in layers. Developmental differentiation of the cerebellar nuclei and Purkinje cells occurs relatively early, followed by the development of Golgi cells. The developmental differentiation of basket cells and astrocytes occurs after birth. Granule cells develop in the uppermost layers of the cortex at E20.

In the postnatal cerebellum, as shown in Figure 4.2, the dividing Purkinje cell layer (PL) is overlaid by a developmentally dividing external granule layer (EGL). Later, the granule cells migrate underneath the PL while stretching their parallel fibers to form the inner granule cell layer (IGL), which consists of granule cells and Golgi cells. At the same time of migration, the number of granule cells in the IGL gradually decreases, and the molecular layer consists of parallel fibers extending from the granule cells, dendrites of Purkinje cells, basket cells, and astrocytes. Finally, the mature cerebellar cortex consists of three layers: the molecular layer, the Purkinje cell layer, and the granule cell layer.

At birth, many Purkinje cells are arranged in multiple layers (multilayer), and dendrites are barely extended. Later, dendrites elongate with the migration of granule cells, and at the same time, the cell body develops into a monolayer by apoptosis. This apoptosis is regulated by the neurotrophic factor (BDNF) released from the ascending fibers. Multiple innervations of epithelial fiber inputs extending from the olive

nucleus have been observed in juveniles. Bergmann glia, a type of glial cell that assists in granule cell migration, develops at the same time as granule cell migration and is thought to play a role in maintaining the environment surrounding the Purkinje cell-granule cell synapse.

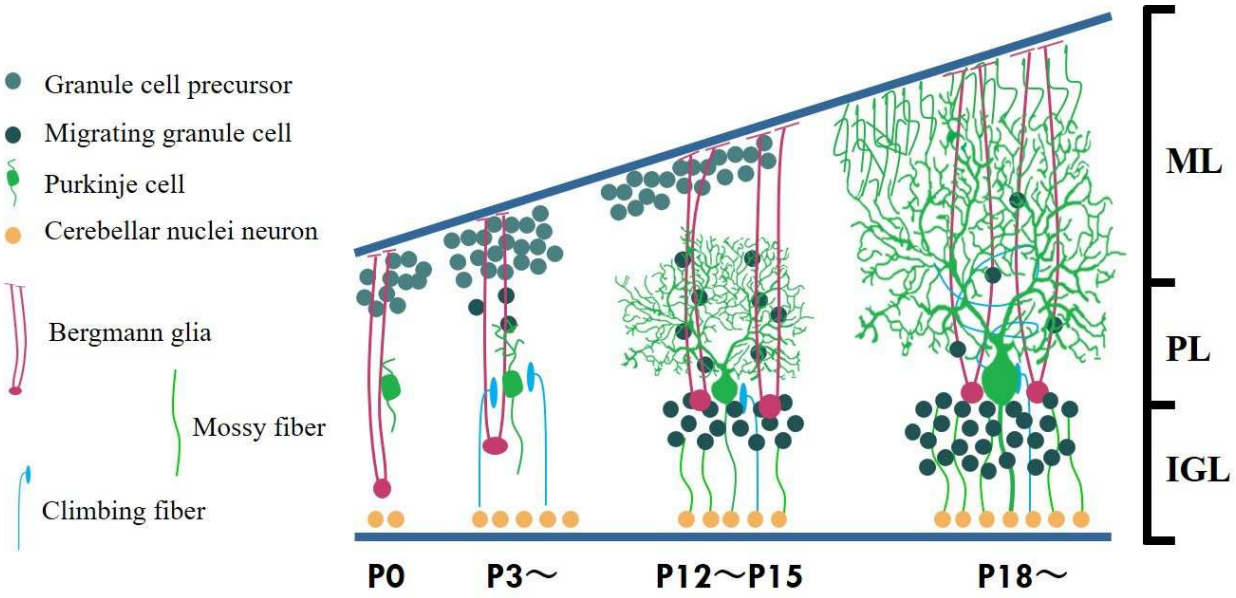

Figure 4.2 Neuronal migration during early cerebellar development, ML: molecular layer; PL: Purkinje layer; IGL: inner granule layer(*91*)

The progenitor cells of granule cells are produced in the limbic region of the rhombic lip. They then migrate, spreading anteriorly just below the meninges on the surface of the brain while preparing for mitosis. As a result, the surface of the cerebellum is covered with a layer of granule cell precursors distributed over EGL. This layer of mitotic cells can be seen just below the meninges, but by the end of embryonic life, the granule layer is distributed in a line just below it.

Purkinje cells are produced in the fourth ventricle of the rhombencephalon. The Purkinje cells then migrate radially away from the ventricular surface, and by late embryonic stage, all cells are localized near the brain surface and arranged in layers. The Purkinje cell layer initially forms multiple layers, but as the

cerebellum develops, apoptosis leads to the formation of a single monolayer within a week of birth. The cerebellum is compartmentalized in symmetrical longitudinal stripes from medial to lateral.

4.2 Experimental section

4.2.1 Animal preparation

Rats used in this section were prepared as previously described in section 3.2.1. Pregnant dam was subjected to the following glyphosate (Glyphosate reference material, Fujifilm Wako, CAS no. 1071-83-6)) treatment. For acute exposure, 25 mg/kg body weight (GP 25), 100 mg/kg body weight (GP 100) and 250 mg/kg body weight (GP 250) were administrated by oral gavage to the pregnant dam on embryonic day 16, E16. For chronic exposure (GPc), 15.625 mg/kg/day was administrated by oral gavage to the pregnant dam for 16 days, starting from E5 until E20. The control animals were prepared by oral gavage of phosphate-buffered saline, 1× PBS diluted from 10× PBS. The composition of 10× PBS was listed in Table 4.2. The body weights of male pups (10 pups per treatment group) were recorded every five days.

Table 4.2 Composition of 10× PBS in 500 mL

NaCl	40.0 g
Na_2HPO_4	5.8 g
KH_2PO_4	1.0 g
KCl	1.0 g

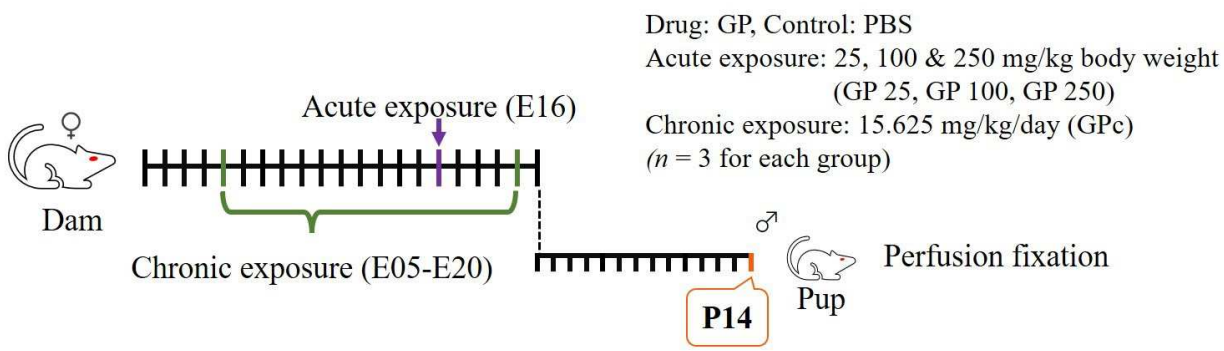

Figure 4.3 The study design to assess the cerebellar alteration in F1 male offspring born from prenatal GP exposed dam

4.2.2 Perfusion fixation

Perfusion fixation is a fixation operation to prevent decay of brain tissue and preserve cell structure, in order to create cerebellar slices for observation. The aldehyde in the fixative solution inhibits the migration of the biomolecules and their enzymatic activity by cross-linking the biomolecules, thus stopping cellular alterations. In this study, F1 male pups were perfusion-fixed at post-natal day 14 (P14).

4% paraformaldehyde (Nacalai Tesque, Inc.) solution was prepared by mixing 10% paraformaldehyde solution with Milli Q water at a ratio of 4 to 6. The prepared 4% paraformaldehyde solution was placed in a 25 mL syringe fitted with a 27G R.B. needle (Terumo, NN-2725R).

2-Bromo-2-chloro-1,1,1-trifluoroethane (Sigma-Aldrich) was used as an anesthetic in this study for animal sacrifice. The animal was placed on its back on the dissection table and with their limbs fixed after they reach a deep anesthesia state. The skin of the chest was first removed, and the ribs of the left chest were removed to expose the heart next so as not to injure other organs. The needle was inserted into the lower right side of the exposed heart, and the fixation fluid was injected into the left ventricle. 5 mL of the fixation fluid was injected, and an incision was made near the right atrium to facilitate the drainage of circulating blood and fixation fluid. After all the fixation fluid was completely injected, the rat was decapitated. Next, the skin of the head and the upper part of the skull was removed. Then, the bone inside the ear that holds the skull and brain together was removed in order to extract the whole brain. The whole brain was then

immersed in the fixation solution for 40 minutes to complete the fixation process. After that, fixation solution was discarded and the whole brain was preserved with 1× PBS containing 0.02% sodium azide and stored in a refrigerator.

4.2.3 Preparation of cerebellar tissue sections

The cerebrum and medulla were removed from the fixed whole brain using a scalpel in order to obtained the cerebellum. Cerebellar hemispheres were excised and sagittal cerebellar vermis slices with a thickness of 50 μm were prepared using a vibrating blade tissue slicer (Linear Slicer PRO7, Electron Microscopy Sciences). The cerebellar slices were placed in a 24-well plate filled with 1× PBS and kept suspended at 4°C.

4.2.4 Immunohistochemical staining

The principle of the method is shown in Figure 2.15 as previously described in section 2.2.6.

Preparation of staining solutions

The solutions used for immunohistochemical staining are shown below.

a: 0.5 wt% Triton X-100 (dilution of 10 wt% Triton X-100 with 1×TBS)

b: 0.05 M NaOH (dilution of 1M NaOH with 1×TBS)

c: 1.2% H_2O_2 (dilution of 30% H_2O_2 with 1×TBS)

d: Blocking solution (Add diluted 10 wt% Triton X-100 with 1×TBS to 1 mL of goat serum)

e: Primary antibody (diluted with blocking solution)

f: Secondary antibody (diluted with blocking solution)

The antibodies used in this study were listed in Table 4.3 as shown below.

Table 4.3 Composition of primary antibody solutions

Target	Primary Antibody	Ratio to blocking solution
Microglia	rabbit antiIba1 (1:1000, Fujifilm Wako 012 26723)	1:100
Purkinje cell	mouse anti Calbindin-D 28k (1:1000, Sigma-Aldrich C9848)	1:1000

Table 4.4 Composition of secondary antibodies

Fluorescent- labeled antibody	Ratio to blocking solution
Alexa-Fluor-488-conjugated goat anti-mouse IgG (Invitrogen A-11005)	1:1000
Texas Red-conjugated goat anti-rabbit IgG (Thermo Fisher T2767)	1:1000

Staining procedure

1. Sliced cerebellar sections were immersed in solution a for 6 minutes. This procedure was repeated three times.
2. Immersion in solution b for 6 minutes.
3. Immersed in solution a for 2 minutes.
4. Soaked in solution c for 20 minutes.
5. Immersed in solution a for 6 minutes. This procedure was repeated twice.
6. Immersed in TBS for 6 minutes. This operation was repeated twice.
7. Immersed in solution d for 40 minutes.
8. Immersed in primary antibody and stored at 4°C overnight.
9. Immersed in 1×TBS for 2 minutes.
10. Immersed in solution d for 6 minutes.
11. Immersed in secondary antibody and stored at 4°C overnight.

12. Immersed in 1×PBS for 3 minutes. This procedure was repeated twice.
13. A drop of glycerin was placed on the cerebellum section of a glass slide, covered with a cover glass, and observed using a confocal microscope.

4.2.5 Hematoxylin and Eosin Staining

Hematoxylin and eosin staining (HE staining) is the most basic and important staining method for histopathological specimens, as it is used to obtain a complete picture of cellular and tissue structures at the light microscope level. The principle of HE staining is that hematein, which is produced by the oxidation of hematoxylin, forms a complex with the metal part of the mordant and becomes positively charged, thereby binding to the phosphate groups of the negatively charged cell nucleus and ribosomes. In addition, eosin is an acidic dye, and since the dye itself is negatively charged, it binds to positively charged cytoplasm, interstitial cells, and fibers to stain them.

HE staining procedure

The procedure for HE staining is shown below. During each step, as much of the staining solution as possible is removed so that no solution remains for later steps.

1. The sliced cerebellar sections were dried and immersed in hematoxylin solution for 5 minutes.
2. Immerse the sliced cerebellum sections in running water at 34°C for 10 minutes (so that the water flow does not directly hit the cerebellum sections).
3. Cerebellar sections were dried and immersed in eosin for 4 minutes.
4. The cerebellar sections were dried and immersed in eosin for 4 minutes.
5. Eosin was washed off with 95% ethanol. This procedure was repeated twice.
6. The cerebellar sections were dried, and MOUNT-QUICK AUEOUS was dropped onto the cerebellar sections as an inclusion agent, covered with a cover glass, and observed using a stereomicroscope.

4.2.6 Confocal microscopy

Cerebellar slices that had undergone immunohistochemical staining were observed using a confocal microscope as described previously in section. The settings used in this observation are shown below.

Fluorescent images were captured with an objective lens with 10× magnification, scan size = 2048, scan speed = 0.125, with 8 times image acquisition for clearer image by averaging. For Calbindin-D 28k imaging, fluorescence wavelength = 488 nm, excitation wavelength = 486.8 nm; for Iba1 imaging, fluorescence wavelength = 561 nm, excitation wavelength = 561.5 nm. The images obtained from confocal microscopy were processed with an open-source image processing software, Fiji(*49*).

4.2.7 Statistical analysis

The data were reported as mean ± standard error of mean (SEM). Dunnett's test was performed to estimate the significance of the result. Data were reported as statistically significance when $p < 0.05$.

4.3 Results and Discussion

The body weight of offspring was recorded to determine whether the prenatal GP exposure was affecting the growth of offspring. The body weight of the F1 male offspring of all GP exposure was lower than the control group. However, the result is not statistically significant (Figure 4.4). Overall, prenatal GP exposure suppressed the growth F1 pups.

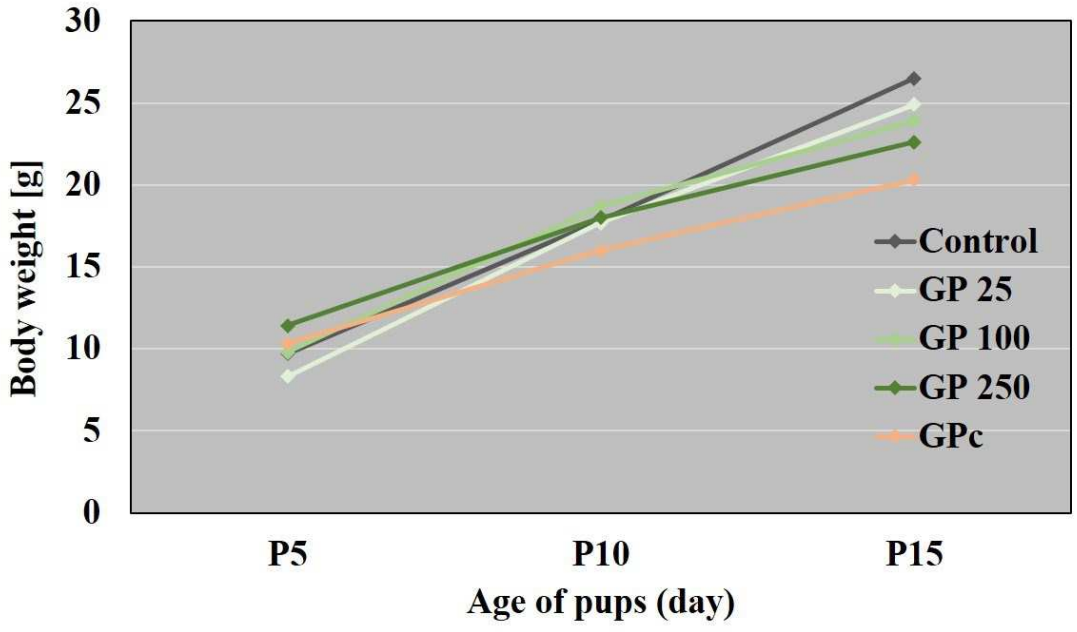

Figure 4.4 Body weight gain in the first two week after birth

Cerebellar development abnormalities are strongly associated with the inflammation in early development, usually manifested as morphological changes, such as the Purkinje cells defect and vermis size change. Therefore, the effect of prenatal GP exposure on cerebellar development was examined in F1 male pups (P14) born from maternal GP 25, GP 100, GP 250 and GPc exposure was confirmed. The region of focus is the V and VI lobes in the rat cerebellum because this region is classically involved in motor function and carried out cognitive function as reported in recent studies(*92*). Thus, anomalies in this region, such as the alteration of Purkinje cells and microglia, were examined to help us better understand the effects of prenatal chemical exposure have on the manifestation of neurodevelopmental disorder.

Figure 4.5 showed that the morphology of the cerebellum was unaltered for both control and GP exposed specimens. Overall, GP exposure did not alter the perspective of the cerebellum but altered the significant components of the cerebellum, the Purkinje cells, and microglia.

Immunostaining with Calbindin-D28k showed decreased Purkinje cells in the cerebellum slices from the F1 pups born from GP exposed dams (yellow triangle in Figure 4.6). The changes in the number of Purkinje cells per 1 mm of the PL were calculated, and a significant decrease was observed across all GP exposure (Figure 4.7 top).

Next, the effects of GP exposure-mediated inflammation had on the microglia, as shown below, were examined through immunostaining with anti-Iba1 antibodies. The result showed that activated microglia were observed in the cerebellum of the GP exposed F1 pup, and they were located in the PL (yellow circle in Figure 4.6). The changes in the number of microglia per 1 mm of the PL were calculated, and a significant increase was observed in across all GP exposure (Figure 4.7 bottom).

This study is designed to assess the alterations of prenatal GP exposure have on the cerebellar development of F1 offspring in the postnatal period and how it affected the behavior in adulthood using a rat model. GP reference material was used in this study instead of commercial formula as the clearance time of Roundup® is relatively short (3.1 hours in human and 14.38 hours in rat)(*53*, *54*). Considering the neurotoxic effects of GP, we think the research on the herbicide formula might not be sufficient compared

to the active chemical ingredient itself. The result also showed that prenatal GP exposure did not cause gender differences in the litter but suppressed the litter size and the bodyweight of F1 male offspring.

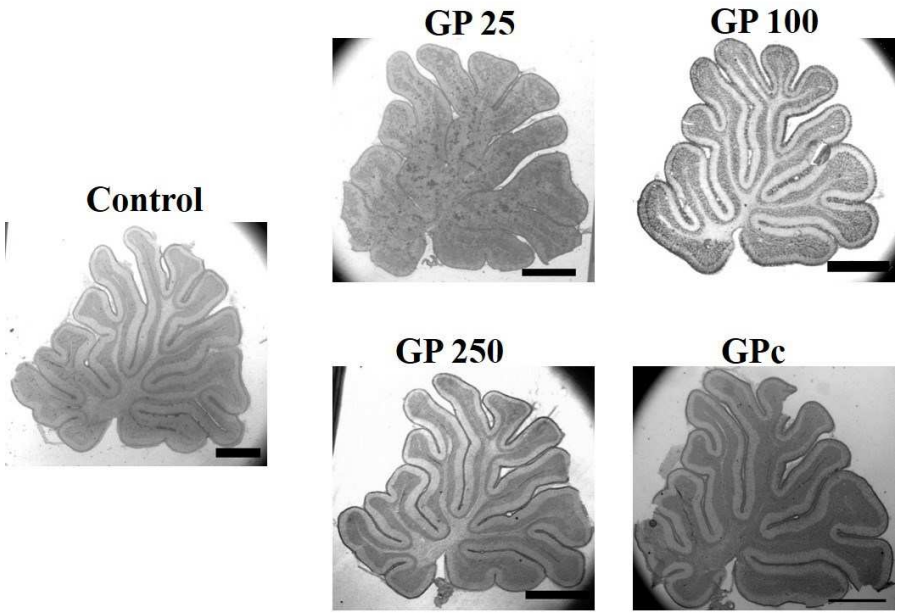

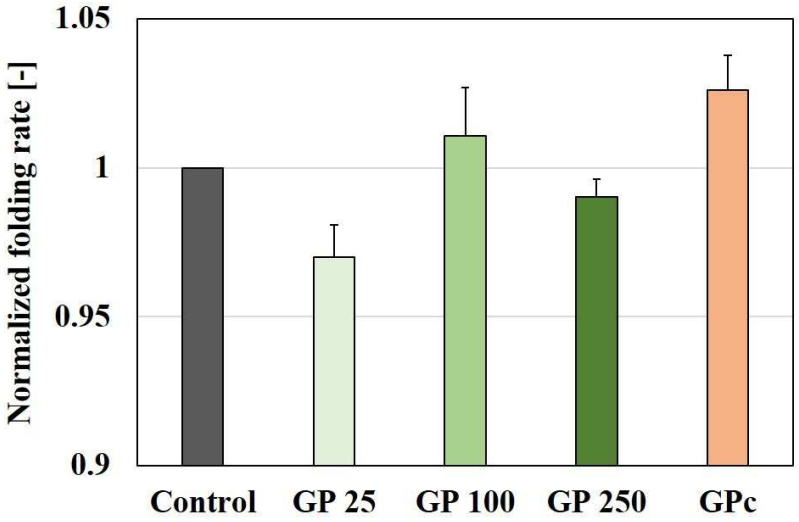

Figure 4.5 Histopathological examination of sagittal cerebellum slices to determine development abnormalities in F1 male pups (P14) born to dams exposed to GP 25, GP 100, GP 250 and GPc. Sagittal cerebellum slices (thickness = 50 µm) were obtained from fixed brain (top). Each bar represents mean ± SEM (n = 3 for each sample, bottom)

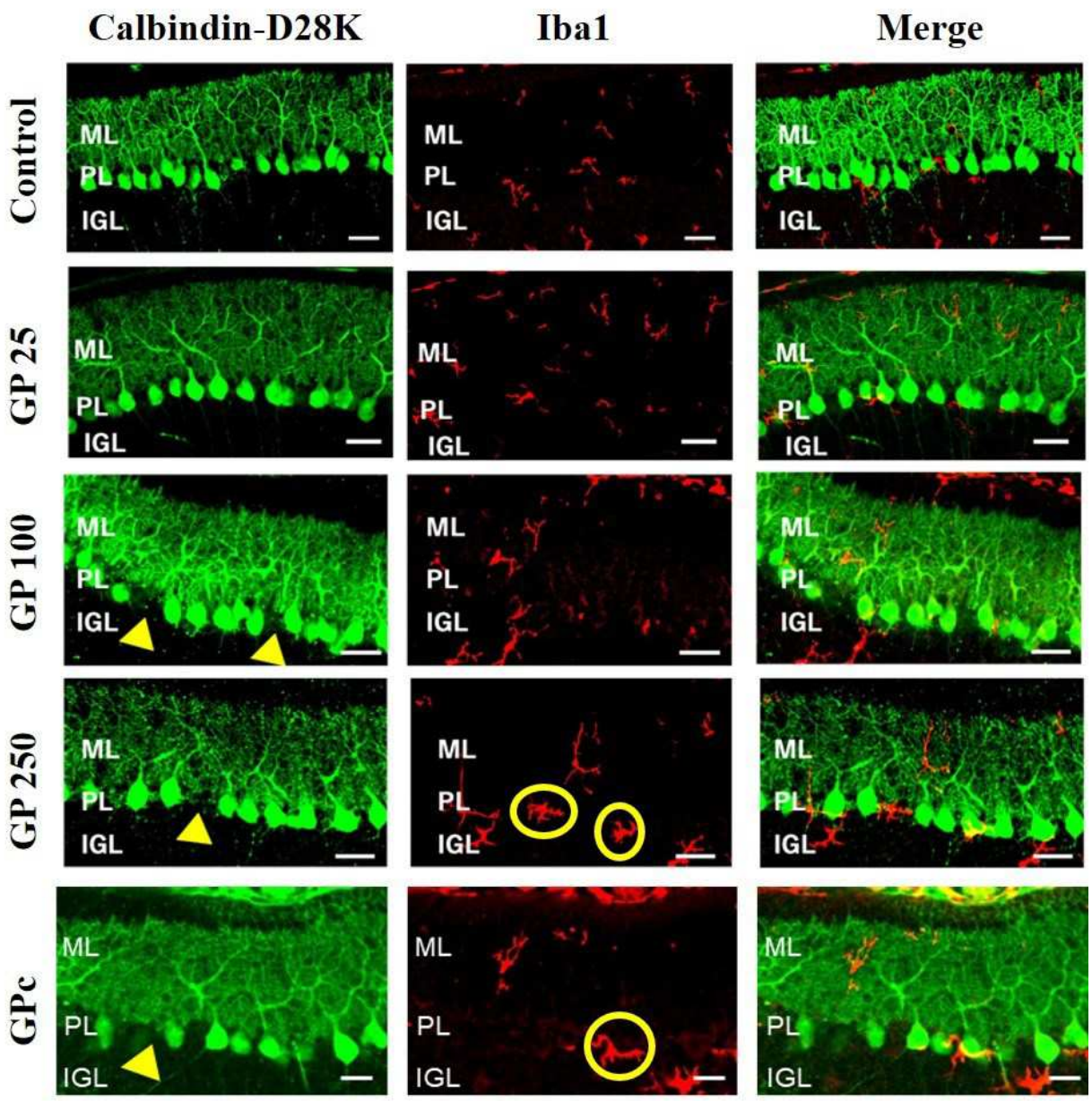

Figure 4.6 Immunostaining of sagittal cerebellum slices to determine development abnormalities in F1 male pups (P14) born to dams exposed to GP 25, GP 100, GP 250 and GPc. Sagittal cerebellum slices (thickness = 50 µm) were obtained from fixed brain (n = 3 for each sample). Yellow triangle indicates Purkinje cells deficit whereas yellow circle indicates activated microglia ascending to PL. ML: molecular layer, PL: Purkinje layer, IGL: inner granular layer. Scale bar = 100 µm

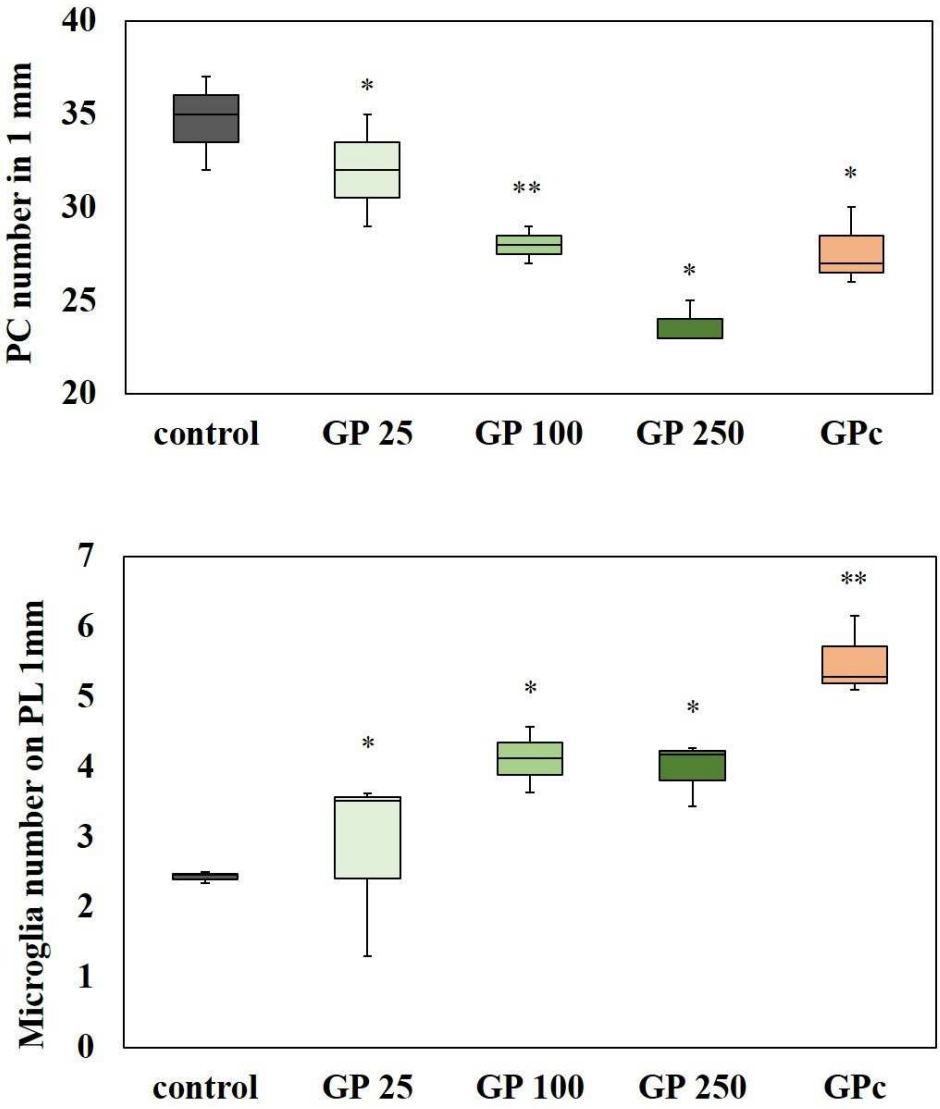

Figure 4.7 Alterations observed in Purkinje cells (top) and microglia (bottom) in F1 male pups (P14) born to dams exposed to GP 25, GP 100, GP 250 and GPc. The significant value was estimated by Dunnett's test (n = 3 for each sample, ∗∗ $p < 0.01$, ∗ $p < 0.05$ compared to control group)

The doses of GP used in this study are decided by referencing the NOAEL of GP in rat developmental toxicity study established by the Food Safety Commission of Japan in 2016. The highest dose GP 250 (250 mg/kg body weight) we used is 1/4 of the established NOAEL (1000 mg/kg body weight/day). However, these doses (acute exposure, 250 or 500 mg/kg body weight) were reported to alter

the neurobehavior of the F1 offspring(*67*), suggesting that dosage lower than the established NOAEL might affect the neurodevelopment in the rat. Therefore, it is necessary to investigate the effects of prenatal GP exposure using a lower dosage set in our study. The result showed no gender difference was observed in the litter, whereas the litter size and the bodyweight of F1 male offspring were decreased compared to the control animals. Although these alterations are not statistically significant, our findings suggest that prenatal GP exposure may jeopardize the health of F1 male offspring as they grow. Emerging evidence showed that GP exposure is a growing health concern, but its effects on cerebellar development remain unclear. Therefore, further investigation of the effect of GP exposure on the offspring is critical to understand the differences.

This thesis focused on the cerebellum because more evidence pointed out that it collaborates with multiple brain regions in order to perform communication and cognitive functions(*93*, *94*), albeit its typical role in fine motor function. These reports implied that any alteration in the cerebellum might contribute to neurological and neurodegenerative disorders as seen in other brain regions. The immunohistochemical analyses and histopathological examination of the cerebellum revealed that the number of Purkinje cells decreased from GP exposure, and the decrement was dosage-dependent and statistically significant across all GP exposure on P14. Defect in Purkinje cells is associated with neurodevelopment disorder as it plays an important role in signal transduction and neural transmission (*90*). Therefore, this alteration could be a direct result of the inflammation in early development following GP exposure. Indeed, in other reported effects of pesticide exposure on Purkinje cells, degeneration of Purkinje cells and decreased spontaneous firing rate were observed, which is strongly associated with the manifestation of neurodegenerative and neurobehavioral disorders(*95*, *96*).

Furthermore, we observed activated microglia ascending to the PL in GP exposed rats. Moreover, the number of microglia also increased in a dosage-dependent manner and statistically significant in GP 100 and GP 250. Our study suggests that dosage much lower than the established NOAEL affected cerebellar development. Activated microglia are responsible for releasing pro-inflammatory cytokines that assist in

proliferation, differentiation, apoptosis, and immune response. Excessively activated microglia in the cerebellum may contribute to the excessive production of pro-inflammatory cytokines.

4.4 Summary

Previously, using rat model, our labs found that prenatal chemical exposure altered the density and alignment of PC, the cerebellar folding, activated microglia, and changed the animal behavior. The study on the cerebellar development under prenatal chemical exposure and its connection towards higher brain function is usually overlooked. This is because until recently, popular opinions still think that it is solely responsible for motor and voluntary movements. However, increasing reports on the defects and alterations observed in developing cerebellum connected it to neurological and neurobehavioral disorders(*97–100*). Therefore, assessing the changes in cerebellar development in these circumstances is vital to better understand the exact roles played by cerebellum.

The result showed that GP exposure did not alter the morphology of cerebellum and pups born from treatment group tend to have lower body weight that control group. Perhaps this is the reason why OECD categorized GP as non-toxic chemicals. However, the results obtained in this study showed significant Purkinje cells deficit and significant increase in activated microglia in the cerebellum of the treatment group. Although the dosage used in this study is lower than NOAEL established, the significant changes occurred in the constituents that form cerebellum were greatly affected. This raised the question whether the GP usage is a health risk factor that need immediate attention.

Chapter 5 Alteration of Pro-Inflammatory Cytokine Found in Offspring Cerebellum

5.1 Introduction

This chapter will describe the alteration of pro-inflammatory cytokine found in offspring cerebellum. Significant alteration of cerebellar development observed in previous chapter might be mediated by systemic inflammation as both acute and chronic exposure showed significant changes. Therefore, finding out the production of pro-inflammatory cytokines during early development is essential to understand the mechanism behind the observed alteration. The result showed that transient inflammation occurred in the cerebellum of juvenile male rat although the production timing differed for the tested pro-inflammatory cytokines, which are inducible nitric oxide synthase (iNOS) and interleukin-1β (IL-1β).

5.1.1 Pro-inflammatory cytokines

The production of pro-inflammatory cytokines in response to the exposome is extremely important as this instigates the primary immune response in our body. This allows the anti-infectious process to take place accordingly, for instance raising body temperature and the recruit of resident macrophages in attacking the pathogens. However, excessive production of pro-inflammatory cytokines during severe inflammation may cause deleterious consequences that might exacerbate the situation. Therefore, understanding the intricated mechanism behind the release of pro-inflammatory cytokine is vital to uncover the disease mechanism.

The capacity of interleukin (IL)-l and tumor necrosis factor-alpha (TNF-α) to induce inflammatory mediators contributes to their pro-inflammatory properties. Phospholipase, cyclooxygenase and lipoxygenase are activated by IL-1 and TNF- α leading to the release of prostaglandins, thromboxane, leukotrienes, and platelet activating factor. Free radicals (superoxide [O_2^-], nitric oxide [NO]), and proteolytic enzymes are other mediators produced by target cells in response to IL-1 and TNF- α. Other

cytokines which are also involved in the cytokine cascade included chemokines such as IL-8, IL-12, and IFN-γ or T-cells derived cytokines such as TNF-β, IL-2, and IL-4. This suggested that various cytokines are at play in driving the cascade(*101*).

Since prenatal GP exposure may elicit systemic inflammation in the pregnant dam, this implied that the flow of such pro-inflammatory cytokines from the mother to offspring through vertical transmission might affect the cerebellar development of the offspring. In this thesis, inducible nitric oxide synthase (iNOS) and interleukin-1β (IL-1β) were investigated. iNOS is released by resident macrophages as an act of immune response against pathogens which induced apoptosis. Meanwhile, IL-1β was intensely produced by macrophages and microglia in central nervous system when invasion is first identified by the immune system(*102–104*).

5.2 Experimental Section

5.2.1 Animal preparation

Rats used in this section were prepared as described in section 3.2.1. Pregnant dam was subjected to acute exposure with 250 mg/kg body weight (GP 250) on E16. The control animals were prepared by oral gavage of phosphate-buffered saline, 1× PBS diluted from 10× PBS.

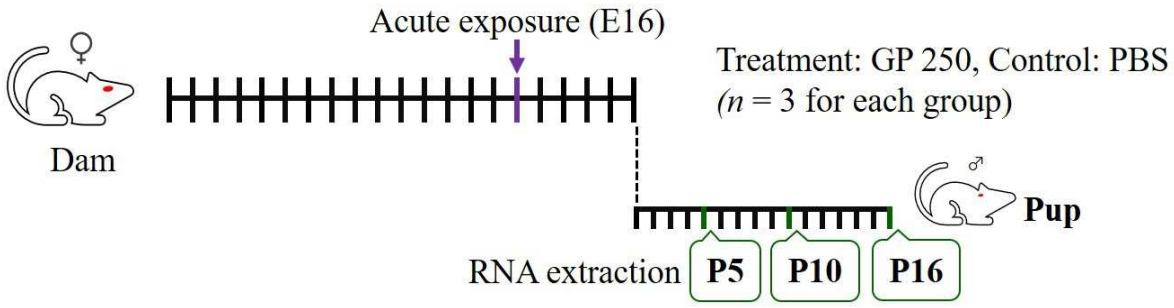

Figure 5.1 The study design to assess the production of pro-inflammatory cytokines in the cerebellum of juvenile F1 male offspring born from prenatal GP exposed dam

5.2.2 RNA extraction

Cerebellum was obtained from F1 male offspring as previously described in section 4.2.2 at P5, P10 and P16. RNA was extracted from the cerebellum using TRIzol® reagent (Thermo Fisher Scientific) following the protocol from the manufacturer. The protocol was briefly described below.

1. Rinse the homogenizer with RNA-free-water twice and then TRIzol™ reagent.
2. Add 50 µL of TRIzol™ reagent to the microtube containing cerebellum, then quick-freezing with liquid nitrogen.
3. Crush the frozen cerebellum with homogenizer. Repeat step 2 and 3 until homogenized.
4. Add 950 µL of TRIzol™ reagent, mix by inverting.
5. Incubate for more than 5 minutes in room temperature.
6. Add 200 µL of chloroform, mix by vigorous shaking, then incubate for 2 minutes.
7. Centrifuge at 12,000 x g for 15 minutes (4°C).
8. Retrieve RNA from the aqueous phase (about 500 µl), then mix with 500 µL of isopropanol.
9. Mix thoroughly by inverting, then incubate for 10 minutes in room temperature.
10. Centrifuge at 15,000 x g for 10 minutes (4°C).
11. Discard the supernatant (gel-like RNA pellet at the bottom of the microtube).
12. Add 1 mL of 70% EtOH, then mix by vortexing.
13. Centrifuge at 15,000 x g for 10 minutes (4°C).
14. Discard the supernatant, then centrifuge up to 15,000 x g and stop (to prevent ethanol carry over).
15. Discard the leftover ethanol, then + 101 µL of RNA-free-water and mix by tapping.
16. Centrifuge at 60 x g for a few seconds, then label the sample accordingly.
17. Take 1 µL of the extracted RNA sample for concentration determination using Qubit RNA HS assay kit (Invitrogen, Q32855).
18. Store all samples in deep freezer (−80°C) for further use.

5.2.3 Quantitative RT-PCR (qRT-PCR)

RNA extracted from section 5.2.2 was analyzed by qRT-PCR using QuantiTect SYBR Green RT-PCR kit (Qiagen, Valencia, CA, USA), with an ABI PRISM 7900HT sequence detection system (Applied Biosystems, Foster City, CA, USA) as previously described(*105*). The concentration of RNA extract was set to 5 μg/μL in this study. The composition of regents used in qRT-PCR was listed in Table 5.1. β-actin was used as the endogenous control and the expression level of inducible nitric oxide synthase (iNOS) and interleukin-1β (IL-1β) were examined. The DNA sequence for all the primers (Invitrogen, Thermo Fisher Scientific) used in this study was listed in Table 5.2. The thermal cycling parameters for qRT-PCR was listed in Table 5.3.

Table 5.1 Composition of reagents used in qRT-PCR

①Primer dilution		②Primer Mix		③Master Mix	
H_2O	180 μL	H_2O	3 μL	H_2O	3.75 μL
Primer	20 μL	Primer A (forward)	1 μL	SYBRgreen	10 μL
		Primer B (reverse)	1 μL	Reaction mix	0.25 μL

Table 5.2 Nucleotide sequence of primers

mRNA	forward primer	reverse primer
β-actin	5’-AAGTCCCTCACCCTCCCAAAAG-3’	5’-AAGCAATGCTGTCACCTTCCC-3’
iNOS	5’-GAGACAGGAAAGTCGGAAGC-3’	5’-GTGTTGAAGGCGTAGCTGAA-3’
IL-1β	5’-TCAGGAAGGCAGTGTCACTCATTG-3’	5’-ACACACTAGCAGGTCGTCATCATC-3’

Table 5.3 Thermal cycling parameters for qRT-PCR

step	RT	Polymerase activation	PCR	
	HOLD	HOLD	Cycle (35 – 45cycles)	
			Denature	Anneal/Extend
Temp. (℃)	48	95	95	60
Time	30 min	15 min	15 sec	1 min

5.2.4 Statistical analysis

The data were reported as mean ± standard error of mean (SEM). Student's *t*-test was performed to estimate the significance of the result. Data were reported as statistically significance when $p < 0.05$.

5.3 Results and Discussion

Neuroinflammation is an important aspect of the neurotoxic event as inflammation-mediated cell proliferation and differentiation during early development(*106*). Therefore, determining the changes of inflammation mediators and pro-inflammatory cytokines after GP exposure is important to evaluate the neurotoxicity of GP. We examined the expression levels of iNOS and IL-1β to evaluate the relation of pro-inflammatory cytokines production in the cerebellum of GP 250-F1 male rats during the neurodevelopmental period. The expression level of iNOS remained constant, slightly higher than the control, during the early neurodevelopmental period and increased significantly on P16 (Figure 5.2 top). On the other hand, the expression level of IL-1 β was significantly increased on P5 transiently but remained unchanged as compared to control after P5 (Figure 5.2 bottom). This result showed that transient inflammation occurred in the cerebellum of the juvenile rat during the postnatal period upon GP exposure, although the production timing for iNOS and IL-1 β differed.

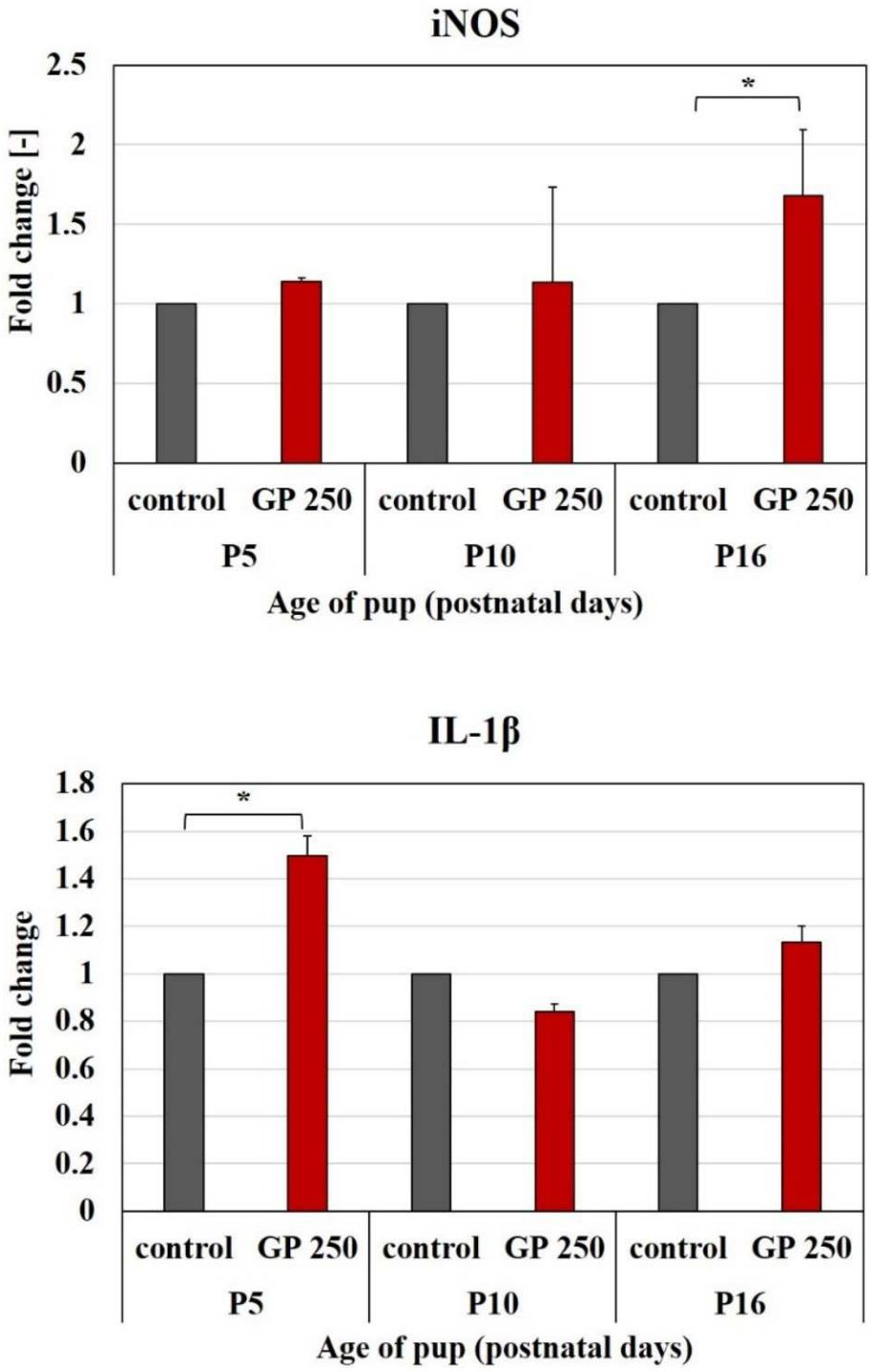

Figure 5.2 Effects of prenatal GP exposure on the expression change of iNOS (top) and IL-1β (bottom) in cerebellum from P5, P10 and P16 F1 male pups. Each bar represents mean ± SEM and the significant value was estimated by Student's *t*-test ($n = 3$ for each sample, $* p < 0.05$ compared to control group)

Indeed, our finding showed that GP 250 exposure causes inflammation in the cerebellum during early development. The expression levels of pro-inflammatory cytokines IL-1β were significantly increased transiently at the early stage of neurodevelopment, while iNOS was significantly increased at the late stage of neurodevelopment. If GP exposure would cause acute inflammation over the neurodevelopment period, all the general markers of inflammation, in this case, both iNOS and IL-1β, should be upregulated even from an early stage. However, we observed the different timing of the upregulation of these pro-inflammatory cytokines in the GP-exposed cerebellum. This implicates that iNOS and IL-1β were playing different roles during neurodevelopment. Expression of IL-1β is usually associated with inflammation in the brain, as they inhibit neurogenesis and induce apoptosis(*99*, *100*).

Meanwhile, the production of iNOS in the brain, which is inducible by IL-1β, indicates cell death caused by infection and inflammation(*101*). Transient increase of IL-1β during early-stage suggested that excessive inflammation occurred then, and these increased cytokines might induce the release of iNOS, which initiated the apoptosis. Perhaps GP exposure might not be causing acute inflammation but progress inflammatory cascade during development.

Interestingly, the production timing of both IL-1β and iNOS differed, which inferred a non-acute inflammation. The early transient increase of IL-1β following the GP exposure observed in the cerebellum might be the first domino block that falls to jump-start the whole alterations observed in this study. Expression of IL-1β stunts the normal cerebellar development by affecting the growth of Purkinje cells and activating microglia. It then facilitated the ascension of activated microglia toward the Purkinje cells and the expression of iNOS, which initiated apoptosis to clean off the degenerated Purkinje cells (Figure 5.3). Although the cerebellum morphological shape remained unaffected after the significant alterations on the Purkinje cells and microglia, their effects on the cerebellar function are still unclear.

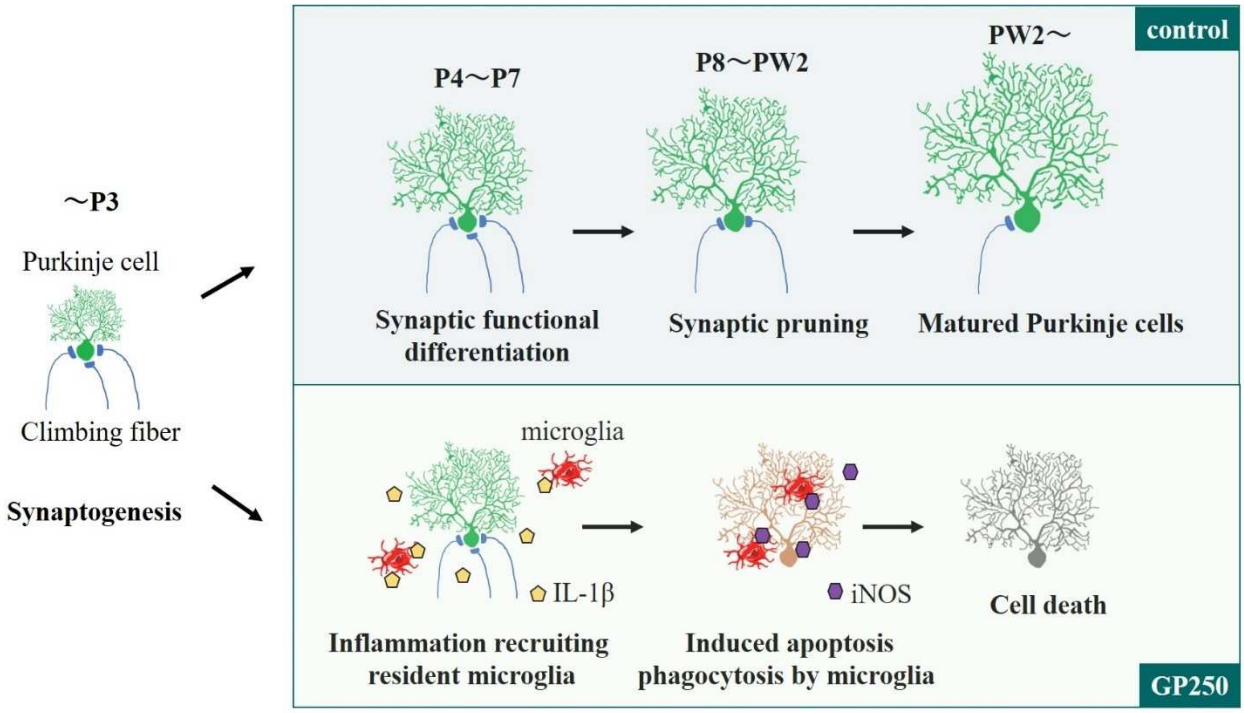

Figure 5.3 Schematic diagram depicting the proposed mechanism that affects the cerebellar Purkinje cells defects and increased microglia as observed in Chapter 4 considering the different production timing of both iNOS and IL-1β.

5.4 Summary

The result showed that transient inflammation occurred in the cerebellum of juvenile rat during postnatal period upon GP exposure although the production timing for iNOS and IL-1 β differed. This implied that systemic inflammation occurred in the F1 male offspring as pro-inflammatory cytokines were detected in their cerebellum long after they were born. This strongly suggested that the origin of such alteration start from the pregnant dams that were exposed to GP during pregnancy. Vertical transmission of pro-inflammatory cytokines might stay with the offspring, affecting their development continuously. This suggests that stress in pregnancy is a good target in studying systemic inflammation as multiple events occur during pregnancy. This causes both the mother and fetus to be more susceptible to the alterations occur over

the pregnancy(*107–109*). Indeed, the result showed that the effects might carry on after the fetus is birth, even in adulthood.

Chapter 6 Effects of Prenatal Glyphosate Exposure on the Social Behavioral Changes in Matured Animal

6.1 Introduction

This chapter expands the research scope into adulthood by examining the effects of prenatal glyphosate exposure on the social behavioral changes in matured animal. Animal behavior study is essential in understanding the brain alteration and disease phenotype. In this thesis, basic motor function and social behavior of adult male rat were observed to determine whether the transient inflammation occurred in early cerebellar development would affect their motor and cognitive function. The result demonstrated that adult male rats born from prenatal GP exposed dam were less explorative, not grooming as much and more anxious in social interaction. Less interested in exploration, decreased grooming frequency and anxiousness is indicative of cognitive impairment, and hence, the result inferred that the effects of prenatal GP exposure carried on into adulthood.

6.1.1 Animal behavior study

Rodents such as rats and mice are among the most commonly used animal models to study animal behavior. Although it is impossible to recognize the behavioral abnormalities of animals from verbal expressions, it is possible to capture behavioral abnormalities, and some behavioral changes in animals that are similar to the alterations observed in human with psychiatric disorders. Rats have been employed a lot since the beginning of animal behavior study as they perform well in the standard behavioral pharmacology experiments in order to investigate brain functions.

There are various behavioral tests that are conducted to evaluate the alterations appeared in rat model corresponding to the disease model employed in the study. Behavioral study that investigated the basic locomotor and sensory function, or analyses of more complex behavior related to cognition and emotionality are among the tests that are commonly carried out in various research setting.

Common behavioral paradigms used in the study of neuropsychiatric disorders such as depression, autism, schizophrenia, and neurodegenerative disorders, for instance Alzheimer's disease and Parkinson's disease are gaining more attention over the year. This is because assessing the behavioral changes using animal model are proven to be effective as the validity of such result is translatable in human study. Therefore, its is crucial to establish a consistent rat behavior model to guarantee the validity of that particular model concerning the behavior or disease being studied.

Basic sensory and motor function are usually tested using the open field test(*110*), horizontal ladder crossing test(*111*), rotarod test(*112*), Y - maze spontaneous alternation(*113*) and so on. These tests are designed to test the ambulatory and exploratory ability of test subjects when they are introduced to the new environment. The movements of the test subjects are usually recorded by the camera after training.

On the other hand, examination of social behavior is designed to investigate the relevance to neuropsychiatric diseases and neurodegenerative disorders. The common tests used to study social interaction and communication involved two chambers test or three chambers test, in which the test subject was placed with unfamiliar animal in a familiar environment to assess their behavioral changes. This test is particularly popular in the study of depression, autism and aggressive behavior(*114*, *115*).

6.2 Experimental section

6.2.1 Behavior test

To assess the effects of prenatal GP exposure to animal mobility and sociality, the behavior of the F1 male offspring born from GP 250-exposed dams was observed on postnatal week 6, PW6(*116*). Rat mobility was determined by the total distanced traveled. Meanwhile, central-field penetration, rearing frequency and grooming frequency were recorded as the changes in rat social behavior, i.e., anxiety-like behavior. Animal behavior was video-recorded with a digital camera on top of the test subject and analyzed using the original application improving from the Open-Source Tools, Tracker (https://physlets.org/tracker/). The rat's behavioral trajectory was displayed in coordinates on the *xy*-plane. Total distanced travelled, *D* was calculated by the equation shown below:

$$D = \sum_{i=0} \sqrt{(x_{i+1} - x_i)^2 + (y_{i+1} - y_i)^2} \qquad (1)$$

6.2.2 Open field test

Animals were habituated to the circular open field (diameter = 80 cm, height = 44 cm, RO-10, Shin Factory) for 2 minutes before the experiment started(*110*, *117*). Each rat was placed in the middle of the open field to record their following behavior changes: total distance traveled, center-field penetration, rearing frequency, and grooming frequency for 10 minutes. The apparatus was cleaned using 70% ethanol in between animals.

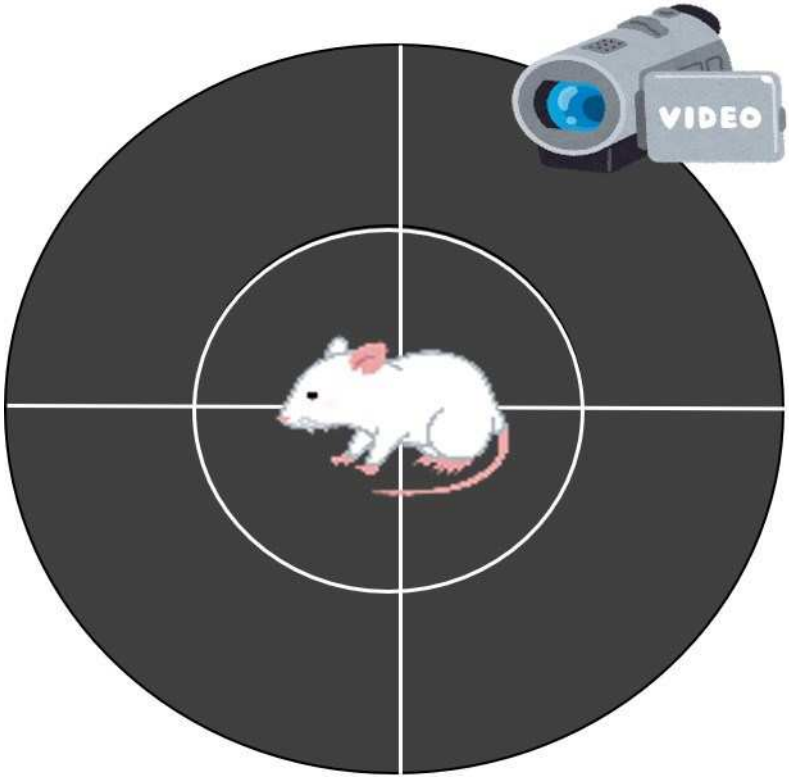

Figure 6.1 Schematic diagram depicting the open field test

6.2.3 Social behavior test

F1 male offspring was placed in the circular open field with an unfamiliar another rat to record their social behavior changes. Two types of unfamiliar rats, a similar sized (PW6) and bigger sized (PW12), were

placed in a cage within the circular open field, one by one, with the test subject and habituated for 2 minutes before the test started(*118*). The total distance traveled, rearing frequency, and grooming frequency of the test subjects were recorded for 10 minutes. The apparatus was cleaned using 70% ethanol in between animals.

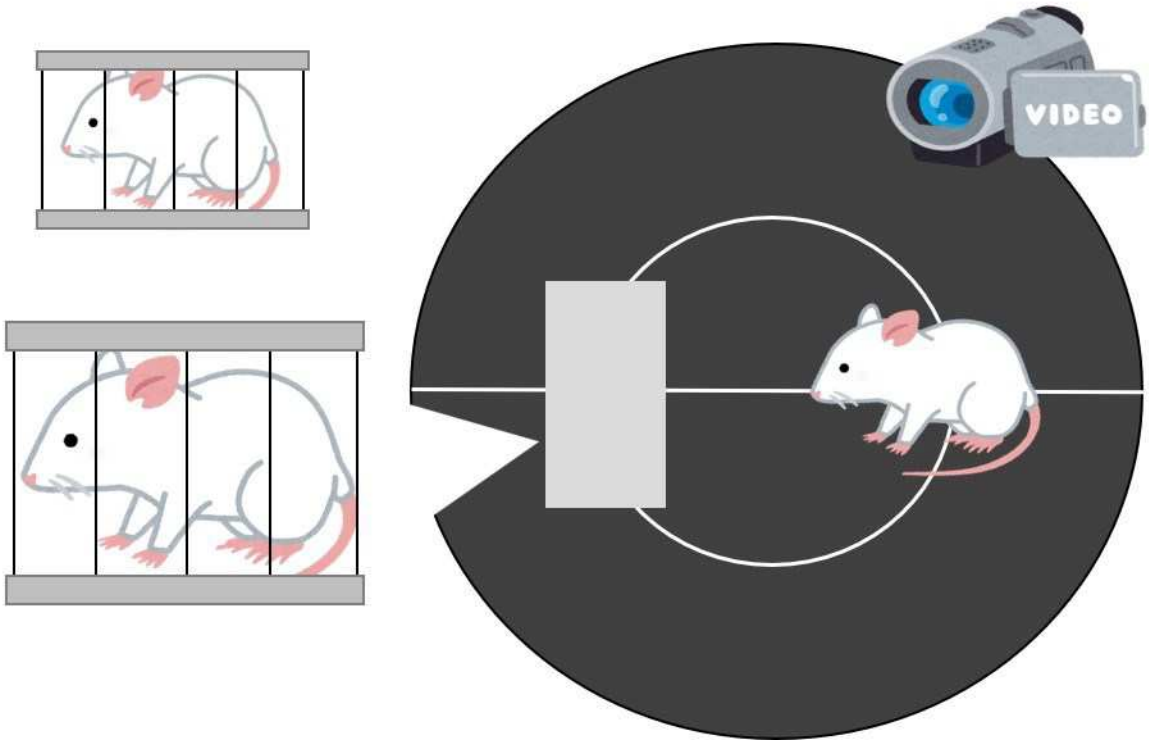

Figure 6.2 Schematic diagram depicting the social behavior test

6.2.4 Statistical analysis

The data were reported as mean ± standard error of mean (SEM). Welch's *t*-test was performed to estimate the significance of the result. Data were reported as statistically significance when $p < 0.01$, and $p < 0.05$.

6.3 Results and Discussion

The effects of GP exposure on the behavior of matured F1 male offspring were assessed via an open field test to uncover the link between behavioral change and cerebellar development abnormalities. The control rats traveled more than the GP250 exposed-mature F1 male offspring (Figure 6.3 top) but stay lesser in the center of the open field as the center-field penetration of control is much lesser (Figure 6.3 bottom). This observation showed that the GP exposed-mature F1 male offspring tend to stop and stay at the open field center during observation.

Test subjects were placed with an unfamiliar rat with different body sizes (similar size and bigger size) in the open field to record their behavior change. The control rat traveled more when placed with both unfamiliar similar-sized rat and unfamiliar bigger-sized rat comparing to the GP exposed-mature F1 male offspring (Figure 6.4).

When placed with an unfamiliar similar-sized rat, the rearing frequency of GP exposed-mature F1 male offspring was higher than the control. However, GP exposed-mature F1 male placed with an unfamiliar bigger-sized showed the rearing frequency close to zero (Figure 6.5 top). As for grooming frequency, GP exposed-mature F1 male offspring showed more grooming when placed with a similar-sized rat than a bigger-sized rat (Figure 6.5 bottom).

Recent studies on neurodegenerative disorders indicated that fear and anxiety-like behavior would connect to the cerebellum (*119*), showing involvement and collaboration of the cerebellum with other brain regions in higher brain function. Thus, it is important to assess the behavioral change of adult F1 offspring upon prenatal GP exposure better to understand the connection between cerebellar development and behavior. The behavior tests showed us that the altered behavior of GP exposed-mature F1 male offspring is linked to fear and anxiety. In the open field test, we observed lower exploratory action from GP exposed-mature F1 male offspring as they froze during exploration, and the grooming and rearing frequency were also lower than control rats, which indicates fear and anxiety towards the novel environment.

Furthermore, in the social behavior test, GP exposed-mature F1 male offspring placed with unfamiliar rats (similar or bigger) showed similar exploratory behavior as seen in the open field test as they traveled less than the control rats. In other words, their fear and anxiety manifested as "frozen" in a fight or flight situation. However, the rearing and grooming frequency differs for GP exposed-mature F1 male offspring in social behavior tests when placed with unfamiliar rats in different body sizes. When placed with an unfamiliar rat of similar size, higher rearing and grooming frequency can be interpreted as anxiety where the test subjects had to be alerted towards the stranger. Meanwhile, lower rearing and grooming frequency when placed with a bigger unfamiliar rat can be interpreted as fear as they froze most of the time.

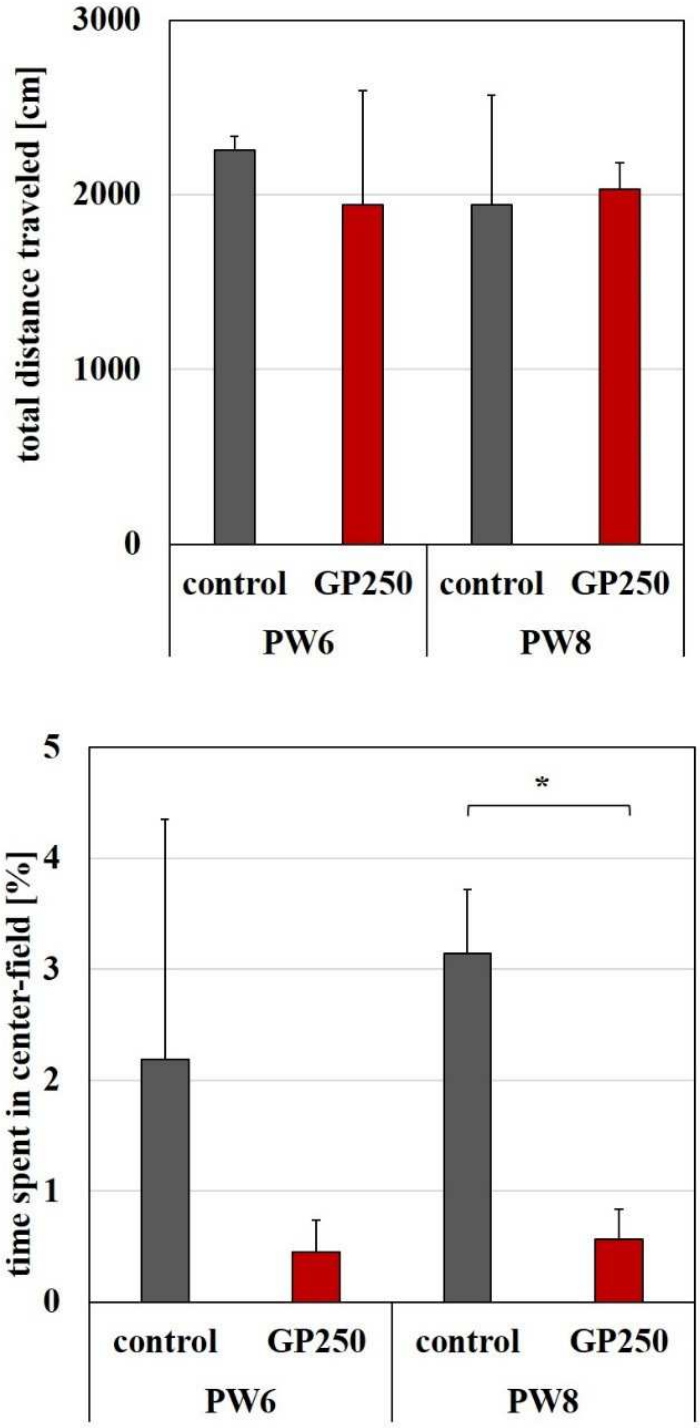

Figure 6.3 Alteration in exploratory behavior of adult male rat, total distanced traveled in cm (top); time spent in center-field in % (bottom). Each bar represents mean ± SEM and the significant value was estimated by Welch's *t*-test ($n = 3$ for each sample, $* p < 0.05$ compared to control group)

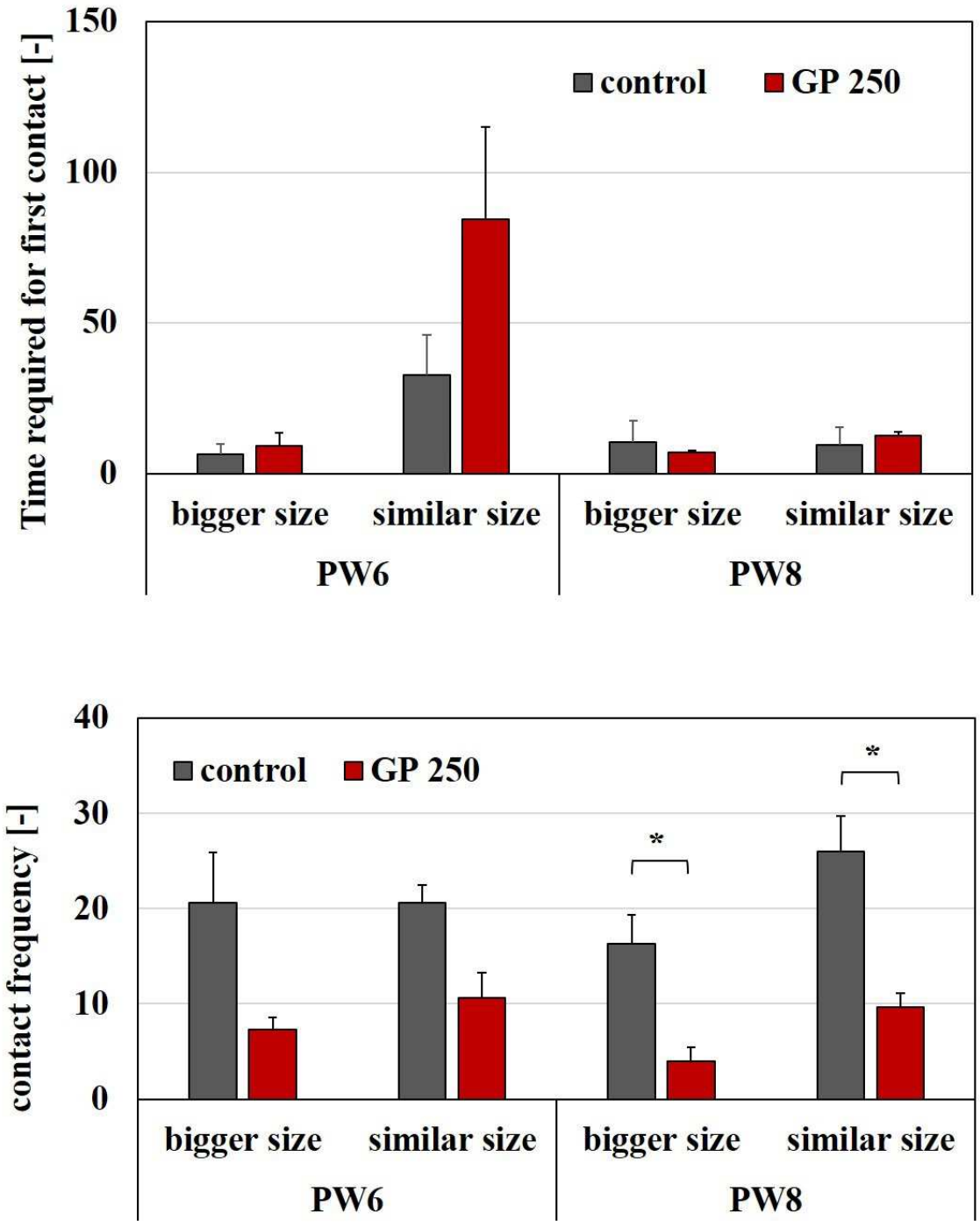

Figure 6.4 Alteration in social behavior of adult male rat, time required for first contact (top); contact frequency (bottom). Each bar represents mean ± SEM and the significant value was estimated by Welch's *t*-test ($n = 3$ for each sample, $* p < 0.05$ compared to control group)

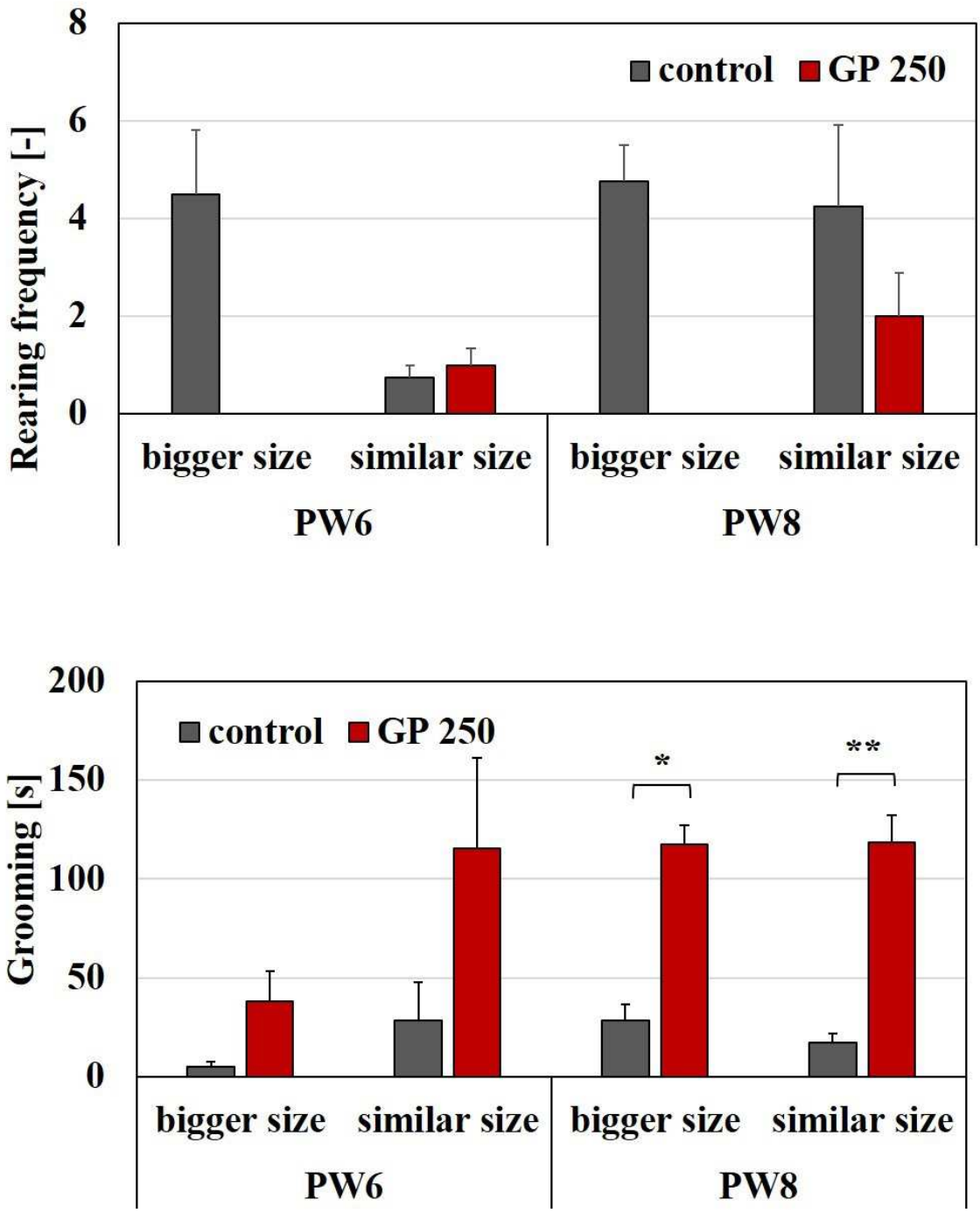

Figure 6.5 Alteration in social behavior of adult male rat, rearing frequency (top); grooming (bottom). Each bar represents mean ± SEM and the significant value was estimated by Welch's *t*-test ($n = 3$ for each sample, $** p < 0.01$, $* p < 0.05$ compared to control group)

6.4 Summary

Behavioral changes such as less time spent in the center-field, less contact frequency and increased grooming strongly implied that adult male rats born from pregnant dams that were exposed to GP prenatally express fear and anxiety when compared to control group. Taken together the results obtained from previous chapters, this suggests that the effects of prenatal GP exposure propagated throughout the life of the affected male offspring. This further strengthens the effectiveness of using the pesticides to induce systemic inflammation. This results also raised concern over the usage of GP in agriculture as the combined result greatly implied that prenatal GP exposure might cause developmental neurotoxicity in offspring.

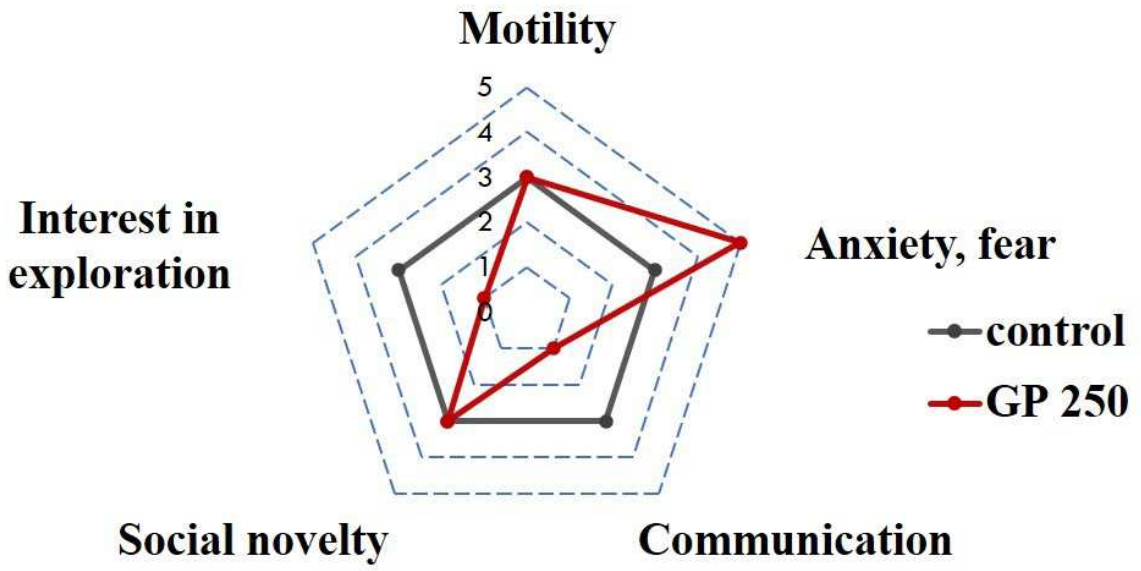

Figure 6.6 Radar chart depicting the alteration observed from behavior tests. Score =±2 when $p < 0.01$, score =±1 when $p < 0.05$ compared to control group

Chapter 7 Conclusion and future prospects

In a nutshell, this study proposed an assessment involving cellular biology, signal processing, rat study and genetic engineering in order to evaluate the alterations coming from the systemic inflammation.

7.1 On the advancement of SAM

Current result demonstrated that SAM is capable to distinguish cell in different mitotic phase based on the changes of acoustic impedance. This result was confirmed with laser confocal microscopy and SAM is proven to be more useful than conventional technique as living observation is possible. Assessing the alterations of malignant cell during mitotic phase was successful, but mapping the true acoustic impedance of cell nucleus and other organelles remained imminent, as they are target of drug study.

Two-dimensional acquisition of cell morphology was successful but distinguishing cell under foreign assault from normal healthy cell remained challenging. This is because assessing mechanical property of various cells under different condition are necessary in order to develop better SAM. Further works are necessary to label cell for comparison and observe the mentioned alteration in three-dimensional to better understand the cellular behavior of cancer cell**.** Three-dimensional acquisition was made possible by processing deconvoluted signals allowing us to observed cellular dynamic changes non-invasively. Better resolution is vital to increase preciseness in measurement in order to provide better understanding on the physiological changes *in vitro*.

Employment of SAM in translational research in close future is highly anticipated as it provides more information than conventional optic microscope.

7.2 Assessing systemic inflammation through prenatal chemical exposure

It is known that the GP, the active ingredient in many herbicides, inhibit 5-enolpyruvylshikimate-3-phosphate synthase (EPSPS), an enzyme participating in the biosynthesis of aromatic amino acids (phenylalanine, tyrosine and tryptophan) through the shikimate pathway in bacteria, fungi, and plants.

Although shikimate pathway does not exist in mammalian metabolic system, the gut flora consists of hundreds of millions of bacteria that possess this pathway, and thus are susceptible to the detrimental effects caused by GP exposure. Since the gut flora also play an important role in regulating immune defense, GP exposure may have the potential to modify the animal and human microbiota that has direct effect on the host health outcomes. Emerging evidence has suggested the GP exposure, even at low levels relevant to human environmental exposure levels can alter the gut microbiome composition and diversity. These Results demonstrated that GP exposed rats showed a decrease in the family of bacteria that are responsible for butyrate production in the gut. Butyrate is one of the essential short chain fatty acids which play important roles in protecting the intestine walls. A loss in these bacteria may present a risk as the intestine wall weakens and loss its barrier function that stops toxic substances from crossing into the bloodstream. A possible underlying mechanistic link between the gut dysbiosis and the abnormality in neurodevelopment may be that these toxic substances penetrate the placenta and affects the neurodevelopment of fetus in utero during pregnancy. However, further extensive investigation will be needed to test this hypothesis.

Moreover, it is shown that prenatal GP exposure is neurotoxic in cerebellar development. The results showed that acute prenatal GP exposure alter the production timing of IL-1β and iNOS in the cerebellum of the F1 offspring during postnatal period. Early transient expression of IL-1β upon GP exposure initiated the inflammation that contributed to the Purkinje cells degeneration and microglia activation observed in P14 cerebellum. Alteration of cerebellum during development could affects the motor function of the F1 offspring throughout their lifetime. Indeed, in both open field test and social behavior test, the matured GP 250-F1 offspring showed fear and anxiety-liked behavior. This is the first report that links the behavior change to the alteration observed in cerebellar development upon GP exposure. Further studies are necessary to unravel the connections of cerebellar development in animal behavior.

Taken together, it is important to ask the question if we can intervene with the brain development trajectory once the chemical exposure is confirmed? Moreover, can the alteration of gut flora influence the fetal brain development? If so, what is the feasible mechanism behind it? The possible hypothesis that garnered the most support right now will be maternal immune activation that bring on cytokines and

chemokines storm that had everlasting effects to the offspring after birth. Indeed, our result showed that the continuous adverse effects were carried onto adulthood, altering the neurobehavior of adult male rats. The possible mediator that drives these events is the systemic inflammation. This begs the question whether systemic inflammation is hereditary during pregnancy. Implication that the alteration occur during pregnancy will last long in the infant even after they enter adulthood is worrisome. Therefore, further research focuses on the pro-inflammatory cytokines that have deleterious consequences during pregnancy can help to shine a light on building better strategies to counter it.

References

1. M. G. Netea, F. Balkwill, M. Chonchol, F. Cominelli, M. Y. Donath, E. J. Giamarellos-Bourboulis, D. Golenbock, M. S. Gresnigt, M. T. Heneka, H. M. Hoffman, R. Hotchkiss, L. A. B. Joosten, D. L. Kastner, M. Korte, E. Latz, P. Libby, T. Mandrup-Poulsen, A. Mantovani, K. H. G. Mills, K. L. Nowak, L. A. O'Neill, P. Pickkers, T. van der Poll, P. M. Ridker, J. Schalkwijk, D. A. Schwartz, B. Siegmund, C. J. Steer, H. Tilg, J. W. M. van der Meer, F. L. van de Veerdonk, C. A. Dinarello, A guiding map for inflammation. *Nature Immunology*. **18**, 826–831 (2017).
2. A. U. Ahmed, An overview of inflammation: mechanism and consequences. *Frontiers in Biology*. **6**, 274 (2011).
3. C. Serhan, P. Ward, D. Gilroy, *Fundamentals of Inflammation* (Cambridge University Press, 2010).
4. J. Henao-Mejia, E. Elinav, T. Strowig, R. A. Flavell, Inflammasomes: far beyond inflammation. *Nature Immunology*. **13**, 321–324 (2012).
5. L. L. Munn, Cancer and inflammation. *WIREs Systems Biology and Medicine*. **9** (2017), doi:10.1002/wsbm.1370.
6. G. Ryan, G. Majno, Acute inflammation. A review. *The American Journal of Pathology*. **86**, 183–276 (1977).
7. M. L. Varela, M. Mogildea, I. Moreno, A. Lopes, Acute Inflammation and Metabolism. *Inflammation*. **41**, 1115–1127 (2018).
8. L. Ferrero-Miliani, O. H. Nielsen, P. S. Andersen, S. E. Girardin, Chronic inflammation: Importance of NOD2 and NALP3 in interleukin-1β generation. *Clinical and Experimental Immunology*. **147** (2007), pp. 227–235.
9. D. Hanahan, R. A. Weinberg, Hallmarks of cancer: The next generation. *Cell*. **144** (2011), pp. 646–674.
10. M. P. Murtaugh, M. J. Baarsch, Y. Zhou, R. W. Scamurra, G. Lin, Inflammatory cytokines in animal health and disease. *Veterinary Immunology and Immunopathology*. **54**, 45–55 (1996).
11. I. Marafini, S. Sedda, V. Dinallo, G. Monteleone, Inflammatory cytokines: from discoveries to therapies in IBD. *Expert Opinion on Biological Therapy*. **19**, 1207–1217 (2019).

12. L. Vitkovic, J. Bockaert, C. Jacque, "Inflammatory" Cytokines. *Journal of Neurochemistry*. **74**, 457–471 (2001).

13. J. R. Challis, C. J. Lockwood, L. Myatt, J. E. Norman, J. F. Strauss, F. Petraglia, Inflammation and Pregnancy. *Reproductive Sciences*. **16**, 206–215 (2009).

14. Y. Saijo, M. Tanaka, H. Okawai, F. Dunn, The ultrasonic properties of gastric cancer tissues obtained with a scanning acoustic microscope system. *Ultrasound in Medicine & Biology*. **17**, 709–714 (1991).

15. X. Tang, T. B. Kuhlenschmidt, J. Zhou, P. Bell, F. Wang, M. S. Kuhlenschmidt, T. A. Saif, Mechanical Force Affects Expression of an In Vitro Metastasis-Like Phenotype in HCT-8 Cells. *Biophysical Journal*. **99**, 2460–2469 (2010).

16. K. Kobayashi, S. Yoshida, Y. Saijo, N. Hozumi, in *Ultrasonics* (Elsevier, 2014), vol. 54, pp. 1922–1928.

17. C. Wild, E. Weiderpass, B. Stewart, editors, *World Cancer Report: Cancer Research for Cancer Prevention* (IARC, 2020).

18. S. Carkaci, L. Santiago, B. E. Adrada, G. J. Whitman, Screening for Breast Cancer with Sonography. *Seminars in Roentgenology*. **46**, 285–291 (2011).

19. R. Berezney, The nuclear matrix: A heuristic model for investigating genomic organization and function in the cell nucleus. *Journal of Cellular Biochemistry*. **47**, 109–123 (1991).

20. J. D. Watson, F. H. C. Crick, The Structure of DNA. *Cold Spring Harbor Symposia on Quantitative Biology*. **18**, 123–131 (1953).

21. L. Pray, Discovery of DNA Structure and Function: Watson and Crick. *Nature Education*. **1** (2008).

22. A. Annunziato, DNA Packaging: Nucleosomes and Chromatin. *Nature Education*. **1** (2008).

23. M. Bhasin, E. L. Reinherz, P. A. Reche, Recognition and Classification of Histones Using Support Vector Machine. *Journal of Computational Biology*. **13**, 102–112 (2006).

24. Tan Lab at Penn State, (available at http://www.personal.psu.edu/sxt30/projects_nucleosomerecogntion.html).

25. R. A. Horton, L. A. Moran, G. Scrimgeour, D. Rawn, M. Perry, *Principles of Biochemistry: International Edition, 4th Edition* (Prentice Hall, Upper Sadle River, NJ, ed. 4, 2006).

26. K. Struhl, Histone acetylation and transcriptional regulatory mechanisms. *Genes & Development*. **12**, 599–606 (1998).

27. P. A. Wade, D. Pruss, A. P. Wolffe, Histone acetylation: chromatin in action. *Trends in Biochemical Sciences*. **22**, 128–132 (1997).

28. R. W. Johnstone, Histone-deacetylase inhibitors: novel drugs for the treatment of cancer. *Nature Reviews Drug Discovery*. **1**, 287–299 (2002).

29. A. J. M. de RUIJTER, A. H. van GENNIP, H. N. CARON, S. KEMP, A. B. P. van KUILENBURG, Histone deacetylases (HDACs): characterization of the classical HDAC family. *Biochemical Journal*. **370**, 737–749 (2003).

30. A. v Chernov, J.-L. Prétet, R. A. Katz, N. Lourenço De Freitas, M. G. Deberaldini, D. Gomes, A. R. Pavan, Â. Sousa, J. Leandro, D. Santos, C. P. Soares, Histone Deacetylase Inhibitors as Therapeutic Interventions on Cervical Cancer Induced by Human Papillomavirus. *Frontiers in Cell and Developmental Biology | www.frontiersin.org*. **1**, 592868 (2021).

31. P. J. van den Elsen, M. CJA van Eggermond, F. Puentes, P. van der Valk, D. Baker, S. Amor, The epigenetics of multiple sclerosis and other related disorders, doi:10.1016/j.msard.2013.08.007.

32. T. J. Mitchison, E. D. Salmon, Mitosis: a history of division. *Nature cell biology*. **3**, E17–E21 (2001).

33. J. Richard Mcintosh, Mitosis. *Cold Spring Harbor Perspectives in Biology*. **8** (2016), doi:10.1101/cshperspect.a023218.

34. M. A. Jordan, L. Wilson, Microtubules as a target for anticancer drugs. *Nature Reviews Cancer*. **4**, 253–265 (2004).

35. Z. Li, X. Chen, X. Sun, Q. Zhou, J. Chen, G. H. Leno, J. F. Engelhardt, Nuclear transfer of M-phase ferret fibroblasts synchronized with the microtubule inhibitor demecolcine. *Journal of Experimental Zoology Part A: Comparative Experimental Biology*. **303A**, 1126–1134 (2005).

36. N. Hozumi, S. Yoshida, K. Kobayashi, Three-dimensional acoustic impedance mapping of cultured biological cells. *Ultrasonics*. **99** (2019), doi:10.1016/j.ultras.2019.105966.

37. R. Nagaoka, H. Hasegawa, K. Tamura, S. Yoshida, N. Hozumi, K. Kobayashi, Suppression of reflected signals from substrate as clutters for cell measurements using acoustic impedance microscopy. *Ultrasonics*. **118** (2021), doi:10.1016/j.ultras.2021.106580.

38. R. H. Rahayu, K. Takanashi, T. Tiong Kwong Soon, I. Seviaryna, R. Maev, K. Kobayashi, N. Hozumi, S. Yoshida, Reaction assessment of cultured breast cancer cells exposed to anticancer agents using microscale acoustic impedance profile. *Japanese Journal of Applied Physics*. **57** (2018), doi:10.7567/JJAP.57.07LF26.

39. T. Tiong Kwong Soon, R. Sasaki, E. B. PRASTIKA, Y. Kawaguchi, K. Kobayashi, N. Hozumi, S. Yoshida, Evaluation of elastic change during mitotic phase of murine breast cancer cells using scanning acoustic microscope. *Japanese Journal of Applied Physics* (2022), doi:10.35848/1347-4065/ac54f7.

40. T. Tiong Kwong Soon, T. W. Chean, H. Yamada, K. Takahashi, N. Hozumi, K. Kobayashi, S. Yoshida, Effects of anticancer drugs on glia-glioma brain tumor model characterized by acoustic impedance microscopy. *Japanese Journal of Applied Physics*. **56** (2017), doi:10.7567/JJAP.56.07JF15.

41. A. I. Gunawan, N. Hozumi, S. Yoshida, Y. Saijo, K. Kobayashi, S. Yamamoto, Numerical analysis of ultrasound propagation and reflection intensity for biological acoustic impedance microscope. *Ultrasonics*. **61**, 79–87 (2015).

42. A. I. Gunawan, N. Hozumi, K. Takahashi, S. Yoshida, Y. Saijo, K. Kobayashi, S. Yamamoto, Numerical analysis of acoustic impedance microscope utilizing acoustic lens transducer to examine cultured cells. *Ultrasonics*. **63**, 102–110 (2015).

43. E. Bagus Prastika, T. Shintani, T. Kawashima, Y. Murakami, N. Hozumi, T. Tiong Kwong Soon, S. Yoshida, R. Nagaoka, K. Kobayashi, Time and frequency domain deconvolution for cross-sectional cultured cell observation using an acoustic impedance microscope. *Ultrasonics*. **119**, 106601 (2022).

44. N. Hozumi, R. Yamashita, C. K. Lee, M. Nagao, K. Kobayashi, Y. Saijo, M. Tanaka, N. Tanaka, S. Ohtsuki, Ultrasonic sound speed microscope for biological tissue characterization driven by nanosecond pulse. *Acoustical Science and Technology*. **24**, 386–390 (2003).

45. N. Hozumi, R. Yamashita, C. K. Lee, M. Nagao, K. Kobayashi, Y. Saijo, M. Tanaka, N. Tanaka, S. Ohtsuki, in *Ultrasonics* (2004), vol. 42, pp. 717–722.

46. T. W. Chean, N. Hozumi, S. Yoshida, K. Kobayashi, Y. Ogura, Mutual conversion between B-mode image and acoustic impedance image. *Japanese Journal of Applied Physics*. **56** (2017), doi:10.7567/JJAP.56.07JF18.

47. Y. Saijo, E. S. Filho, H. Sasaki, T. Yambe, M. Tanaka, N. Hozumi, K. Kobayashi, N. Okada, Ultrasonic tissue characterization of atherosclerosis by a speed-of-sound microscanning system. *IEEE Transactions on Ultrasonics, Ferroelectrics, and Frequency Control*. **54**, 1571–1576 (2007).

48. A. Nakano, T. Uemura, N. Hozumi, M. Nagao, S. Yoshida, K. Kobayashi, S. Yamamoto, Y. S. Tohoku, in *Proceedings - IEEE Ultrasonics Symposium* (2008), pp. 1893–1896.

49. J. Schindelin, I. Arganda-Carreras, E. Frise, V. Kaynig, M. Longair, T. Pietzsch, S. Preibisch, C. Rueden, S. Saalfeld, B. Schmid, J. Y. Tinevez, D. J. White, V. Hartenstein, K. Eliceiri, P. Tomancak, A. Cardona, Fiji: An open-source platform for biological-image analysis. *Nature Methods*. **9** (2012), pp. 676–682.

50. D. L. Wen, Q. Yang, J. Tong CHEN, H. Zhou, R. Ming LIU, X. Tai HUANG, Dynamic distribution of Ser-10 phosphorylated histone H3 in cytoplasm of MCF-7 and CHO cells during mitosis. *Cell Research*. **15**, 120–126 (2005).

51. S. He, J. R. Davie, Sp1 and Sp3 foci distribution throughout mitosis. *Journal of Cell Science*. **119**, 1063–1070 (2006).

52. Atsdr, Toxicological Profile for Glyphosate - Draft for Public Comment (2020).

53. C. Cox, Glyphosate (Roundup). *Journal of Pesticide Reform*. **18**, 3–16 (1998).

54. Glyphosate. *Food Safety*. **4**, 93–102 (2016).

55. D. M. Roberts, N. A. Buckley, F. Mohamed, M. Eddleston, D. A. Goldstein, A. Mehrsheikh, M. S. Bleeke, A. H. Dawson, A prospective observational study of the clinical toxicology of glyphosate-containing herbicides in adults with acute self-poisoning. *Clinical Toxicology*. **48**, 129–136 (2010).

56. A. Anadón, M. R. Martínez-Larrañaga, M. A. Martínez, V. J. Castellano, M. Martínez, M. T. Martin, M. J. Nozal, J. L. Bernal, Toxicokinetics of glyphosate and its metabolite aminomethyl phosphonic acid in rats. *Toxicology Letters*. **190**, 91–95 (2009).

57. O. S. von Ehrenstein, C. Ling, X. Cui, M. Cockburn, A. S. Park, F. Yu, J. Wu, B. Ritz, Prenatal and infant exposure to ambient pesticides and autism spectrum disorder in children: population based case-control study. *BMJ*. **364**, 962 (2019).

58. C. E. Gallegos, M. Bartos, C. Bras, F. Gumilar, M. C. Antonelli, A. Minetti, Exposure to a glyphosate-based herbicide during pregnancy and lactation induces neurobehavioral alterations in rat offspring. *NeuroToxicology*. **53**, 20–28 (2016).

59. O. K. Borggaard, A. L. Gimsing, Fate of glyphosate in soil and the possibility of leaching to ground and surface waters: a review. *Pest Management Science*. **64**, 441–456 (2008).

60. E. Sherwin, S. R. Bordenstein, J. L. Quinn, T. G. Dinan, J. F. Cryan, Microbiota and the social brain. *Science*. **366** (2019), doi:10.1126/SCIENCE.AAR2016.

61. J. F. Cryan, K. J. O'riordan, C. S. M. Cowan, K. v. Sandhu, T. F. S. Bastiaanssen, M. Boehme, M. G. Codagnone, S. Cussotto, C. Fulling, A. v. Golubeva, K. E. Guzzetta, M. Jaggar, C. M. Long-Smith, J. M. Lyte, J. A. Martin, A. Molinero-Perez, G. Moloney, E. Morelli, E. Morillas, R. O'connor, J. S. Cruz-Pereira, V. L. Peterson, K. Rea, N. L. Ritz, E. Sherwin, S. Spichak, E. M. Teichman, M. van de Wouw, A. P. Ventura-Silva, S. E. Wallace-Fitzsimons, N. Hyland, G. Clarke, T. G. Dinan, The microbiota-gut-brain axis. *Physiological Reviews*. **99**, 1877–2013 (2019).

62. E. A. Mayer, K. Tillisch, A. Gupta, Gut/brain axis and the microbiota. *Journal of Clinical Investigation*. **125**, 926–938 (2015).

63. I. Sekirov, S. L. Russell, L. Caetano, M. Antunes, B. B. Finlay, Gut Microbiota in Health and Disease. *Physiological reviews* (2010), doi:10.1152/physrev.00045.2009.-Gut.

64. S. Roy Sarkar, S. Banerjee, Gut microbiota in neurodegenerative disorders. *Journal of Neuroimmunology*. **328** (2019), pp. 98–104.

65. S. M. Jandhyala, R. Talukdar, C. Subramanyam, H. Vuyyuru, M. Sasikala, D. N. Reddy, Role of the normal gut microbiota. *World Journal of Gastroenterology*. **21**, 8836–8847 (2015).

66. S. Ghaisas, J. Maher, A. Kanthasamy, Gut microbiome in health and disease: Linking the microbiome-gut-brain axis and environmental factors in the pathogenesis of systemic and neurodegenerative diseases. *Pharmacology and Therapeutics*. **158** (2016), pp. 52–62.

67. Y. Aitbali, S. Ba-M'hamed, N. Elhidar, A. Nafis, N. Soraa, M. Bennis, Glyphosate based- herbicide exposure affects gut microbiota, anxiety and depression-like behaviors in mice. *Neurotoxicology and Teratology*. **67**, 44–49 (2018).

68. J. G. Caporaso, J. Kuczynski, J. Stombaugh, K. Bittinger, F. D. Bushman, E. K. Costello, N. Fierer, A. G. Pẽa, J. K. Goodrich, J. I. Gordon, G. A. Huttley, S. T. Kelley, D. Knights, J. E. Koenig, R. E. Ley, C. A. Lozupone, D. McDonald, B. D. Muegge, M. Pirrung, J. Reeder, J. R. Sevinsky, P. J. Turnbaugh, W. A. Walters, J. Widmann, T. Yatsunenko, J. Zaneveld, R. Knight, QIIME allows analysis of high-throughput community sequencing data. *Nature Methods*. **7**, 335–336 (2010).

69. E. Bolyen, J. R. Rideout, M. R. Dillon, N. A. Bokulich, C. C. Abnet, G. A. Al-Ghalith, H. Alexander, E. J. Alm, M. Arumugam, F. Asnicar, Y. Bai, J. E. Bisanz, K. Bittinger, A. Brejnrod, C. J. Brislawn, C. T. Brown, B. J. Callahan, A. M. Caraballo-Rodríguez, J. Chase, E. K. Cope, R. da Silva, C. Diener, P. C. Dorrestein, G. M. Douglas, D. M. Durall, C. Duvallet, C. F. Edwardson, M. Ernst, M. Estaki, J. Fouquier, J. M. Gauglitz, S. M. Gibbons, D. L. Gibson, A. Gonzalez, K. Gorlick, J. Guo, B. Hillmann, S. Holmes, H. Holste, C. Huttenhower, G. A. Huttley, S. Janssen, A. K. Jarmusch, L. Jiang, B. D. Kaehler, K. bin Kang, C. R. Keefe, P. Keim, S. T. Kelley, D. Knights, I. Koester, T. Kosciolek, J. Kreps, M. G. I. Langille, J. Lee, R. Ley, Y.-X. Liu, E. Loftfield, C. Lozupone, M. Maher, C. Marotz, B. D. Martin, D. McDonald, L. J. McIver, A. v. Melnik, J. L. Metcalf, S. C. Morgan, J. T. Morton, A. T. Naimey, J. A. Navas-Molina, L. F. Nothias, S. B. Orchanian, T. Pearson, S. L. Peoples, D. Petras, M. L. Preuss, E. Pruesse, L. B. Rasmussen, A. Rivers, M. S. Robeson, P. Rosenthal, N. Segata, M. Shaffer, A. Shiffer, R. Sinha, S. J. Song, J. R. Spear, A. D. Swafford, L. R. Thompson, P. J. Torres, P. Trinh, A. Tripathi, P. J. Turnbaugh, S. Ul-Hasan, J. J. J. van der Hooft, F. Vargas, Y. Vázquez-Baeza, E. Vogtmann, M. von Hippel, W. Walters, Y. Wan, M. Wang, J. Warren, K. C. Weber, C. H. D. Williamson, A. D. Willis, Z. Z. Xu, J. R. Zaneveld, Y. Zhang, Q. Zhu, R. Knight, J. G.

Caporaso, Reproducible, interactive, scalable and extensible microbiome data science using QIIME 2. *Nature Biotechnology*. **37**, 852–857 (2019).

70. A. Bunn, M. Korpela, An Introduction to dplR (2019), doi:10.1016/j.dendro.2008.01.002.

71. J. Oksanen, F. G. Blanchet, M. Friendly, R. Kindt, P. Legendre, D. Mcglinn, P. R. Minchin, R. B. O'hara, G. L. Simpson, P. Solymos, M. Henry, H. Stevens, E. Szoecs, H. W. Maintainer, Package "vegan" Title Community Ecology Package Version 2.5-7 (2020).

72. F. Rohart, B. Benoıˆt Gautier, A. Singh, K.-A. L. Cao, mixOmics: An R package for 'omics feature selection and multiple data integration (2017), doi:10.1371/journal.pcbi.1005752.

73. H. Wickham, ggplot2: Elegant Graphics for Data Analysis Second Edition (2009) (available at http://www.springer.com/series/6991).

74. A. Duncan Murdoch, E. D. Chow, M. Duncan Murdoch, Package "ellipse" Title Functions for Drawing Ellipses and Ellipse-Like Confidence Regions (2020).

75. H. SAITOH, K. GAMOH, Liquid chromatography/mass spectrometric analysis of 2-nitrophenyihydrazide derivatives of low-molecular organic acids. *BUNSEKI KAGAKU*. **52**, 923–929 (2003).

76. Y. Amakura, K. Kondo, H. Akiyama, H. Ito, T. Hatano, T. Yoshida, T. Maitani, スギヒラタケに含まれる特徴的な長鎖脂肪酸について. 食品衛生学雑誌. **47**, 178–181 (2006).

77. A. Geirnaert, M. Calatayud, C. Grootaert, D. Laukens, S. Devriese, G. Smagghe, M. de Vos, N. Boon, T. van de Wiele, Butyrate-producing bacteria supplemented in vitro to Crohn's disease patient microbiota increased butyrate production and enhanced intestinal epithelial barrier integrity OPEN. *Scientific reports*. **7**, 1–14 (2017).

78. M. Vital, A. Karch, D. H. Pieper, Colonic Butyrate-Producing Communities in Humans: an Overview Using Omics Data. *mSystems*. **2** (2017), doi:10.1128/MSYSTEMS.00130-17/FORMAT/EPUB.

79. T. Konikoff, U. Gophna, Oscillospira: a Central, Enigmatic Component of the Human Gut Microbiota. *Trends in Microbiology*. **24**, 523–524 (2016).

80. Y. chen, H. Zheng, G. Zhang, fang-lan chen, L. chen, Z. Yang, High Oscillospira abundance indicates constipation and low BMi in the Guangdong Gut Microbiome project (2020), doi:10.1038/s41598-020-66369-z.

81. M. Boutard, T. Cerisy, P.-Y. Nogue, A. Alberti, J. Weissenbach, Functional Diversity of Carbohydrate-Active Enzymes Enabling a Bacterium to Ferment Plant Biomass. *PLoS Genet*. **10**, 1004773 (2014).

82. F. Wu, X. Guo, J. Zhang, M. Zhang, Z. Ou, Y. Peng, Phascolarctobacterium faecium abundant colonization in human gastrointestinal tract. *Experimental and Therapeutic Medicine*. **14**, 3122–3126 (2017).

83. C. Willyard, Could baby's first bacteria take root before birth? *Nature*. **553**, 264–266 (2018).

84. B. Gottwald, Z. Mihajlovic, B. Wilde, H. M. Mehdorn, Does the cerebellum contribute to specific aspects of attention? *Neuropsychologia*. **41**, 1452–1460 (2003).

85. P. Bugalho, B. Correa, M. Viana-Baptista, Role of the cerebellum in cognitive and behavioural control: scientific basis and investigation models. *Acta Médica Portuguesa*. **19**, 257–67 (2006).

86. S. M. Ravizza, C. A. Mccormick, J. E. Schlerf, T. Justus, R. B. Ivry, J. A. Fiez, S. Ravizza, Cerebellar damage produces selective deficits in verbal working memory. *Brain*. **129**, 306–320 (2006).

87. 俊也真鍋, 寿森, 雅彦渡辺, 栄之岡野, 剛宮川, *改訂第3版 脳神経科学イラストレイテッド-分子・細胞から実験技術まで* (羊土社, 2013; https://www.yodosha.co.jp/yodobook/book/9784758120401/?ad=fb).

88. Postnatal Neurogenesis in the Developing Cerebellum | Brain Development, (available at https://braindevelopmentmaps.org/home/brain-map-sets/postnatal-neurogenesis-in-the-developing-cerebellum/).

89. J. E. Slemmer, C. I. de Zeeuw, J. T. Weber, Don't get too excited: mechanisms of glutamate-mediated Purkinje cell death. *Progress in Brain Research*. **148**, 367–390 (2005).

90. M. Ito, Historical review of the significance of the cerebellum and the role of Purkinje cells in motor learning. *Annals New York Academy of Sciences*. **978**, 273–288 (2002).

91. M. Rahimi-Balaei, H. Bergen, J. Kong, H. Marzban, Neuronal migration during development of the cerebellum. *Frontiers in Cellular Neuroscience*. **12** (2018), , doi:10.3389/fncel.2018.00484.

92. C. J. Stoodley, J. D. Schmahmann, Evidence for topographic organization in the cerebellum of motor control versus cognitive and affective processing. *Cortex*. **46**, 831–844 (2010).

93. T. D. Rogers, E. Mckimm, P. E. Dickson, D. Goldowitz, C. D. Blaha, G. Mittleman, Is autism a disease of the cerebellum?: An integration of clinical and pre-clinical research. *Frontiers in Systems Neuroscience* (2013), doi:10.3389/fnsys.2013.00015.

94. D. R. Hampson, G. J. Blatt, Autism spectrum disorders and neuropathology of the cerebellum. *Frontiers in Neuroscience*. **9** (2015), , doi:10.3389/fnins.2015.00420.

95. J. Kimura-Kuroda, Y. Komuta, Y. Kuroda, M. Hayashi, H. Kawano, Nicotine-like effects of the neonicotinoid insecticides acetamiprid and imidacloprid on cerebellar neurons from neonatal rats. *PLoS ONE*. **7** (2012), doi:10.1371/journal.pone.0032432.

96. T. Sadakata, W. Kakegawa, A. Mizoguchi, M. Washida, R. Katoh-Semba, F. Shutoh, T. Okamoto, H. Nakashima, K. Kimura, M. Tanaka, Y. Sekine, S. Itohara, M. Yuzaki, S. Nagao, T. Furuichi, Impaired cerebellar development and function in mice lacking CAPS2, a protein involved in neurotrophin release. *Journal of Neuroscience*. **27**, 2472–2482 (2007).

97. W. E. Kaufmann, K. L. Cooper, S. H. Mostofsky, G. T. Capone, W. R. Kates, C. J. Newschaffer, I. Bukelis, M. H. Stump, A. E. Jann, D. C. Lanham, K. Krieger, Specificity of Cerebellar Vermian Abnormalities in Autism: A Quantitative Magnetic Resonance Imaging Study. *Journal of child neurology*. **18**, 463–470 (2003).

98. J. Skefos, C. Cummings, K. Enzer, J. Holiday, K. Weed, E. Levy, T. Yuce, T. Kemper, M. Bauman, Regional alterations in Purkinje cell density in patients with autism. *PLoS ONE*. **9** (2014), doi:10.1371/journal.pone.0081255.

99. E. Hoxha, P. Lippiello, F. Zurlo, I. Balbo, R. Santamaria, F. Tempia, M. C. Miniaci, J. Mariani, J. Rossignol, E. Tamagno, The Emerging Role of Altered Cerebellar Synaptic Processing in Alzheimer's Disease (2018), doi:10.3389/fnagi.2018.00396.

100. E. Hoxha, I. Balbo, M. Mc, F. Tempia, Purkinje Cell Signaling Deficits in Animal Models of Ataxia. *Purkinje Cell Signaling Deficits in Animal Models of Ataxia. Front. Synaptic Neurosci*. **10**, 6 (2018).

101. J.-M. Cavaillon, M. Adib-Conquy, The Pro-Inflammatory Cytokine Cascade. *Immune Response in the Critically Ill*, 37–66 (2002).

102. B. Becher, S. Spath, J. Goverman, Cytokine networks in neuroinflammation. *Nature Reviews Immunology 2016 17:1*. **17**, 49–59 (2016).

103. A. Tozzi, A. J. Hannan, S. D. Skaper, L. Facci, M. Zusso, P. Giusti, An Inflammation-Centric View of Neurological Disease: Beyond the Neuron. *Frontiers in Cellular Neuroscience | www.frontiersin.org*. **12** (2018), doi:10.3389/fncel.2018.00072.

104. A. S. Mendiola, A. E. Cardona, The IL-1b phenomena in neuroinflammatory diseases. *Journal of Neural Transmission*. **125**, 781–795 (2018).

105. S. Yamada, D. Yamazaki, Y. Kanda, 5-Fluorouracil inhibits neural differentiation via Mfn1/2 reduction in human induced pluripotent stem cells. *The journal of Toxicological Sciences*. **43**, 727–734 (2018).

106. A. D. Kraft, G. Jean Harry, Features of microglia and neuroinflammation relevant to environmental exposure and neurotoxicity. *International Journal of Environmental Research and Public Health*. **8**, 2980–3018 (2011).

107. J. Finik, Y. Nomura, Cohort Profile: Stress in Pregnancy (SIP) Study. *International Journal of Epidemiology*. **46**, 1388–1388k (2017).

108. W. Zhang, Q. Li, M. Deyssenroth, L. Lambertini, J. Finik, J. Ham, Y. Huang, K. J. Tsuchiya, P. Pehme, J. Buthmann, S. Yoshida, J. Chen, Y. Nomura, Timing of Prenatal Exposure to Trauma and Altered Placental Expressions of HPA-Axis Genes and Genes Driving Neurodevelopment. *Journal of neuroendocrinology*. **30**, e12581 (2018).

109. W. Zhang, K. Rajendran, J. Ham, J. Finik, J. Buthmann, K. Davey, P. M. Pehme, K. Dana, A. Pritchett, H. Laws, Y. Nomura, Prenatal exposure to disaster-related traumatic stress and developmental trajectories of temperament in early childhood: Superstorm Sandy pregnancy study. *Journal of Affective Disorders*. **234**, 335–345 (2018).

110. T. D. Gould, D. T. Dao, C. E. Kovacsics, The Open Field Test. *Neuromethods*. **42**, 1–20 (2009).

111. G. A. Metz, I. Q. Whishaw, Cortical and subcortical lesions impair skilled walking in the ladder rung walking test: a new task to evaluate fore-and hindlimb stepping, placing, and co-ordination. *Journal of Neuroscience Methods*. **115**, 169–179 (2002).

112. H. Shiotsuki, K. Yoshimi, Y. Shimo, M. Funayama, Y. Takamatsu, K. Ikeda, R. Takahashi, S. Kitazawa, N. Hattori, A rotarod test for evaluation of motor skill learning. *Journal of Neuroscience Methods*. **189**, 180–185 (2010).

113. R. L. Bell, S. Powell, S. Rahman, S. Momeni, L. Segerström, E. Roman, Supplier-dependent differences in intermittent voluntary alcohol intake and response to naltrexone in Wistar rats. *Frontiers in Neuroscience | www.frontiersin.org*. **9**, 424 (2015).

114. B. L. Pearson, E. B. Defensor, D. C. Blanchard, R. J. Blanchard, C57BL/6J mice fail to exhibit preference for social novelty in the three-chamber apparatus. *Behavioural Brain Research*. **213**, 189–194 (2010).

115. O. Kaidanovich-Beilin, T. Lipina, I. Vukobradovic, J. Roder, J. R. Woodgett, Assessment of Social Interaction Behaviors. *JoVE (Journal of Visualized Experiments)*, e2473 (2011).

116. Q. Hou, Y. Wang, Y. Li, D. Chen, F. Yang, S. Wang, A developmental study of abnormal behaviors and altered GABAergic signaling in the VPA-treated rat model of autism. *Frontiers in Behavioral Neuroscience*. **12** (2018), doi:10.3389/fnbeh.2018.00182.

117. R. N. Walsh, R. A. Cummins, The Open-Field Test: A Critical Review. *Psychological Bulletin*. **83**, 482–504 (1976).

118. L. Olexová, P. Štefánik, L. Kršková, Increased anxiety-like behaviour and altered GABAergic system in the amygdala and cerebellum of VPA rats — An animal model of autism. *Neuroscience Letters*. **629**, 9–14 (2016).

119. J. Moreno-Rius, The cerebellum in fear and anxiety-related disorders. *Progress in Neuro-Psychopharmacology and Biological Psychiatry*. **85** (2018), pp. 23–32.

Acknowledgements

First, I would like to express my sincere gratitude to my supervisor, Dr. Sachiko Yoshida for the last 6 years guiding me from master course (April 2016 – March 2018) till doctoral course (April 2018 – March 2022). Without her professional inputs and guidance, it would be extremely difficult to finish my study and research. It has been a great privilege to be her student as she shared a lot of knowledge and experience which help in grooming me to become a better researcher in the future.

I would like to extend my appreciation towards Professor Dr. Naohiro Hozumi from Department of Electrical and Electronic Information Engineering, Toyohashi University of Technology. The collaboration in between our labs have been generating a lot of breakthroughs in the visualization and evaluation of various cells using acoustic impedance microscope. I am deeply grateful for all the suggestions and support you gave me when I needed them the most.

Also, my sincere gratitude to the thesis committee: chief jury, Professor Dr. Toshihiko Eki and jury, Professor Dr. Kazunori Takashima for their valuable and critical comments.

Furthermore, I sincerely appreciated all the insightful discussion, useful guidance and collaborations to help me complete my doctoral dissertation from all the people listed below.

Assistant Professor Dr. Yuu Hirose	Department of Applied Chemistry and Life Science Toyohashi University of Technology Toyohashi, Aichi, Japan
Assistant Professor Dr. Jianzhong Hu	Department of Genetics and Genomic Sciences, Ichan School of Medicine at Mount Sinai New York, NY, USA
Professor Dr. Yoko Nomura	Queens College, City University of New York New York, NY, USA

Dr. Yasunari Kanda	National Institute of Health Sciences Kawasaki, Kanagawa, Japan
Dr. Kazuto Kobayashi	R&D division, Honda Electronics Co., Ltd. Toyohashi, Japan
Mr. Noriyuki Asai	Ichibiki Co., Ltd. Toyohashi, Aichi, Japan
Associate Professor Dr. Masahiro Koshimura	National Institute of Technology, Sasebo College Sasebo, Nagasaki, Japan

I would also like to thank all of my lab mates for all the help and support provided, be it helps in experiment and research or advices when I encountered obstacles in school life. Thank you all for the creation of great atmosphere when I was first transferred into Physiological Bioscience Laboratory. I am extremely grateful for all your kindness that help me interact better with fellow lab mates. I cherished the curiosity we shared in exploring the unknown and all the joyous moments we created together. Moreover, many thanks to Mr. Kyoichi Takanashi, Mr. Mamoru Washiya, Ms. Rahma Hutami Rahayu, Mr. Edo Bagus Prastika, Ms. Kana Miyamoto, Mr. Ken Futagami, Ms. Haruko Ohtsuka, Mr. Takuhei Ohmuro, Ms. Christine Lee Li Mei, Mr. Takaya Inakawa and Mr. Ruka Sasaki for their moral support, assistances and contributions in completing this thesis.

My deepest thanks to Sato Yo International Scholarship Foundation (SISF) too for providing me a generous scholarship, so that I did not have to worried about my livelihood. The 3.5 years financial support, starting April 2018 to September 2021, tremendously improve my life as an international student here in Japan. I am really grateful for all the support I get from the SISF and other students I met via this foundation. Also, special thanks to Mr. Masanori Tomida, for his never-ending kindness and advices even after the scholarship sponsorship (Rotary Yoneyama Memorial Foundation) for my Master degree had ended. In addition, many thanks to the Tahara Rotary Club members for all the kindness you blessed me with.

My deepest gratitude to my family and friends too. No word can express how grateful I am to always have their love and support all these years when I am set to pursue a dream that no one in the family dare to dream. Thanks for all the moral support and prayers to help me realized my dream and complete the doctoral program.

List of Publications

I. Papers

1. **Effects of anticancer drugs on glia--glioma brain tumor model characterized by acoustic impedance microscopy**

   Thomas Tiong Kwong Soon, Tan Wei Chean, Tan Wei Chean, Hikari Yamada, Kenta Takahashi, Naohiro Hozumi, Kazuto Kobayashi, Sachiko Yoshida

   Japanese Journal of Applied Physics, 2017, Vol. 56, 07JF15.

2. **Reaction assessment of cultured breast cancer cells exposed to anti-cancerous agents by means of micro-scale acoustic impedance profile**

   Rahma Hutami Rahayu, Kyouichi Takanashi, Thomas Tiong Kwong Soon, Inna Seviaryna, Roman Maev, Kazuto Kobayashi, Naohiro Hozumi, Sachiko Yoshida

   Japanese Journal of Applied Physics, 2018, Vol. 57, 07LF26.

3. **Non-invasive intracellular observation of cancer cells associated with proliferation**

   Thomas Tiong Kwong Soon, Rahma Rahayu Hutami, Kyouichi Takanashi, Naohiro Hozumi, Sachiko Yoshida, Kazuto Kobayashi

   2018 IEEE International Ultrasonics Symposium (IUS), pp. 1-9. IEEE, 2018.

4. **Three-Dimensional Acoustic Impedance Imaging for Cultured Biological Cells**

   Naohiro Hozumi,, Nur Dalila Binti Jalaluddin, Thomas Tiong Kwong Soon, Tomohiro Kawashima, Yoshinobu Murakami, Sachiko Yoshida, Kazuto Kobayashi

   2018 IEEE International Ultrasonics Symposium (IUS), pp. 1-9. IEEE, 2018.

5. **Evaluation of elastic change during mitotic phase of murine breast cancer cells using scanning acoustic microscope**

   Thomas Tiong Kwong Soon, Ruka Sasaki, Edo Bagus Prastika, Yuki Kawaguchi, Kazuto Kobayashi, Naohiro Hozumi and Sachiko Yoshida

   Japanese Journal of Applied Physics 2022 (accepted at 9th February 2022)

6. **Time and frequency domain deconvolution for cross-sectional cultured cell observation using an acoustic impedance microscope**

   Edo Bagus Prastika, Taichi Shintani, Tomohiro Kawashima, Yoshinobu Murakami, Naohiro Hozumi, Thomas Tiong Kwong Soon, Sachiko Yoshida, Ryo Nagaoka, and Kazuto Kobayashi

   Ultrasonics 119 (2022): 106601.

II. Domestic Conferences

1. **細胞観察のためのフィルム型培養器の新規開発**

   Thomas Tiong Kwong Soon, Tan Wei Chean, Yasuhiro Yokoyama, Masaki Imayasu, Kazuto Kobayashi, Naohiro Hozumi, Sachiko Yoshida

   第 9 回バイオ超音波顕微鏡研究会, Hamamatsu, Shizuoka, oral presentation, November 2016

2. **Gene-labeled cultured tumor model inspection for anticancer drugs using acoustic impedance microscope**

   Rahma Hutami Rahayu, Thomas Tiong Kwong Soon, Tan Wei Chean, Kyouichi Takanashi, Kenta Kishikawa, Hirofumi Kurita, Kazunori Takashima, Kazuto Kobayashi, Naohiro Hozumi, Sachiko Yoshida

   Physiological Society of Japan, Hamamatsu, Shizuoka, poster presentation, March 2017

3. **超音波顕微鏡を用いた培養がん細胞の抗がん剤に対する細胞内変化の観察**

   Thomas Tiong Kwong Soon, Rahma Hutami Rahayu, Kyouichi Takanashi, Kazuto Kobayashi, Naohiro Hozumi, Sachiko Yoshida

   The Japan Society of Ultrasonics in Medicine, Utsunomiya, Tochigi, oral presentation, May 2017

4. **Quantitative research of the effects of anticancer drugs on cultured breast cancer cells using ultrasonic microscope**

   Rahma Hutami Rahayu, Kyouichi Takanashi, Thomas Tiong Kwong Soon, Inna Seviaryna, Roman Maev, Kazuto Kobayashi, Naohiro Hozumi, Sachiko Yoshida

   Symposium on Ultrasonic Electronics (USE 2017), Tagajyou-shi, Miyagi, poster presentation, October 2017

5. **Altered gut microbiota observed in valproate-administrated autistic model rats**

   Thomas Tiong Kwong Soon, Chihiro Nishikawa, Yukiko Fueta, Susumu Ueno, Yuko Sekino, Yasunari Kanda, Yoko Nomura, Sachiko Yoshida

6. The 95th Annual Meeting of the Physiological Society of Japan, poster presentation, March 2018. **バルプロ酸誘発性自閉症モデルラットにおける腸内細菌叢の変化**

   宮本佳菜, Thomas Tiong Kwong Soon, 広瀬侑, 笛田由紀子, 上野晋, 諫田泰成, Yoko Nomura, 吉田祥

   第 65 回 中部日本生理学会, poster presentation, November 2018.

7. **Intracellular dynamics observation of breast cancer cells using acoustic impedance microscopy**

   Thomas Tiong Kwong Soon

   第 13 回バイオ超音波顕微鏡研究会, December 2018

8. **Alteration of cerebellar developmental structures and metabolic condition in prenatal famine rat**

   Kana Miyamoto, Thomas Tiong Kwong Soon, Seta Sato, Yoko Nomura, Yasunari Kanda, Sachiko Yoshida

   The 42nd Annual Meeting of the Japan Neuroscience Society, poster presentation, July 2019

9. **Developmental abnormality induced LPS, bacteria-derived inflammatory agent in rat cerebellar cortex**

   Haruko Ohtsuka, Noriyuki Asai, Thomas Tiong Kwong Soon, Yasunari Kanda, Sachiko Yoshida

   The 42nd Annual Meeting of the Japan Neuroscience Society, poster presentation, July 2019

10. **Chronic glyphosate exposure elicits neuronal cell death and microglia activation in developing rat cerebellum**

    Ken Futagami, Thomas Ting Kwong Soon, Christine Lee Li Mei, Hang Yong Lin, Yoko Nomura, Yasunari Kanda, Sachiko Yoshida

    The 47th Annual Meeting of the Japanese Society of Toxicology, e-poster presentation, June 2020

11. **Comparison of the effects of glyphosate neurotoxicity and HDACi neurotoxicity from the gut flora**

    Thomas Tiong Kwong Soon, Noriyuki Asai, Ken Futagami, Takaya Inakawa, Yoko Nomura, Yasunari Kanda, Sachiko Yoshida

    The 63rd Annual Meeting of the Japanese Society of Neurochemistry, e-poster presentation, September 2020

12. **Delayed neurotoxicity of prenatal glyphosate exposure and microglial activation**

    Ken Futagami, Thomas Ting Kwong Soon, Christine Lee Li Mei, Haruko Ohtsuka, Yoko Nomura, Yasunari Kanda, Sachiko Yoshida

    The 63rd Annual Meeting of the Japanese Society of Neurochemistry, e-poster presentation, September 2020

13. **Real time observation of collagen release from cultured human fibroblasts**

Shizuka Nakada, Thomas Tiong Kwong Soon, Edo Bagus Prastika, Kazuto Kobayashi, Naohiro Hozumi, Sachiko Yoshida

The 63rd Annual Meeting of the Japanese Society of Neurochemistry, e-poster presentation, September 2020

14. **The neurodevelopmental toxicity of chronic glyphosate exposure in developing rat cerebellum**

Shigehisa Satake, Ken Futagami, Thomas Tiong Kwong Soon, Yoko Nomura, Yasunari Kanda, Sachiko Yoshida

The 63rd Annual Meeting of the Japanese Society of Neurochemistry, e-poster presentation, September 2020

15. **High-dose neonicotinoid insecticide, Acetamiprid induces Purkinje cell malformation and behavioral alteration**

Christine Lee Li Mei, Takuhei Omuro, Thomas Tiong Kwong Soon, Johnny Ademir Lopez, Yoko Nomura, Yasunari Kanda, Sachiko Yoshida

The 63rd Annual Meeting of the Japanese Society of Neurochemistry, e-poster presentation, September 2020

16. **Physiological properties of cultured microglia from glyphosate-exposed rat cerebellum**

Kiyoshi Umemura, Misaki Iwanaga, Shizuka Nakada, Thomas Tiong Kwong Soon, Edo Bagus Prastika, Kazuto Kobayashi, Naohiro Hozumi, Yoko Nomura, Yasunari Kanda, Sachiko Yoshida

The 63rd Annual Meeting of the Japanese Society of Neurochemistry, e-poster presentation, September 2020

17. Cytological mechanism of developmental neurotoxicity embryonic LPS exposure

Haruko Otsuka, Sharumadhi Veloo, Kazunobu Tsunemoto, Thomas Tiong Kwong Soon, Yasunari Kanda, Sachiko Yoshida

The 63rd Annual Meeting of the Japanese Society of Neurochemistry, e-poster presentation, September 2020

18. Evaluation of elastic change during mitotic phase of murine breast cancer cells using scanning acoustic microscope

Thomas Tiong Kwong Soon, Ruka Sasaki, Edo Bagus Prastika, Yuki Kawaguchi, Kazuto Kobayashi, Naohiro Hozumi, Sachiko Yoshida

The 42nd Symposium on Ultrasonic Electronics (USE 2021), e-poster presentation, October 2021

19. Evaluation of collagen release from cultured human fibroblasts via ultrasonic microscope

Shigehisa Satake, Taichi Shintani, Shizuka Nakada, Thomas Tiong Kwong Soon, Edo Bagus Prastika, Kazuto Kobayashi, Naohiro Hozumi, Sachiko Yoshida

The 42nd Symposium on Ultrasonic Electronics (USE 2021), e-poster presentation, October 2021

20. Directly assessing the reactivity of rat-derived microglia with scanning acoustic microscope

Christine Lee Li Mei, Kiyoshi Umemura, Mai Murakami, Thomas Tiong Kwong Soon, Kazuto Kobayashi, Naohiro Hozumi, Sachiko Yoshida

The 42nd Symposium on Ultrasonic Electronics (USE 2021), e-poster presentation, October 2021

III. International Conferences

1. **Quantitative Research on the Effects of Anticancer Drugs on Glia-Glioma Brain Tumor Model Using Ultrasonic Microscope**

   Thomas Tiong Kwong Soon, Tan Wei Chean, H. Yamada, K. Takahashi, N. Hozumi, K. Kobayashi, S. Yoshida

   Symposium on Ultrasonic Electronics (USE 2016), Busan, Korea, poster presentation, November 2016

2. **Non-invasive intracellular observation of cancer cells associated with proliferation**

   Thomas Tiong Kwong Soon, Rahma Rahayu Hutami, Kyouichi Takanashi, Naohiro Hozumi, Sachiko Yoshida, Kazuto Kobayashi

   2018 IEEE International Ultrasonics Symposium (IUS), Kobe, Japan, poster presentation, October 2018.

3. **Altered gut flora and cerebellar development abnormalities in VPA rat model of ASD**

   Thomas Tiong Kwong Soon, Seta Sato, Kana Miyamoto, Yuu Hirose, Yasunari Kanda, Sachiko Yoshida

   The 9th Federation of the Asian and Oceanian Physiological Societies Congress (FAOPS 2019), Kobe, Japan, poster presentation, March 2019

4. **Alteration of gut microbiota and cerebellar structures in Glyphosate-exposure rat**

   Kana Miyamoto, Ken Futagami, Thomas Tiong Kwong Soon, Yuu Hirose, Jianzhong Hu, Yoko Nomura, Yasunari Kanda, Sachiko Yoshida

   The 9th Federation of the Asian and Oceanian Physiological Societies Congress (FAOPS 2019), Kobe, Japan, poster presentation, March 2019